ANALYSIS OF SURFACE INTEGRITY IN ELECTRICAL DISCHAGE MACHINING (EDM) PROCESS FOR TUNGSTEN CARBIDE MATERIAL

A THESIS SUBMITTED IN THE FULFILLMENT OF THE REQUIREMENTS FOR THE AWARD OF THE DEGREE OF DOCTOR OF PHILOSOPHY

Submitted By

CHANDER PARKASH KHATTER

9010555

DEPARTMENT OF MECHANICAL ENGINEERING

THAPAR UNIVERSITY

PATIALA – 147004, INDIA

FEBRUARY, 2009

CERTIFICATE

This is to certify that the thesis entitled "**Analysis of Surface Integrity in Electrical Discharge Machining (EDM) Process for Tungsten Carbide Material"** which is being submitted by Mr. Chander Parkash Khatter to Department of Mechanical Engineering, Thapar University, Patiala in fulfilment of the requirements for the award of the degree of Doctor of Philosophy, is a record of candidate's own work carried out by him under our guidance and supervision. The matter presented in this thesis has not been submitted in part or full for the award of any degree in any other University or Institute.

Date: August 19, 2010

Place: Patiala

19/8/2010

Dr. B.L. Sethi
Professor & Director
Mechanical Engineering Department
Guru Nanak Institute of Technology
Mullana (Distt. Ambala)
Haryana, INDIA

19/8/10

Dr. O. P. Pandey
Professor and Head
School of Physics & Material Sciences
Thapar University
Patiala-147004 (India)

ACKNOWLEDGEMENTS

I acknowledge with deep sense of gratitude and humility, the inspiring help and guidance rendered by my supervisors, **Dr. B.L. Sethi**, Director, Guru Nanak Institute of technology, Maullana and **Dr. O.P. Pandey**, Professor and Head, School of Physics and Material Sciences, Thapar University, Patiala for their interest and encouragement throughout the course of this research effort. Their deep insights into the problem and ability to provide guidance and solutions have been of immense value in improving the quality of my research work at all stages.

My special thanks are due to **Prof. K.K. Raina**, Deputy Director, **Dr Sushil Mittal** dean research and **Dr. S.K. Mohapatra** Professor and Head, Mechanical Engineering Department, Thapar University, Patiala for their encouragement and moral supports.

I am very much grateful to additional Secretary and Development Commissioner Ministry of MSME Govt. of India for allowing me to enrol for PhD programme at Thapar University Patiala. I sincerely thank my colleagues and staff of Central Institute of Hand Tools, Jalandhar where I served as a Principal Director for more than six years and applied the EDM technology to assist various industrial units in general and MSME in particular.

My sincere thanks are due to **Dr. J.K. Sharma**, Director, Prof**. P.L. Bali,** Head, Mechanical Engineering and Dean Research and Development, **Dr. Chander Mohan**, Prof. Computer Science and Engineering Department, Ambala College of Engineering and Applied Research, Ambala for their valuable help and constant encouragement.

Thanks are also due to **Dr. Dinesh Shukla**, Lecturer, Department of Mechanical Engineering, B.R. Ambedkar Natoinal Institute of Technology, Jalandhar for being associated with technical association and contributing his bit during my research efforts at different stages.

Very special thanks to Research Scholars **Mr. Akshay**, **Ms. Kamalpreet**, **Ms. Manwinder**, **Ms. Bhupinder** for helping and supporting me at all the time. I take this opportunity to express my respect and thankfulness to all my well wishers and colleagues for their encouragement and support.

I express my love and gratitude to my wife **Jyoti** and other family members for their affectionate, patience, personal sacrifices and moral support throughout the research project.

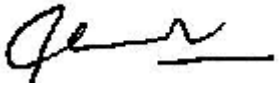

(Chander Parkash Khatter)

CONTENTS

LIST OF FIGURES

Page No

Chapter 4

Chapter 5

LIST OF TABLES

LIST OF PUBLICATIONS

1. Effect of processing parameters on structural features of tungsten carbide after electric discharge machining (EDM), **C.P. Khatter**, Dr. O.P. Pandey, Tribology – Materials, Surfaces & Interfaces, **2/2**, 2008, 65-71.

2. Analysis of energy distribution parameters of Electric discharge machining (EDM) for Tungsten Carbide, **C.P. Khatter**, Dr. O.P. Pandey, Tribology – Materials, Surfaces & Interfaces, **3**, 2009, 1-15.

3. Failure analyses of cemented tungsten carbide extrusion die, **C.P. Khatter**, Dr. B.L. Sethi, Dr. O.P. Pandey, Dr. B.L. Sethi, Tribology – Materials, Surfaces & Interfaces (Published).

4. Structural analysis of electrodischarge machined surfaces of EN 31 tool steel, O. P. Pandey, C. P. Khatter, R. Choudhary and R. K. Garg,Electric discharge machining (EDM) of WC-Co cermet, Tribology – Materials, Surfaces & Interfaces, **3/2,** 2009,74-83.

5. Study of surface cracks on electrodischarge machined tungsten carbide cermet, **C.P. Khatter**, Dr. O.P. Pandey, Tribology – Materials, Surfaces & Interfaces, **0**, 2010, 0-0. (Accepted)

PREFACE

The current need of machining requires high surface finish with ease of manufacturing. Engineers and technologists are working on Electrical Discharge Machining (EDM) for more than five decades but accelerated research and development activities in this area have started only during the last few years. In EDM process melting and re-solidification at the surface of the material being machined occurs, i.e. thermal and chemical factors intervene [1-4]. Cobalt is used as binder in the sintered WC material. The amount and grain size of cobalt which may vary from 6% to15%, determines the hardness and toughness of the carbide. During EDM process cobalt which is used as binder melts first because of low melting point as compared to tungsten carbide. If the machining conditions are not optimized properly then it may lead to development of cracks. Formations of these cracks are because of high tensile and compressive stresses that build up at the interface of the WC and Co binder. The network crack formation is associated with the development of high tensile stresses, exceeding the fracture strength of the material [5-8].

Extensive research in the field has led to better understanding of the phenomenon of the metal removal in the presence of electric impulses. EDM is an advanced machining process which has steadily gained importance over the years because of ability to cut and shape wide variety of materials irrespective of the high hardness [9]. Lee Soo Hiong [10] has presented a comprehensive study of the surface integrity of the machined work piece of the tungsten carbide by EDM. It has been reported that there is a little difference between the hardness of the EDMed surface and the original hardness of the work piece for all EDM conditions. Several investigators have shown that the energy distribution in the EDM process influences the material removal rate and accuracy to great extent [11, 12]. The adoption of larger pulse current and smaller pulse on duration is effective in suppressing the formation of surface cracks. In general the material removal rate and machining characteristics during the EDM process depend on the distribution of the input energy to electrode and work piece [13, 14]. The input energy supplied during machining is distributed to various components i.e. work piece, electrode, dielectric etc. Part of this input energy is utilized for machining and remaining goes as waste.

The effectiveness of the EDM process is evaluated in terms of the material removal rate (erosion of work piece material per unit time), relative wear ratio and

the surface roughness of the EDM machined surface. All these parameters depend upon the distribution of the energy supplied during the process. It is also observed that copper and aluminium electrodes results in poor machined surface at high currents, which is due to the fact that higher MRR of Cu and Al metal electrodes is accompanied by larger and deeper craters, resulting in a greater surface roughness [15-18]. For a particular application and with given technical conditions Juhr [19] has studied the thermal load using different simulation conditions of different pulse wave forms. In many applications EDM of cemented carbide is restricted by the basic properties of this family of materials. A specific electrical voltage is supplied to both of electrode and work piece. Once the gap between two electrodes is narrow enough, electrical discharge occurs. Material removal is accomplished through the thermal functions caused by the discharge, including evaporation and melting and the function of force, including discharge impact pressure and explosive force [19]. In EDM, the choice of electrode polarity is an important factor. The effect of polarity on the material removal rate, relative wear ratio and surface roughness can be clearly seen [20]. Puertas et al.[21] reported that most important factor was intensity, followed by duty cycle factor, the pulse time factor and the interaction effect of first two.

Electro-discharge machining (EDM) appears as an alternative to grinding and hard turning for the machining of tool steels because EDM allows the machining of any type of conducting material, regardless of its hardness. In order to achieve high level of surface finish most users have resorted to manual lapping (hand polishing). The abrasive nature of the lapping, not only provides better surface appearance but the tensile residual stresses induced by the EDM process can be reduced and even transformed into compressive residual stresses [22]. It was found that thermal stresses exceed the yield strength of the workpiece mostly in an extremely thin zone near the spark [23]. Vinod Yadav et al. [24] observed that after one spark, substantial compressive and tensile stresses develop in a thin layer around the spark location. It is reported for different substances that maximum material removal occurs at both optimum power and pulse duration [25-27].

The aim of the present study is to optimize the experimental conditions for an effective energy distribution which is available in electric discharge machining for tungsten carbide. The write up of the thesis is divided into six chapters which is described below.

Chapter1

Introduction

Chapter1 describes comparative study of different manufacturing processes including traditional and modern methods. Main parameters and the related parameters of the study have been described. Input energy parameters include peak current, pulse duration and polarity. Output in the form of surface integrity has been chosen for this study which includes surface roughness micro hardness and microstructure. A brief idea about problems associated with machining of tungsten carbide through non-traditional machining is given. The EDM process, which is most suitable for machining of tungsten carbide, has been described in detail. At the end the problem selection and organizing the thesis is described.

Chapter2

Literature review

Extensive research in the field of EDM has led to better understanding of the phenomenon of metal removal rate in the presence of electrical impulses. The key interest of scientists and technologist is for the development of efficient generators leading to higher rates of metal removal with excellent surface finish and low tool wear. This has lead to development of some machines with numerical and adoptive controls. This chapter has been divided in six different sections i.e. EDM Process, factors effecting machining rate, energy distribution and material parameters, surface integrity in EDM with proper references. Accordingly the literature review has been done. In each and every section attempt has been made to club the work of different authors working on the same or similar field. The literature survey indicate that not much work has been carried out on machining of tungsten carbide so the work done on other similar materials like metal matrix composites have been considered and compared with the tungsten carbide.

Chapter3

Effect of processing parameters on structural features of tungsten carbide after EDM

This chapter presents the experimental work done for the machining of tungsten carbide. The process parameters required for the machining of WC-Co cermet materials have been optimized to achieve targeted surface finish with optimum material removal rate. Experiments have been performed in the range of 10-20 amp discharge current. The results show that material removal rate (MRR) increases from 5.5 to 8.5 mm^3/min with increase in the density of the electrical discharge energy. However, it deteriorates the surface roughness (R_a factor) which varies from 2.8 to 4.0 microns for CuW electrode. Similar variation was observed for Cu where R_a varies from 0.9 to 2.3. The structural features of the EDMed surface was analysed under SEM. The reasons for formation of different size of craters have been discussed. At the end the nature of cracks observed at the surface is described.

Chapter4

Study of surface cracks on EDMed tungsten carbide cermet

In order to improve the technological performance during EDM process it is essential to understand the formation of cracks, distribution of cracks, size of the cracks, and the structure of cracks to distinguish between fatigue cracks and EDM cracks. An experimental study on surface cracks on EDMed tungsten carbide is presented. The copper tungsten electrode has been used for the study. Current and pulse duration have been selected as variable parameters. The objective of this study is to establish upper limit of machining at which the formation of micro cracks at different energy input levels occurs. It is observed that very good surface finish can be achieved using the machining parameters at low pulse energy. The detail of this study has been presented in this chapter.

Chapter5

Energy distribution in EDM Process

It is well established fact that EDM is thermal erosion process. The amount of energy available for this process is generated through plasma. In order to understand the actual amount of energy utilized for machining of WC this work was planned. Experiments have been conducted in a planned sequence to take an account of the total energy input and to find out what part of the energy have been utilized for the purpose of material removal or useful part and how much energy goes waste. This was done to optimize the process parameter so that maximum amount of energy is used for the useful purpose. Some theoretical work in literature has been reported but no evidence of experimental proof has been reported. For this purpose special tanks for the experiments have been designed and executed. Experimental data was used to calculate the amount of energies utilized by electrode and workpiece material with the help of heat transfer the results so obtained were put to analysis of variance (ANOVA) and have been proved with in significance level of acceptance. It was observed that only 17% of total available energy is utilized for machining of WC.

Chapter 6

Conclusions and scope of future work

In this chapter summery of the findings of entire work has been presented. The conclusions drawn from the work are given and also future plan of the work is proposed.

SELECTED RELATED REFERENCES (1981 -2008)

1. Guu Y H, Hocheng H, Chou C Y, Deng C S, (2003)," Effect of electrical discharge machining on surface characteristics and machining damage of AISI D2 tool steel", *Material Science and Engineering*, **A 358**, 37-43

2. Navas V. Garcia, Ferreres I., Maranon J.A., Garcia-Rosales, Sevillano J.Gil,(2008), "Electro-discharge machining versus hard turning and grinding - Comparison of residual stresses and surface integrity generated in AISI O1 tool steel", *Journal of Material processing technology*,**195**,186-194.

3. Rebelo J. C., Morao Dias A., Krener D., Lebrun J. L., (1998),"Influence of EDM pulse energy on surface integrity of martensite steels" *Journal of Material Processing Technology,* **84**, 90-96.

4. Marafona J., Wykes C, (2000), "A new method of optimizing material removal rate using EDM with copper tungsten electrode", *Int. J. of Machine Tools & Manufacture,* **40(2),** 153-164

5. Shu Kuen-Ming and Tu G. C., (2001), Fabrication and characterization of Cu-SiC_p composites for Electrical Discharge Machining applications, *International Journal of Machine Tools & Manufacture*,**16(4)**, 483-502.

6. Shankar Singh , S. Maheshwari , P.C. Pandey, (2004), "Some investigations into the electric discharge machining of hardened tool steel using different electrode materials", *Journal of Material Processing Technology*, **149**, 272–277.

7. Singh Sehijpal, Shan H S and Kumar Pradeep (2002), "Parametric optimization of magnetic field assisted abrasive flow machining by Taguchi method", *Journal of Quality and reliability engineering International*",**18**, 273-283

8. Kansal H K, Singh S and Kumar P, (2005)**,** "Parametric optimization of powder mixed electrical discharge machining by response surface methodology", *Int. Journal of materials Processing Technology,* **149**, 427-436.

9. Pandit S. M., Rajurkar K. P., (1983),"A stochastic approach to thermal modeling applied to electro-discharge machining", *J. of Heat Transfer*, **105,** 555-562.

10. Lee S. H., Xiaoping Li, (2003),"Study of the surface integrity of the machined work piece in the EDM of tungsten carbide", *Journal of Materials Processing Technology*, **139,** 315–321.

11. Daryl D., Di Bitonto, Philip, Eubank T, Patel, Mukund, Maria and Barrufet, (1989), " Theoretical Models of the Electrical Discharge Machining Process- The Anode Erosion Model" *Journal of Applied Physics*, **66/9,** 4095-4103.

12. Daryl D., Di Bitonto, Philip, Eubank T, Patel, Mukund, Maria and Barrufet, (1989), "Theoretical Models of the Electrical Discharge Machining Process- The Cathode Erosion Model" *Journal of Applied Physics*, **66/9** , 4104-4112.

13. Marafona J., Wykes C, (2000), "A new method of optimizing material removal rate using EDM with copper tungsten electrode", *Int. J. of Machine Tools & Manufacture,* **40(2),** 153-164

14. Montgomery D C, (2005),"Design and analysis of Experiments", 5th Edition, John Wiley & Sons, ISBN 9971-51-329-3

15. Abbas Norliana Mohd, Solomon Darius G., Bahari Md. Fuad, (2007), " A review on current research trends in electrical discharge machining (EDM)", *International Journal of Machine Tool & manufacture*, **47,** 1214-1228.

16. Ho K. H., Newman S.T., (2003), State of the art electrical discharge machining (EDM), *International Journal of Machine Tools & Manufacture*, **43**, 1287-1300.

17. Guitrau E.B., The EDM Hand book, Henser Gardner Publications, 1997.

18. Juhr. H, Schulze, (2004) "Improves cemented carbide properties after wire EDM by pulse shaping", *Journal of Materials Processing Technology*, **149,** 178-183.

19. Liao Y.S, Yu. Y. P, (2004),"The energy aspect of material property in WEDM and its applications" International *Journal of Machine Tools & Manufacture"*, **149,** 77-82.

20. Lee S.H., Li X.P., (2001),"Study of the effect of machining parameters on the machining characteristics in electrical discharge machining of tungsten carbide", *Journal of Materials Process Technology*, **115**, 344-358.

21. Puertas I, Luis C J, Alvarez, (2004),"Analysis of the influence of EDM parameters on surface quality, MRR and EW of WC-Co", *Journal of Materials and Processing Technology,*

22. Ramasawmy H., Blunt L.,(2002), " 3D topography assessment of the effect of different electrolytes during electrochemical polishing of EDM surfaces, *International Journal of Machine Tools & Manufacture*, **42**, 567-574.

23. Yadav Vinod, Jain Vijay K., Dixit Prakash M.,(2002), "Thermal stesses due to electrical discharge machining ", *International Journal of Machine Tools & Manufacture,* **42**, 877-888.

24. Jeswani M L, (1981), "Effect of addition of graphite powder to kerosene used as a dielectric fluid in electrical discharge machining", *Wear*, **70**, 133-139.

25. Kangarajan D, Kerthkeyan R, Palani Kumar K, Davim J. Paulo, (2008), "Optimization of electric discharge machining characterization of WC-Co composites using non dominated sorting genetic algorithm", *International Journal of Advanced Manufacturing Technology,* Springer, **36**, 1124-1132.

26. Simao J., Lee H. G., Aspinwall, Dewes E. M., Aspinwall, (2003), "Workpiece surface modification using electrical discharge machining", *International Journal of Machine Tools & Manufacture,* **43,**121-128.

Chapter 1

AN INTRODUCTION

Overview

Machining is an inherent pre requisite manufacturing process to shape any machine component. This chapter describes comparative study of different machining processes including traditional and modern methods. Main parameters and also the related parameters which influence the machining have been described. Input parameters for electro discharge machining as energy includes peak current, pulse duration and polarity which influences the machining has been described in detail. Output parameters in the form of surface integrity have been chosen for this study which includes surface roughness micro hardness and microstructure. Sequential development to control these parameters by different group of scientist has been described. A brief idea about problems associated with machining of tungsten carbide through nontraditional machining is given. The EDM process, which is most suitable for machining of tungsten carbide, has been discussed in detail. At the end of the chapter the reasons for problem selection and organizing the thesis is described.

1.1 Introduction

The era of conventional machining, used the machine tools like lathe, shaper and milling machines where the carbon steel was used as a cutting tool which further improved when high speed steel (HSS) tools were introduced. The invention of tungsten carbide tools facilitated the machining and material removal rate (MRR) many folds. With the development of 3D milling machines and machining centers, an innovative and versatile tool for productivity improvement has been developed. Emphasis is on high material removal rates to reduce machining time. The same can be achieved through tungsten carbide cutters. Research and developments are on for developing strategies and parameters to develop the best carbide, geometry, coating combinations to realize good tool lifetime and good price performance ratio. During this period nontraditional machining was also developed and many areas for machining were considered, such as electric sparks, high velocity material jets, pulse magnetic fields, light beams, electro thermal, chemical reactions etc. were considered. These nontraditional methods were discovered to overcome difficulties such as complexity of shape, distortion sensitivity, brittle and hard materials. The solutions due to micro machine, difficult to handle jobs and difficult to machine materials such as cermets, ceramics, metal matrix composites etc. were the area of interest for researchers. For superior performance, machining of components made from such materials to close tolerances and higher surface finish is must. For the sake of economy the components must be machined at a fast rate in minimum number of set ups. These requirements are partly been met by the use of number of advance machining processes. These processes, often called as non-conventional machining methods, advance machining processes or modern machining processes are characterized by the absence of plastic deformation and chip formation, as is normally the case in conventional machining. For metal removal, non conventional methods directly utilize some form of the energy viz., thermal, mechanical and chemical. Thermal process mainly included Electrical discharge grinding (EDG), Electron beam welding (EBW), Electron beam machining (EBM), Laser Machining (LM), Plasma arc cutting (PAC), Thermal energy deburring (TED) etc. Some of mechanical processes included Abrasive jet machining (AJM), Abrasive wear jet machining (AWJM), Abrasive flow machining (AFM), Ultrasonic machining (USM) and Ultrasonic welding (USW). Similarly some of other notable electro-chemical methods included Electro-chemical machining (ECM), Electro-chemical grinding (ECG), Electro-stream drilling (ESD), Electro-chemical honing, turning etc. In some of the typical cases chemical milling and chemical blanking registered its importance due to various advantages. Classification of advance machining

processes is shown in Table 1.1. Some of the advance machining processes, amongst which the notable ones are EDM and ECM, have found fairly widespread applications in industry [1-3]. Industry saw improved finishes at very high spindle speeds and because of this new heights of MRR were observed till twentieth century. Till then the scientist were busy at the laboratories to develop newer machining methods. Basic machining parameters to improve the amount of energy utilized for machining were developed. Limitations of the various processes were studied for improving the efficiency of the processes. Other area of development was the tool used to remove the material; the iron based tools were changed to air, abrasives, laser, electricity etc. The Electro discharge machining (EDM) used electricity as a source of energy and conductive materials as tool. Work piece and the tool were used as cathode and anode. Data bank is created for EDM for further investigations by statistical analysis and is used in industries as well as for the research purposes [4-5].

Table 1.1: Classification of Advanced Machining Processes [1]

Type of Energy	Mechanism of Metal removal	Transfer media	Energy source	Processes
Mechanical	Erosion	High velocity Particles	Pneumatic/ Hydraulic Pressure	AJM,USM, WJM
	Shear	Physical contact	Cutting tool	Conventional Machining
Electrochemical	Ion displacement	Electrolyte	High Current	ECM,ECG
Chemical	Ablative Relation	Reactive Environment	Corrosive Agent	CHM
Thermoelectric	Fusion	Hot gases Electrons	Ionized Material High voltage	IBM,PAM, EDM
	Vaporization	Radiation	Amplified Light	LBM
		Ions stream	Ionised material	PAM

AJM	Abrasive Jet Machining	IBM	Ion Beam machining
CHM	Chemical machining	LBM	Laser Beam machining
ECG	Electrochemical Grinding	PAM	Plasma machining
ECM	Electrochemical machining	USM	Ultrasonic machining
EDM	Electric Discharge Machining	WJM	Water Jet Machining

Source: Pandey P.C., and Shan,H.S.(2008), "Modern Machining Process", Tata McGraw Hill, New Delhi [1]

Although the process capability of ECM in terms of metal removal rate is much higher as compared to EDM but application wise EDM is more popular. An idea of the popularity of EDM may be obtained from survey conducted in USSR where EDM accounts for more than 75% of total utilization of newer machining processes. In USA a four-fold increase in the number of EDM machines installed in the industry was observed between the year 1990 and 2000. Technological characteristics like material removal rate, energy distribution of EDM process has been investigated by various researchers [6-8]. Considering all these findings it is believed that EDM has superseded other advanced manufacturing processes because of its easiness and compatibility.

1.2 The EDM Process

Electrical discharge machining (EDM), also referred as spark erosion machining, is a process consisting of the removal of metal particles from a work piece surface by a rapid succession of short time electric discharges. The tool used for spark erosion is an electrode whose shape is a negative replica of the contour to be produced on the work. The tool electrode and the work are held at an accurately controlled distance from one another, which are dependent on the operating conditions and referred to as spark gap. By means of suitable electrical equipment, accommodated in a generator, provisions are made for consecutive spark discharge of approximately 20 V between the electrode and the work piece, which serve the purpose of stock removal. Both the tool and the work are submerged in a dielectric medium [9-12].

Daryl et al. [13, 14] investigated into the theoretical models of the EDM process and reported that spark discharge causes the release of electrical energy, which is converted into thermal and mechanical energy. As a result, certain volume of work piece material and also electrode material are heated to melting and vaporizing temperatures and thrown out in an explosion manner by mechanical and electrical forces. This process leave tiny pits and craters on the work and electrode surfaces, the size of such craters being dependent on the energy content of the spark. If high pulse energy is used, the craters will be relatively large, producing a rough surface. This type of eroding is called “roughing’. On the other hand, the use of low pulse energy will lead to smaller craters and thus smoother surface, the process being called “finishing”. The large number of mutually overlapping discharge craters results in a pitted structure of the surfaces, causing certain roughness and giving spark eroded surfaces, a characteristic matte appearance without any directionally oriented tool marks. The particles removed are carried off from the gap by the dielectric with the aid of a pressure

or vacuum flushing arrangement and are later separated from the liquid in a filtration unit. The rate of stock removal is dependent on the polarity of the work electrode and tool electrode [15]. The dielectric liquid has the function of reducing the cross-sectional area of the discharge channel to increase the energy density, i.e., to concentrate the energy of the spark on a small area and thus increase the efficiency of stock removal. In addition, the dielectric has a shielding function by preventing the access of air; detrimental oxidation will be eliminated during spark discharges. Finally, apart from cooling the work piece and the electrode, the dielectric serve the purpose of flushing the spark gap for the removal of debris. The process can be applied, in general, to any electrically conductive material. Other properties like strength, brittleness etc. do not impose any restrictions to the application of the EDM process. There are no physical cutting forces between the tool and work piece. Due to the process capability EDM has proved especially valuable in the machining of super tough materials such as the new space age alloys.

1.2.1 Historical Background

The origin of electrical discharge machining goes back to 1770, when English scientist Joseph Priestly discovered the erosive effect of electrical discharges on metals. In 1943, Soviet Scientists B.R. Lazarenko and N.I. Lazarenko had the idea of exploiting the destructive effect of an electrical discharge and developing a controlled process for machining materials that are conductors of electricity. With that idea, the EDM process was born, but it was only during the year 1948-1950 that the industrial world became really interested in this process. EDM as a new comer in the industrial machining environment showed relevant importance since the EMO tool fair in Milan in 1954. The first British patent was granted to Rudorff in 1950. USA, Japan and Switzerland developed their machines around 1952. D.F Draw reported the EDM progress in six phases starting with first from 1945-1960. During this period electric breakdown analysis in gases, arc behavior and gas discharge were studied in detail. In second phase (1960-1975), during these 15 years EDM discharge analysis, mono discharge modeling and physical mathematical modeling came into existence. During third phase from 1975 to 1985, multi arc analysis, discharge classification, adoptive control optimizations [ACO] and adoptive control constraints were studied and used for EDM Process. Jeswani M. L. [16] reported the effect of addition of graphite powder to kerosene used as a dielectric fluid in EDM and researchers tried many other additives to improve and modify the EDMed surface. It was only in 1980 with the event of computer numerical control (CNC) in EDM that brought tremendous advances in

improving efficiency of the machining operation. CNC has facilitated total EDM, which implied automatic and unattended machining from inserting the electrode in the automatic tool changer (ATC) (Fig. 1.1) to a finished polished cavity or cavities [17].

Fig. 1.1: Automatic Tool Changer

Fourth phase 1985-1990 brought revolution in improvement of the process. During this period pulse recognition, real time analysis, A.C. tool wear analysis, controls and expert systems for wire EDM machine [WEDM] touched the new heights of performance. Fifth phase 1990-95 brought the parametric approach, Neutral net works and Fuzzy controllers. Modern era from 1995 till date brought in various new aspects in EDM machining such as micromachining by EDM and machining without liquid dielectric. EDM of new conductive materials changed the total scenario. Now EDM is much accepted technique for material removal next to CNC Milling.

1.2.2 EDM Set-up

Nearly all the EDM machines are of vertical C type construction consisting of a base, a column and a head. The column is fixed to the base and supports the head. A coordinate table, which supports the work piece, is usually mounted on the base. Machines with fixed work-table are also available at a lower cost. A dielectric tank is constructed around the

table and is provided with an automatic level controller [18, 19]. It is also equipped with a safety device to shut down operation in case the temperature exceeds a certain limit. Work piece can be mounted on the table with any suitable work-holding devices like magnetic table, vice, chucks or special work holding fixtures. However, it should be ensured that there is a good circulation and flushing of the dielectric fluid. It is some time convenient to hold the workpiece on suction and injection pots that provide a built in arrangement for circulation of dielectric fluid. Controlled removal of material, from the workpiece in EDM, is achieved by the application of electrical energy between the tool and work electrodes in the form of short duration electrical pulses. Apart from supplying the adequate voltage to initiate and maintain the discharge, the generator can also adjust the discharge current and the pulse duration. The pulse generators operate in conjunction with a servo system, which helps to maintain efficient and stable spark gap and ensure the progressive advance of the tool electrode during machining. Fig. 1.2 shows the schematic diagram for the EDM process [20].On CNC EDM it is possible to make threads in hard surfaces Fig 1.3 shows making of threads on hardened die.

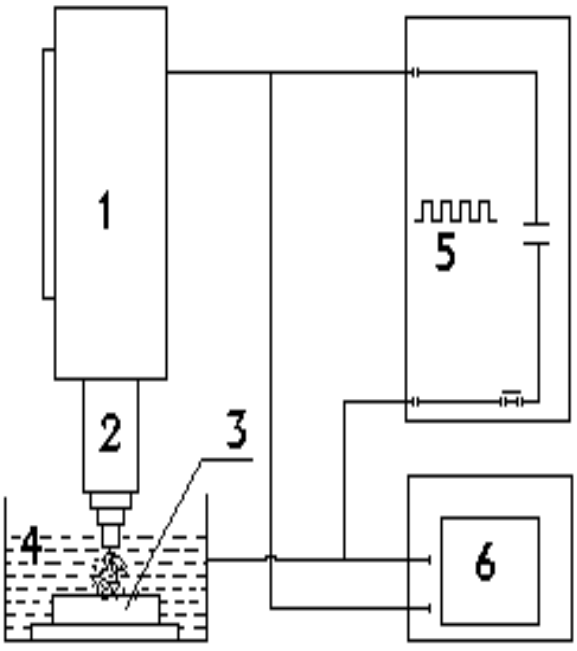

Fig. 1.2: Schematic diagram of the EDM process (1: servo-control; 2: electrode; 3: specimen; 4: dielectric fluid; 5: pulsed generator; and 6: oscilloscope).

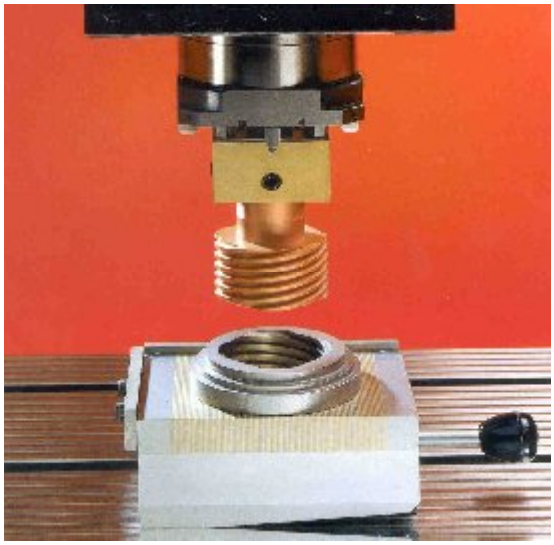

Fig. 1.3: Making threads on hardened die

1.2.3 Mechanism of Metal Removal Rate in EDM

Electro-discharge machining (EDM) appears as an alternative to grinding because the process allows the machining of any type of conducting material, regardless of its hardness. Nevertheless, other factors must be taken into account in the selection of machining processes, especially in the case of aero space parts. The exact mechanism of the EDM process is not clearly understood. However, several theories have been proposed by the early researchers [21-24] to account for the erosion mechanism of EDM process. Generally it has been accepted that the metal removal phenomenon is predominantly thermal in nature. During the electro discharge, an ambulance of electrons strikes the work electrode, which generates enormous amount of heat, causing local melting and evaporation of the electrodes. The heat also causes cracking of dielectric and high pressure generated expels the molten metal in all direction. With each discharge, a small crater is formed on the work piece, and a smaller one on the tool electrode.

1.3 Applications of EDM

EDM can be employed to machine any material provided it shows some minimum electrical conductivity. EDM can be used for making dies for molding, casting, forging, stamping, coining, forming etc. It is also used to make dies for extruding, wire drawing which require through holes [25]. It is employed for tiny holes, orifices and fragile features (micro sized slots). In case of making of intricate shaped dies, the machining time has come down to 50% or even less. Some of the industries claim that because of EDM technology die changing is

faster. EDMed dies are free of burrs and have higher life as a compared to that made by using conventional methods. It permits the use of more durable die material, viz carbide, hardened steel, exotic, etc. Matte finish obtained during EDM minimizes the required polishing time.

Fig. 1.4: CNC EDM milling

One of the common applications of EDM is the removal of broken taps, drills studs, reamers and pins [26]. By using EDM, one can eliminate handwork (breaking sharp edges). We can do EDM (including rework) after heat treatment and can choose better die material without worrying about its machining problems. It can be used to produce shapes which are extremely difficult to make otherwise, viz. squares, 'D' holes, splines, narrow slots and grooves, blended features etc.

1.3.1 Specific Industrial Examples

The evolution of EDM from disintegrator to a fully automated machining center clearly indicates the importance of EDM in modern manufacturing industry. Machine tools are getting smarter with time. The machines themselves are now handling many of the functions that once were assigned to human operators. The automation in EDM fulfills some of the specific applications in support of the process as high aspect holes. There are many different methods used to produce micro holes including discharge machining. Each have its merits and demerits, but for certain applications such as ink jet nozzle manufacture, where it is essential to produce a smooth internal bore inside the hole to encourage laminar flow of ink and an exit perimeter without adherent burrs that would break up the flow of the ink, then micro EDM becomes a strong answer [27]. The two-stage process recently developed

provide two separate micro EDM processes using one NC-machine to fabricate the electrode and a second machine to generate the holes. The fabrication of microelectrode is also possible.

1.4 Trend of Research in EDM

There has been a continuous effort towards enhancing the capabilities of the EDM process so as to make it more versatile and competitive. Fig1.4 shows CNC EDM milling. It has become very common practice to use EDM as milling. Here the electrode works as cutter and the profile is generated without making complex electrode. This has also resulted into the development of a number of EDM assisted processes such as wire EDM, electro discharge grinding (EDG) and micro-spark erosion. New development such as multiple electrode setups and multi-lead power supplies, have made it possible to achieve higher cutting rates, making the process more competitive. On the other hand, introduction of fully automatic numerically controlled machine with adaptive control systems for in-process optimization of the process have resulted into highly efficient metal removal systems. Researchers have also been conducted towards the development of power supply systems for EDM, electrode materials and dielectric fluids. Some reports have been published on basic studies on discharge mechanism, optimization and numerical control of the process [28].

New dielectrics, other than hydrocarbon oils have also been tried to improve upon the efficiency of working and better environment. Data bank is developed, which assists the EDM user in selecting optimum parameters to achieve the desired results. The use of such a data bank would contribute towards increase in productivity and lead to more predictable lead-time and reduced costs [29].

Since EDM is a thermal process where material is removed by a succession of electrical discharges occurring between an electrode and work piece plunged in a dielectric fluid, the basic studies on the mechanism of metal removal in EDM has attracted the attention of many scientists. Several mathematical models are available which, for the given situation, can compute the optimum pulse parameters for maximizing the metal removal rate. However, the existing analytical models are complex, difficult to evaluate and are based on a number of simplified assumptions that do not enable one to describe the process satisfactorily. Thermal action of EDM process affects the surface integrity of a machined component. The first step in the prediction of thermal stresses analysis of temperature distribution. Then thermal stresses due to the non-uniform temperature distribution can be analyzed for finding

the thermal residual stresses in the work piece [22, 30]. EDM of cobalt-bonded tungsten carbide (WC-Co), whose field of application is in constant growth, is carried out. Consequently, an analysis on the influence of current intensity, pulse frequency, electrode rotational speed and flushing pressure on technological variables such as surface roughness and metal removal rate (MRR) is performed, using design of experiments (DOE) and regression analysis. The use of these techniques has enabled to create the second order polynomial models, which made it possible to explain the variability associated with each of the technological variables studied [31].

1.5 Tungsten Carbide

Tungsten carbide, which is extremely hard material second to diamond, is used extensively in the manufacturing. Its machining present some of the most difficult challenges to the engineers. EDM is the only economical method to machine this extremely hard material. Tungsten is obtained from wolframite. The ore of the element is wolfram. In preparation for making tungsten carbide, it is reduced to a fine powder in a hammer or ball mill before being shifted, screened and graded. Carbide powder is produced by heating a mixture of 94 parts tungsten power and 6 parts carbon to approximately 1537° C, to carburize this mixture into tungsten carbide. Even after pressing and sintering, it cannot be used commercially, a binding agent, usually cobalt, is added to add strength. Cobalt is very hard, conductive metal and it is the most common matrix material for cemented carbides. Cobalt powder, in amount ranging from 3 to 30% by weight, is ball milled together with tungsten carbide forming very intimate blend. A high percentage of cobalt will increase the material strength while reducing its hardness. Decreasing the cobalt content has opposite effect [31].

Small amount of paraffin is added to the powder mix to help hold the mixture together when it is pressed into shape and to act as a lubricant to aid pressing and reduce wear of compacting dies. Tungsten carbide is very important material produced by powder metallurgy largely used for tool material, die-casting, machine parts, aeronautics industry, automobile industry, jewelry industry, surgical instrument etc. because of its distinctive properties like high hardness, wear resistance, strength, high melting point etc. To cobalt matrix that holds the tungsten particles in place has greater conductivity than tungsten. In addition, there is large difference in their melting temperatures; Cobalt melts at approximately 1480°C while the tungsten melts at approximately 3370°C. This material can be machined conveniently by EDM process [32]. The spark tends to flow around the tungsten particles and strikes the less resilient cobalt binder. This can leave a surface of

partially melted tungsten particles bounded loosely by an insufficient amount of cobalt binder. When EDMing carbide, the most efficient part of the EDM cycle is the initial impact of the spark which result in the vaporization.

The part EDMed with the oil dielectric will not experience any electrolytic damage but instead will become more susceptible to thermal damage and micro-cracking. This is primarily due to to the heat insulating effects of the oil and the carbon rich environment of the spark gap. The high concentrations of the carbon trapped within the re-melted material can make the EDMed surface much harder and more brittle. Therefore, the potential for the thermal damage is much higher when using oil for the dielectric.

1.6 Surface Morphology

It is the science of the form and structure of material. The surface morphology of the spark eroded surface can be studied through the following:

- Surface finish
- Structural change in the surface

1.6.1 Surface Characteristic

EDM machined surfaces generally have a matt appearance covered by shallow craters globules of debris and pock marks formed by entrapped gases escaping from the re-deposited material. In general, at low discharge energy, the craters are shallow and the density of global appendages and pockmarks is low. Whereas at high energy, the craters are deeper and global the appendages are most evident. Another common feature on EDMed surface is the abundance of cracks, especially at high discharge energies. These cracks are formed as a result of the exceedingly high thermal stresses prevailing at the specimen surface as it was cooled at faster rate after charge.

1.6.2 Surface Microstructure

The microstructure of an EDMed surface is complex and generally differs remarkably from that of the parent metal. Previous studies by various researchers have shown that under the extreme condition of the discharge, both the work piece and the tool material have locally melted and the effect of dielectric cracking during the process. Alloying takes place not only

between the electrode materials but also with the pyrolysis product of the dielectric. This highly alloyed metal is then cooled at an extremely fast rate to room temperature.

In addition to the molten surface the underlying metal has been subjected to a very sharp temperature gradient. The exact profile of the temperature gradient depends on the electrode materials, the dielectric and the actual discharge condition. Complex phase transformation has been reported in this heat affected layer, especially in ferrous alloys where the micro-structure is known to depend sensitively on the condition of the heat treatment [33, 34]. According to Rebelo et al. [28] and Lee et al. [35] residual stress within the EDM surface is the result of phase transformation of the metal and the high temperature gradient established during the process.

Generally, three distinct layers can be identified in the micro-structures of the surface. The outer most layer an intermediate layer and the unaffected parent metal. It has been also found that micro hardness increases with increase of thermal conductivity.

1.7 The present state of research of EDM processes

The EDM has been a very fast growing manufacturing process and demand for optimization of its output parameters has been a matter of serious concern for the researchers. EDM research carried out by recent researchers include ultrasonic aided EDM, dry EDM machining, EDM with powder additives, EDM in water and EDM in gas. Various process modeling techniques for predicting EDM performance have also been developed. These developments employ novel techniques like use of ultrasonic vibration and powder additives, gas and water as medium to take care of high efficiency as well environmental factor. Mathematical models have been used for validating and predicting EDM performance. Below a brief description is presented to highlight the efforts of researchers and reflect the current trends in EDM research.

1.7.1 Ultrasonic Aided EDM

The study of the effects of ultrasonic vibration on the EDM electrode has been undertaken since mid 1980s. The higher efficiency gained by the use of ultrasonic vibration is mainly attributed to enhanced dielectric circulation which facilitates the debris removal and the creation of a large pressure change between the electrode and work piece, resulting in enhancement of molten metal ejection from the surface of the work piece[12].

Ultrasonic vibration aided EDM is suitable to produce deep and small holes. Cu is most frequently selected as the tool electrode either in gas machining or in dielectric machining. This may be due to the characteristics of the material which is stable under spark conditions. The range of the ultrasonic frequency used during the experiment is between 17 and 25 kHz. Most of the researchers have evaluated the performance of steel based work piece materials being widely used in industries.

Fig. 1.5 shows the progress of the method in combining ultrasonic vibrations with EDM from year 1995 to 2006 [12]. The method gained popularity from year 2003 and continues being developed till date.

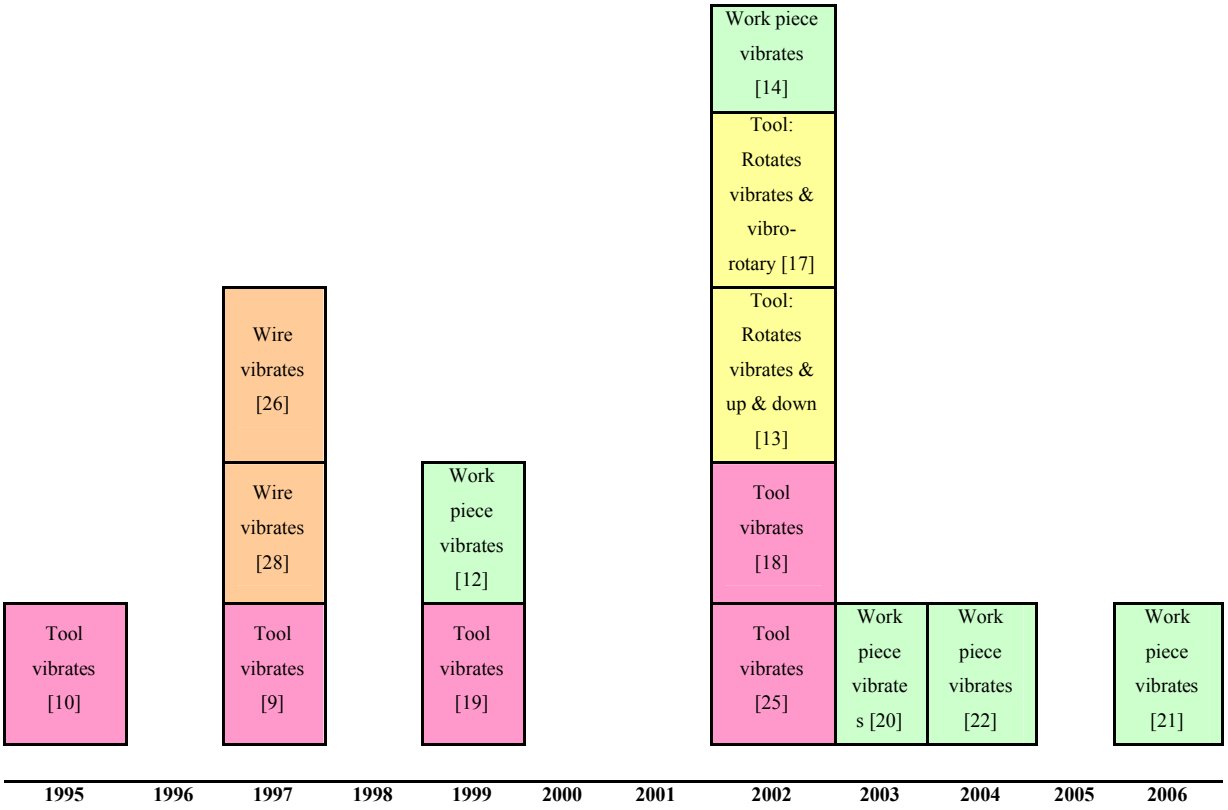

Fig. 1.5: Progress of method in combining ultrasonic vibration with EDM from 1995 to 2006 [12]

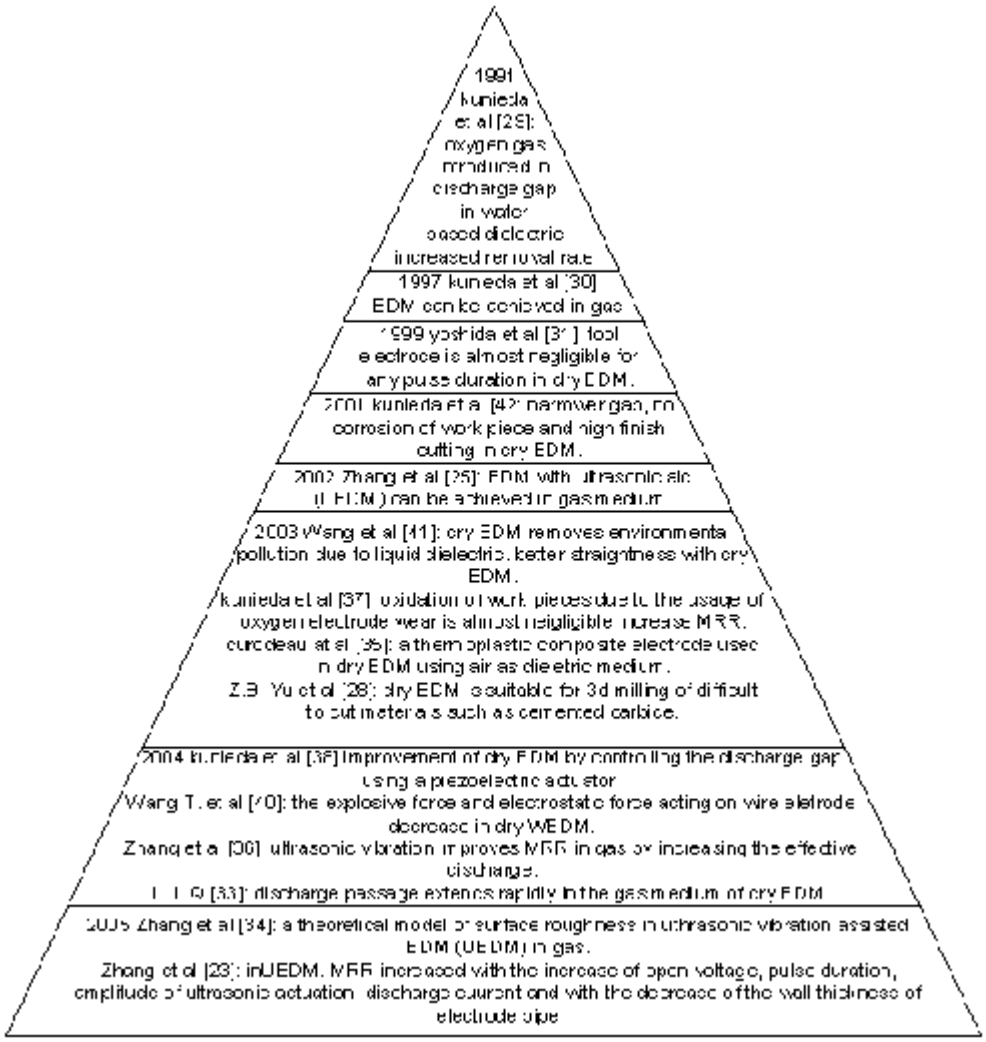

Fig. 1.6: Progress in dry EDM research*[12]

*References given in the fig are as per source

1.7.2 Dry Machining

Sequential growth of dry EDM is shown in Fig1.6 In dry EDM, tool electrode is formed as a thin walled pipe. High-pressure gas or air is supplied through the pipe. The role of the gas is to remove debris from the gap and to cool the inter electrode gap. Fig. 1.7 shows the principle of dry EDM. The technique was developed to decrease the pollution caused by the use of liquid dielectric which leads to production of vapour during machining as well as to manage the waste economically. The researchers from Japan and China made major contribution to the progress of research in this area. The characteristics of dry EDM as listed by Kunieda [36] are:

1. The electrode wear is negligible for any pulse duration.
2. The processing reaction force is much smaller than in conventional EDM.

3. It is possible to change supply of gas according to different applications.
4. The residual stress is small since the melting re-solidification layer is thin.
5. Working gap is narrower than in conventional EDM.
6. The process is possible in vacuum condition as long as there is gas flow.
7. The machine structure can be made compact since no working basin, fluid tank and fluid circulation system are needed.

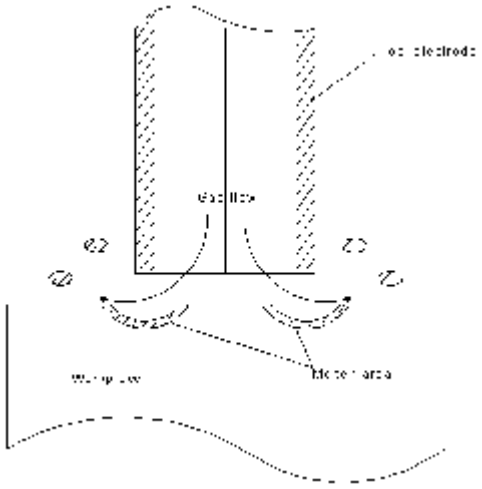

Fig. 1.7: The principle of dry EDM [Q.H. Zhang, 2002]

This technique has focused more on enhancement of the MRR. The MRR in this case is lower as compared to conventional machining. Fig. 4 shows the proportion of typical research studies conducted in this area. It can be seen that dry EDM can be applied to EDM, UEDM, WEDM, EDM Milling and a few other techniques. Fig 5 & 6 show the removal of material from work piece and anode respectively. The results shown are self expla*n*atory.

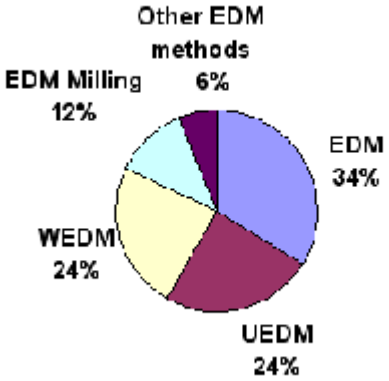

Fig. 1.8: Research studies conducted in dry EDM [12]*.

*References given in the fig are as per source

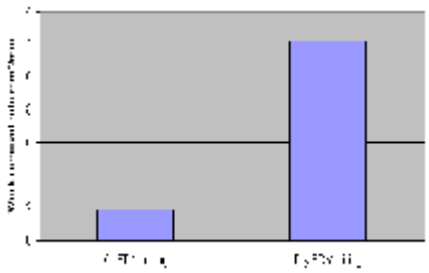

Fig. 1.9: Work piece removal rate [Z.B. Zu, 2004]

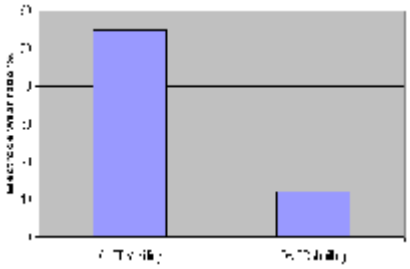

Fig. 1.10: Electrode wears [Z.B. Zu, 2004]

A suitable abrasive powder is mixed into the dielectric fluid. The hybrid material removal process is called Powder Mixed EDM (PMEDM) where it works at low pulse energy [12] and it significantly affects the performance of EDM process. Electrically conductive powder reduces the insulating strength of the dielectric fluid and increases the spark gap between the tool and work piece. EDM process becomes more stable and improves machining efficiency, MRR and Surface Quality (SQ). However, most studies were conducted to evaluate the surface finish since the process can provide mirror surface finish which is a challenging issue in EDM. The characteristics of the powder such as the size, type and concentration influence the dielectric performance.

The earliest paper mentioning about PMEDM was published in 1981[12]. A number of researchers have worked in this area and investigated various types of powders with different concentrations and grain sizes on different types of work pieces. The effect of adding powder in dielectric was studied and many researchers have shown that it improves surface finish to a great extent. It is observed that the addition of copper powder makes almost no difference to the pure kerosene dielectric. From the collected literature a bar chart is prepared to show the type of powder used and to compare the number of works dealing with each type of powder Fig. 7. It is seen that aluminum powder suspension attracted many researchers since it contributes considerably to improvement of MRR as well as the surface finish.

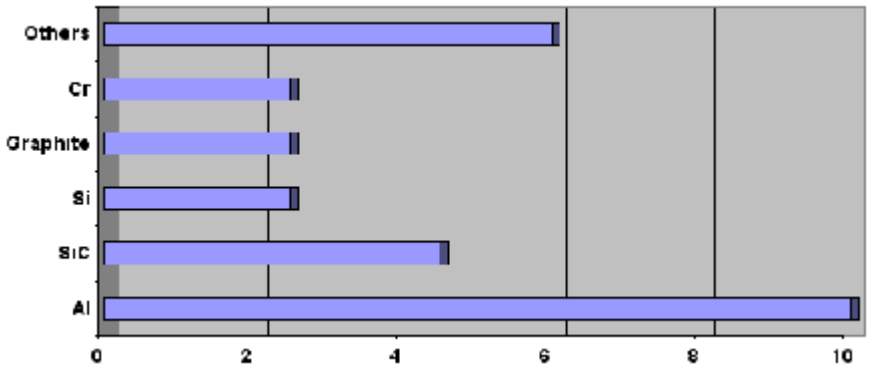

Fig. 1.11: Distribution of type of powder used based on the collected papers [12]*.

*References given in the fig are as per source

1.7.4 EDM in water

Water as dielectric has been found to be an alternative to hydrocarbon oil. The approach is adopted to promote better health and safe environment while working with EDM. This is because hydrocarbon oil such as kerosene will decompose and release harmful vapour (CO and CH_4). Research over the last 25 years has involved the use of pure water and water with additives. Jeswani [16] compared the performance of kerosene and distilled water over the pulse energy range 72-288 mJ. Machining in distilled water resulted in a higher MRR and a lower wear ratio than in kerosene when a high pulse energy range was used. In distilled water, the machining accuracy was poor but the surface finish was better. Water based dielectric can replace hydrocarbon oils since it is environmentally safe.

1.7.5 Modeling

EDM process is influenced by many input factors but it is amenable to modelling, though with difficulty. Various techniques viz. dimensional analysis, artificial neural network (ANN) and thermal modeling have been employed to predict the output of the process mainly the surface finish, tool wear and MRR. Fig 8 shows various theoretical models available in literature for simulating the input and output parameters using different concepts. These models are an effort to understand the various aspects of the EDM process and to support & validate the experimental work.

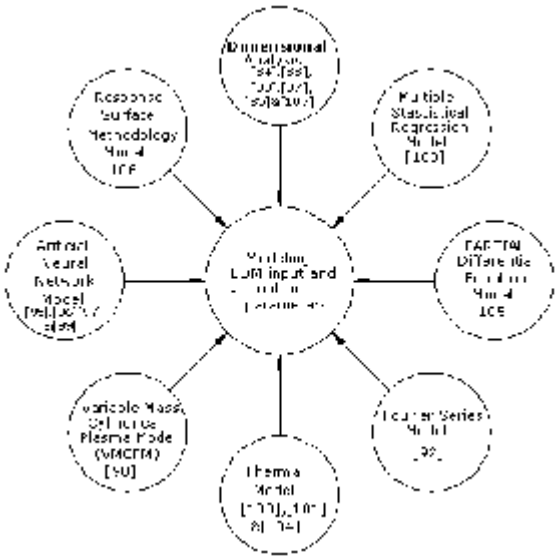

Fig. 1.12: Modelling of input and output parameters by various researchers [12]*.

*References given in the fig are as per source

1.8 Back ground of the problem

Though the EDM process by now is a well established machining option for manufacturing geometrically complex and very hard material parts that are extremely difficult to machine by conventional process yet there are several under explored or partially attempted areas. Despite the fact this process has several advantages like non contact machining, no direct mechanical stresses and no chatter and vibration problems its commercial exploitation in machining of material like tungsten carbide is still problematic, particularly at high machining rates. It is a highly complex process which has defied complete understanding till date. There are several divergent views and theories which have been put forward by different researchers to explain its mechanism of material removal and parameters affecting the process satisfactorily. Up till now there is virtually no universal or single unified theory.

The process requires a detailed study, both by experimentation and mathematical modeling under various operating conditions in order to optimize the process outputs. Most of the work has been reported on machining of steel and steel alloys and non ferrous material etc. using graphite, copper, brass, alumium as tool material. It has found application in mould dies, aeronautical and surgical industries.

The author has been involved in commercial application of Electric discharge machining for more than two decades in its various forms like die sinking, wire cut, and EDM drilling including the CNC versions thereof. Over the years several practical problems were faced,

particularly while trying to achieve high removal rate for forging dies and excellent machining finish for moulds where mirror finish was the requirement. Another major problem faced in tungsten carbide was the premature failure of dies. To address this problem in depth, practical study was under taken and available literature was surveyed on EDM of Tungsten Carbide. It was found that little work was done in this area. The available research papers were studied to have better grasp of the problem.

In the above context it was found essential that a clear and better understanding of the EDM process in terms of process elements, parameters, energy input and output be undertaken. The work of several researchers over the past couple of decade was examined to comprehend experimental and theoretical aspects of investigations previously carried out; based on which the frame work of the study was evolved.

1.9 Organizing the Thesis

The write up of the thesis has been divided into six chapters: (1) Introduction (II) Literature Review (III) EDMing of WC-Co and Effect of Processing Parameters (IV) Surface Cracks on EDMed Tungsten Carbide Cermet (V) Energy Distribution in EDM process (VI) Conclusion. At the end, all the references of research work in the related area, which were consulted and utilized for the interpretations of the results, have been listed under the heading "Reference". Further the list of publications, conference papers and invited lectures, which are related to present study, have also been included.

In this research, Material Removal Rate (MRR), Energy Distribution and Surface Integrity have been investigated to optimize the Electrical Discharge Machining (EDM) process. A comprehensive mathematical model has been developed and validated by experiments using copper, tungsten and graphite as tool electrodes. Experimental work has been conducted on tungsten carbide, using commercial grade of kerosene as dielectric fluid. Statistical methods also have been used to test the confidence level of the data collected through the experiments.

Chapter 2

LITERATURE REVIEW

Overview

Extensive research in the field of EDM has led to better understanding of the phenomenon of metal removal rate by employing high energy electrical impulses. The key interest of scientists and technologists has been the development of efficient generators leading to higher rates of metal removal with excellent surface finish and low tool wear. This has lead to development of EDM machines with numerical and adaptive controls. This chapter has been divided in six different sections namely. EDM Process, factors effecting machining rate, energy distribution and material parameters and surface integrity in EDM each duly reference. Accordingly, the literature review has been carried out. In each highest and organise section has been studied and attempt has been made to club the work of different authors working on the same or similar array. The literature survey indicates that not much work has been carried out on machining of tungsten carbide. Here, work done on other related materials has been considered and compared with the tungsten carbide for better understanding and process improvement.

2.1 Introduction

Technological developments have led to an increased use of high strength, high hardness materials in manufacturing industries. Selection of correct machining conditions, in the majority of manufacturing processes is the most important aspect to be taken into consideration while machining a component. In the machining of above type of materials, traditional manufacturing processes are being increasingly replaced by more advanced techniques such as electro-discharge machining (EDM). Extensive research in this field has led to better understanding of the phenomenon of metal removal with the help of electrical impulses. The researchers have concentrated on one or more machining aspects of the process different types of steels for more than five decades and contributed to the knowhow and technology of EDM process. Also studies have also been carried in the areas where influence of the most important machining parameters for machining of composites like tungsten carbide (WC-Co), conductive ceramics needed to be explained critically. Since the machining parameters like pulse current, pulse duration, type of flushing influence the surface characteristics differently in composites so their in depth study is very important [1].

The key interest of scientists and technologist has been development of efficient pulse generators leading to higher rates of metal removal with excellent surface finish and low tool wear. This has lead to development of EDM machines with numerical and adaptive controls [37-39]. In addition, a number of electrically assisted erosion processes e.g., electric discharge wire cutting, electro erosion grinding and electric discharge electro-chemical machining etc. have also been developed and used widely in industrial applications.

Due to the rapid heating and cooling effects induced by the EDM process, a thermally affected layer formed on the surface of the component. The structure of this layer is quite different from the parent material. Although it is beneficial in terms of enhanced abrasion and erosion resistance but the defects within it such as voids, cracks, induced stresses etc. cause an overall deterioration of the component's mechanical properties[37]. There has been continuing development of miniaturized, lighter and higher density products in a wide variety of fields, including micro components for cellular phones and semiconductors. This has led to the active research and development of advanced machining technologies for these micro components. Takashi Endo et al. [38] studied vibration assisted micro EDM and remarkable reduction of the machining time by applying vibration to the tool electrode was reported. It was also confirmed that vibration assisted micro EDM will achieve the machining of complicated shapes as well as high speed machining of small components.

Materials exhibiting electric conductivity can be machined in complicated shapes by EDM

with high accuracy regardless of their hardness. Especially, micro-EDM is applied for the machining of holes, such as nozzles, orifices and slit and dies for micro components for dimensions ranging from few micrometers to hundreds of micrometers as shown in Fig. 2.1 [40].

Fig. 2.1: Showing small angular holes of a turbine component

This chapter carries reviews of the published literature. These are relevant to the topic of the thesis have been presented under the following three heads:

- EDM Process
- Energy Distribution
- Surface Integrity

2.2 EDM Process

EDM Process consists of material removal through electric discharge. The phenomenon of metal removal by electrical discharges is quite complex to analyze. This is because of the fact that a number of interdependent variables have a controlling effect on the process. Till date, there is no established mechanism to describe the metal erosion process. Not even single conclusive theory has been established for this complex machining process. However, empirical evidences suggest the following events that occur during EDM. The applied voltage creates an ionized channel between the nearest points of the work piece and the electrode in the initial stage. In the next stage, the actual discharge takes place with a heavy flow of current and the resistance of the ionized channel gradually decreases. The high intensity of current continues to further ionize the channel and a powerful magnetic field is generated. This magnetic field compresses the ionized channel and results in localized heating.

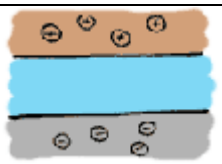	Stage-1 The electrode approaches the workpiece. Both the electrode and workpiece are energized
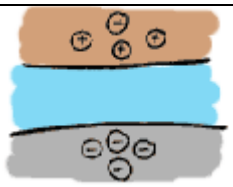	Stage-2 Concentration of the electrical field towards the point where the space between the electrode and workpiece is smallest
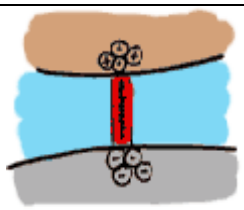	Stage-3 Creation of an ionized channel between the electrode and workpiece
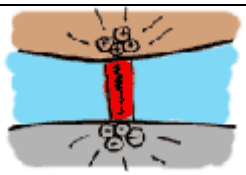	Stage-4 Breakdown of the spark. The workpiece material melts locally and disintegrates. The electrode only wears out slightly
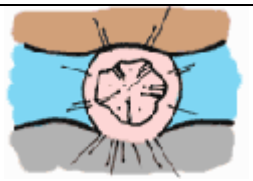	Stage-5 The current is cut off, causing implosion of the spark
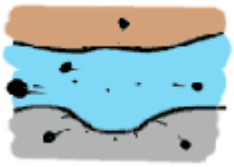	Stage-6 Evacuation of the metallic particles by flushing with dielectric

Fig. 2.2: Different stages of EDM Process

Even with sparks of very short duration, the temperature of the electrode can be raised locally to more than the normal boiling point of work piece material due to transformation of the kinetic energy of electrons into heat. This mechanism of EDM process is illustrated in Fig. 2.2.

Although most of EDM machines available today have some kind of process control, still selecting and maintaining optimum settings is an extremely difficult job. The lack of data on conventional as well as advanced materials, precise gap monitoring devices, and an adaptive control strategy that accounts for the time variant and stochastic nature of the process are the main obstacles toward achieving the ultimate goal of unmanned EDM operation. A few

attempts related to EDM machining and surface integrity data, thermal modeling and adaptive control have been made. When harmful or unproductive machining takes place i.e. arcs, short circuits or open circuits, the controller provides so called "test pulses" with shorter pulse on-time and much longer interval time than the machine pulse as selected by the operator. These low energy pulses allow the gap to restart machining.

However, as far as machining conditions, tool and work piece materials are concerned, most of these attempts are limited in scope. A comprehensive investigation into the surface generating mechanism is one of several essential steps for exploring and developing the overall knowledge and technology base of the EDM process.

The existing hypotheses proposed by several researchers are all based on a number of conflicting assumptions mainly due to major differences in the experimental conditions employed by them. Considering all aspects one can summarise that the mechanism of metal removal in EDM should be studied under the following headings:

- Electro mechanical theory
- Thermal theory
- Thermal mechanical theory

This classification, though useful, has certain difficulties in interpretation of the results and hence is considered to be unsatisfactory. However, this approach is useful to understand the process. Basically the high energy density erodes a part of material from both the electrode and the work piece by locally melting and vaporizing and this is the dominant erosion process [41].

2.2.1 Electro-mechanical theory

Williams [42] has attributed metal erosion in EDM to electric field forces, which arise due to the presence of extremely high current densities in the vicinity of the areas of spark impingement. He calculated the magnitude of these forces and found them to be much higher than the yield point of the work material. This according to him is responsible for the fracture and wear of the exposed area. In subsequent works Williams demonstrated that the work piece (anode) erosion is closely related to its tensile strength.

The electro-mechanical theory of Williams [42]was also supported by Rudorff [43] who found no evidence of melting of the electrode surface during EDM. In other reporting also [44, 45], it is agreed that for very short duration pulses (<2 μs) some material indeed may be removed by mechanical fracture of the electrode. However, the researchers describe that for pulses greater than 2 μs duration, the erosion phenomenon is basically thermal in nature. The

over whelming evidence is provided by high speed photographic records of metal erosion dynamics in EDM. Fuzhu Han et al. [46] described the development of parallel spark EDM method. In the discharge circuit, the electrode is divided into multiple electrodes, each of which is electrically insulated and connected to the pulse generator through a diode. A capacitor is inserted parallel to each discharge gap between each electrode and work piece (here the work piece is common for each electrode). Compared with conventional EDM in which only a singular discharge can be generated for each pulse, multiple discharges can be generated for each pulse in parallel sparks, but the Machining speed and surface roughness can also be improved with parallel spark EDM.

To generate discharges that occur at two or more places, Chen et al. [47] developed a multi-circuit system using a number of discharge circuits and corresponding number of electrodes in the circuit. It was reported that this method can improve the machining speed. However, the demerit of this system is that it needs a number of discharge circuits, which results in a high making cost when the size of the electrode is larger.

Better correlation of eroded crater volume with thermal properties of the electrode material [48,49] and also the evidences of melting and heat affected zone as observed in photomicrographs published by several researchers [42, 50, 51] confirm beyond doubt that the electrode erosion is primarily electro thermal in nature.

2.2.2 Thermal Theory

The temperature of the electrode at the point of spark impingement is instantaneously raised to an extremely high value (about 12000ºC) due to high temperature of the plasma channel. This results in some metal erosion from the electrode. Thermal nature of the EDM process has been discussed by several investigators [52]. However, there are certain conflicting reports regarding the nature of the discharge column. Some believe that the discharges are multi channeled whereas; others maintain that it occurs in a single channel [53, 54]. In order to simplify the analysis, metal removal in these studies has been considered as single channel discharge only. According to thermal theory of metal erosion, material from the electrodes is predominantly removed due to evaporation [9, 55, and 56]. This, however, is in contradiction with experimental observation of others [57, 58]. The distribution of the erosion products in the electrode gap after being ejected from the discharge zone has been studied using trace pattern analysis method (a technique where traces of the discharge are recorded on special photographic plates under controlled conditions) by Willey [58]. By analyzed the debris produced during EDM, under Scanning Electron Microscope (SEM) he

concluded that in EDM, some metal is removed in vapor and even solid phase but the bulk is ejected in the liquid form from the molten pool. He also determined the ratios of vapors and liquid phases for various metals and for different working conditions.

2.2.3 Thermo-mechanical Theory

Deng [53] experimentally determined the magnitudes of the electrodynamics and non-electrodynamics (mainly thermal) forces acting over the electrode during the discharge and found that, in some cases, these forces may be comparable. He further reported that electrodynamic forces are a function of the pulse current and act only during the duration of the discharge, whereas the forces arising due to non electrodynamic effects act for a much longer period.

The thermo-mechanical theory for metal erosion which is applicable to majority of the cases, suggests that during machining, the metal is partly removed due to vaporization and tearing off the grains either completely or partially followed by melting. This pool of liquid gets ejected out due to combined action of a number of forces viz., electromagnetic and electrostatic forces arising due to the presence of electric field accompanying the electric discharge; hydrodynamics forces due to the flow of dielectric; mechanical pressure waves due to explosion of gas bubbles; and gas pressure waves due to vaporization of the dielectric and gases liberated in the molten metal [50, 59-61].

Zolotych [62] using high speed photography observed that the ejection of molten metal from the molten pool is a continuous process till the end of the discharge and is accompanied by the evolution of the gases. These observations were largely confirmed by Williams [42]. However, their interpretations of the observed phenomenon are different. Zolotych [62] attributes this to violent boiling of the molten metal in the pool. This drops down further under pressure of gas bubbles and collapses with the end of discharge channel of plasma. On the other hand, according to Williams [42], when vapour bubble collapses at the end of the discharge, liquid jets impinge upon the crater from all directions causing metal removal. These somewhat different conclusions were attributed to the fact that his experiments were performed with a pulse of 15 μs duration whereas the pulse duration used by Zolotych [62] was much longer.

In a recent and exhaustive physico-mathematical study of the EDM process, Snoyes and Dijck [61, 63] concluded that electrostatic forces play a significant role in metal removal during the early stages only (up to 1 μs duration of the spark), but immediately after the end of the pulse duration, boiling of a part of the molten metal in the pool is mainly responsible

for its evolution. Analytical computation of the metal removal based upon this assumption has been shown to be in fairly good agreement with the experimental data.

On the basis of the findings presented in the above survey it can be concluded that metal erosion in EDM depends upon the energy level and duration of the discharge under particular circumstances. Some erosion may occur due to electrostatic forces [64] or mechanical impacts of the particles but in majority of the cases it is predominantly thermally controlled.

2.3 Surface Integrity in EDM

Each successive pulse discharge in EDM produces a distinct crater on the surface of work piece and the tool electrode. The resulting surface consists of a series of randomly distributed overlapping craters with depth to diameter ratio varying from 5 to 50 μm.

The quality of surface largely depends on the pulse energy and pulse duration. For small energy pulses (tenths of a joule) surface finish comparable to that obtained in turning, planning or milling operations may be obtained [41]. An interesting feature of EDM surface is that unlike conventionally machined surfaces, it has no definite direction of layer. This gives the surface a 'Matte' appearance, and better functional properties due to retention of surface oil film.

2.3.1 Surface Deformation

Immediately at the end of the discharge in EDM, the molten metal left over the crater is still at a sufficiently high temperature. This is cooled rapidly by the dielectric leading to epitaxial solidification of the molten layer onto the substrate. High stresses produced due to contraction on cooling, and shock waves produced due to electric discharge can cause severe slip, twining, and cleavage in the affected layer depending upon the machining conditions employed. These defects accumulate at the grain boundaries and can lead to surface cracking. Even in ductile materials practically all spark-machined surfaces show some cracking and presence of high residual stresses. Nevertheless, the severity of damage may be reduced by a judicious choice of machining parameters.

2.3.2 Metallurgical Changes during EDM Process

The surface integrity of a component describes the topological, mechanical, metallurgical and chemical conditions of the surface region which includes the surface and subsurface structure. After spark machining of steel, if an etched cross-section of the machined surface is examined it would show three distinct zones: (a) a white surface layer (b) a heat-affected

zone and (c) the unaffected parent metal [50, 51]. The top surface layer is found enriched with carbon picked up from the dielectric and electrode material. When etched, it shows a columnar structure indicating that its origin is from solidification from the molten state. Below this, and extending up to 20 times the thickness of the white layer is a metallurgical and chemically affected region which is mainly due to thermal release and diffusion of material from the molten layer.

The re-solidified layer frequently undergoes unusual phase changes caused mainly by the reaction products derived due to cracking of the dielectric, and due to alloying of the work material layer with the transferred tool material [54, 65- 67]. In general, pure non-ferrous materials exhibit few phase changes, whereas, ferrous pure iron, carbon steels, and alloy steels exhibit changes of increasing complexity.

The dielectric appears to be a major factor in determining the extent of phase changes. Several authors have studied the surface deposition and diffusion of tool material on the machined surfaces [3, 62, 68]. They observed that essentially the changes in chemical composition remain confined to the re-solidified layer and also up to very thin zone below it. While machining tool steel with copper electrodes, it was found that up to 10% copper is concentrated in a zone of 5μm depth of the work material and this concentration decreases sharply beyond 20 μm depth. It has further been reported [68] that materials with poor thermal conductivity show lower depth of diffusion, which, however, increases as higher energy pulses are employed.

These changes in chemical composition of the work surface layer, mainly caused by the absorption of carbon from decomposed dielectric and the transfer of material from the tool electrode, can lead to considerable changes in the physical properties of the material. Increase in hardness values has been reported in several cases [35, 36, and 69]. However, the hardness falls rapidly at depth in excess of the thickness of the re-solidified layer [44, 51].

2.3.3. Residual Stresses in EDM

EDM generates residual stresses, these being mainly due to the non homogeneity of heat flow and metallurgical transformations [36-40]. Investigation of the residual stresses of EDMed components revealed their inature is tensile. An increase of their magnitude is observed at the surface layers with increasing pulse energy. Since the integrity of the EDM surface is degraded by the unstable arcing which always occurs during the machining process, the quality of an EDM product is evaluated in terms of surface integrity, which is

characterized by the surface roughness, presence of surface cracks, and the residual stresses. The roughness of the EDM surface is associated with the distribution of the craters formed by the electric sparks [35]. Kunieda et al. [36] have reported that only 15% of the molten work piece material is flushed away by the dielectric. The remaining material re-solidifies on the EDM surface due to fast cooling rate generated by the dielectric. This recast layer is referred to as the white layer since it is very difficult to etch and looks white and when observed under an optical microscope. It has been suggested previously that the electric sparks generated during machining decompose the kerosene dielectric, and the resulting carbon penetrates into the machined surface [41, 42]. High cooling rates of the molten metal left over in the crater, combined with shrinkage of the re-solidifying layer can introduce considerably large tensile stresses in the work surface. These residual stresses are essentially confined to the immediate vicinity of the top surface area of the machined workpiece and fall off rapidly with depth below the top surface to a relatively low value further, at certain distance below the surface the nature of the stress changes over to compressive [37,38,51]. Consequently, an inspection of the white layer reveals that it is densely infiltrated with carbon elements [26, 27]. The formation of surface cracks can be attributed to the differentials of contraction stress within the white layer i.e. molten material with a higher carbon ingression contracts to a greater degree than the remaining molten material on the EDM surface and when the contraction stress exceeds the material's ultimate tensile stress of the material, cracks will form. According to Rebelo et al. [28] residual stress within the EDM surface is the result of phase transformation of the metal and the high temperature gradient established during the EDM process. In terms of mechanical properties of the white layer, it has high hardness and good wear resistance due to the quenching effects of the dielectric and the carbon penetration. However, the cracks and residual stress which usually appear in this brittle white layer may lead to the failure of the EDM product, particularly under conditions of fatigue and impact loading. If the quality of the EDM product is to be improved, it is essential to develop a thorough understanding of the relationship between the EDM machining parameters and the resulting surface roughness, white layer, surface cracks and residual stress [31]. However, the surface integrity of an EDM product is dependent on the electrode material. Hence it is worthwhile exploring the EDM surface integrity associated with the use of a tungsten carbide as work piece. Since the ASTM Standard E837 for residual stress measurement [79-80] specifies that the diameter of the drilled hole should be in the range of 1.5-2.6 mm. a cylindrical electrode was used with diameter of 1.5 mm for study by the above researches. The Hole-Drilling Strain Gage Method is a semi-destructive measurement method which was first proposed by Mathar [82] in 1934. This technique

involves drilling a hole in the center of a rosette strain gage attached to the surface of the work piece. According to elastic mechanics theory, the stress within a component can be calculated by measuring the stain released on the specimen surface as the hole is drilled vertically in to the work piece. Following substantial investigation and calibration this method is now a mature technique which has been widely applied throughout industry due to its intrinsic advantages of a smaller drilled hole and its non interference with the work piece functionality. This method has been quoted in ASTM Standard E837 since 1981. The electric-resistance rosette gage is first attached to the surface of non stressed AISI 1045 work piece. The stain gage used throughout the experiment was the TEA-06-062E device manufactured by Measurements Group Inc. The relieved strain caused by the drilling operation is detected by the rosette strain gage and displayed on a P-3500 Strain Indicator (Measurements Group Inc). The three values of measured stain i.e. ε_1, ε_2 and ε_3, are then substituted into Eq. (1) in order to calculate the minimum and maximum principal residual stresses within the work piece.

$$\sigma_{min},\sigma_{max} = \frac{\varepsilon_3+\varepsilon_1}{4A^-} \pm \frac{\sqrt{(\varepsilon_3-\varepsilon_1)^2(\varepsilon_3+\varepsilon_1-2\varepsilon_2)^2}}{4B^-} \quad (2.1)$$

Where $\overline{A}$ and $\overline{B}$ are calibration coefficients for, the area effect of the strain gage then finite-element calculation are used to determine the values of these calibration coefficients. The numerical solutions of $\overline{A}$ and $\overline{B}$ can be expressed as:

$$\overline{A} = -\frac{1+v}{2E} \times \overline{a} \quad (2.2a)$$

$$\overline{B} = -\frac{1}{2E} \times \overline{b} \quad (2.2b)$$

Where $\overline{a}$ and $\overline{b}$ are dimensionless coefficients, E is Young's Modulus, and v is Poisson's ratio. The values of the dimensionless coefficients $\overline{a}$ and $\overline{b}$ are virtually material-independent and are correct to within 1% for a Poisson's ratio between 0.28 and 0.33. The exact values of the two coefficients depend upon the ratio of Do/D and are available from in ASTM Standard E837 [61]. If the material properties E and v are known, the calibration coefficients $\overline{A}$ and $\overline{B}$ are given by Equations (2a) and (2b) respectively.

Opitz [78] has reported a high degree of carburization of ferrous metals when machined in

kerosene. Titanium, which is a highly reactive metal, forms a carbon rich layer in kerosene, but when machined in distilled water, TiO_2 is normally produced [51].

Aleksandrov [71], and Crookall and Khor [72] made quantitative measurements of the magnitude of the residual stresses in EDM surfaces and found that the re-solidified layer is stressed close to ultimate tensile stress of the base metal. No appreciable difference in residual stress pattern in the work surface was observed when water and kerosene were used as dielectrics.

Since the surface layer of a workpiece machined by EDM is brittle and has low strength, the work surfaces after machining have often been found to exhibit a network of micro-cracks, sometimes penetrating into the parent material [39-40]. The depth of this surface damage depends upon the parameters of the discharge (pulse duration playing a more important role) and may be between 2.5 and 5 times the roughness (R_a) value of the surface [69] for steel (1% carbon). Others [39] mention it to be 1.5 to 2.0 times the thickness of the molten zone.

2.3.4 Effect of EDM on Mechanical Properties of Work Material

The presence of high surface residual stresses and micro cracks in components produced by EDM have a significant effect on the properties of the work material such as, fatigue life, and stress corrosion behavior. Several investigators have reported a significant decrease in fatigue strength of the spark machined components [39, 42 and 69]. Aleksandrov [71] has quote a 10-30% reduction in fatigue strength of alloy steel parts when machined by EDM, whereas a 60% decrease in endurance limit in case of Inconel 718. Aleksandrov [71] further claimed that even finish machining by EDM can also prove to be detrimental to fatigue strength. Barash [41, 82] has reported considerable lowering of the fatigue and impact strengths of tool steel specimen when processed by EDM.

Some improvement in fatigue life of the machined specimen is possible by imparting suitable heat treatment to the components machined by this process. However, if surface cracks are present, the damage is of permanent nature and the affected zone must be removed by lapping, polishing or by some other suitable means [15,83]. Bhattacharya et al. [84] correlated the spark gap with size of the damaged zone and recommended that removal of a layer equivalent to half the gap width will eliminate the entired damaged zone.

2.4 Factors Effecting Machining Rate

Based on current knowledge, the main inconvenience when applying the technology involved in die-sinking electrical discharge machining for ceramic materials is the electrical

conductivity of these materials, the limits being fixed for the case of electrical resistivity of between 100 and 300 Ω cm. Machining rate in EDM depends on a large number of variables, which vary oftenly and cannot be controlled or quantified. The number of factors thought to be significant is formidable but it is quite possible that many of these quantities may have very little or no significant effect on the process and might possibly be ignored [85].

2.4.1 Generators for Use in EDM

There appears to be a very large difference between various electric discharge machining systems especially as regards to their erosion rates, tool wear, machining accuracy, cost, and power consumption etc. The "Relaxation" of RC circuit employed during the earlier investigations on spark machining is still widely used, especially in the range of low energy sparks (0.5 μJ on 0.1μs) or when very fine finish is desired. It is cheap, simple and robust but has its own limitations such as, low efficiency and oscillating nature of discharge. These results in low metal removal rates and high tool wear respectively [57].

The charging efficiency of an RC circuit may be improved by adding inductors in the circuit (RCL or RCLL circuit). This leads to increased erosion rates (Maximum of 300mm^3/mm) with low relative tool wear (5%-30%) but this probably causes increased damage to the work. Diodes in the discharge circuits have been used to minimize the discharge oscillations but they are not wholly effective owing, at least in part, to self-capacitance. The rotary generators provide long duration pulses as compared to RC circuits [58]. The generators are capable of much higher erosion rates and are generally used for fast rough cutting only. For fine finishing the R-C generators are still preferred.

In engineering applications, however, the relaxation and rotary machines have been largely replaced by the transistorized (controlled pulse) generators. The transistorized generators are particularly effective in roughing and medium fine finishing and yield much lower tool wear than relaxation or rotary machines and can achieve higher cutting rates for a given surface finish. Currents ranging from 1A to 100A and pulse times varying between 2μs and 2000 μs are normally possible on such machines. However, generators with 600 A to 700 A output current and capable of giving erosion rates of 5500 mm^3/min are also available. These generators allow independent control on pulse 'ON' and 'OFF' times and provide unidirectional rectangular wave pulses to the electrodes and normally operate on two different models: (i) Fixed Frequency (voltage pulse timing), and (ii) variable frequency (current pulse timing). In the former, the effect of increasing ignition delay is to reduce the current pulse duration. In the latter it is the current pulse duration, which is fixed. The fixed

pulse energy is supplied in each cycle, hence metal removal per pulse is normally constant, and the effect of increase in ignition delay is therefore to reduce the pulse frequency. Considering the overall performance pulse generators allow faster MRR, low tool wear and better surface quality. Recently, use of bipulse and programmable waveform generators, capable of generating pulses other than rectangular, have also been reported. Use of trapezoidal pulses has been shown to result into high erosion rates and low tool wear [68]. Apart from the type of generator used, other important variables controlling erosion rate are the pulse parameters, work shape, electrode material properties and the machining fluid [42, 48].

2.4.2 Pulse Parameters

Pulse parameters are significant in determining the erosion rates of the given work material. An increase in working voltage, pulse current and pulse 'ON' time generally results in higher metal removal rates(MRR). However, for the given configuration these variables invariably show an optimum value for which MRR would be maximized. On the other hand, an increase in pulse 'OFF' time reduces the pulse duty factor and consequently lowers the machining rate [36, 66].

Dependence of machining rates on tool work polarity cannot be explained only by the material properties of the electrodes and pulse duration. It is a complex phenomenon associated with the ignition mechanism of the spark and the electrical power distribution between the cathode and anode. In R-C circuits a straight polarity (tool cathode, work-anode) is generally employed, whereas a reverse polarity (tool anode) is sometimes preferred in transistorized pulse generators. Heuvelman [37] reported a rapid fall in the REW with decreasing pulse duration while using sinusoidal waveform pulses and negative tool electrode polarity. With longer pulses, the polarity has to be altered in order to keep the electrode wear low. At the beginning of the pulse the number of electrons is larger than the number of ions; hence, the anode wears at the faster rate. At sometime, after the pulse has been switched ON the electron to ion ratio changes and the number of generated ions increase. When this happens, the cathode wears increases. In their experiments, Rajurkar et.al [87] changed the polarity of the electrodes when the ion current become predominant, and thus obtained low relative tool wear. Snoeys and Van Dijck [61, 63] calculated the ratio of electron to ion current (i_c-/i_c+) and the anode/ cathode (P_a/P_c) power distribution for two cases (Copper and Iron) for different current densities and for various cathode temperatures. They found that the power ratio (Pa/P_c) decreases with the total current density and

concluded that in general all parameters leading to a decrease in the current density would result into a reduction in the positive electrode wear [61]. As the energy density decreases with increasing pulse duration, a negative tool polarity is often recommended for use in case of relaxation generators, which normally produce high current amplitudes (100 – 1000A) and short pulse durations (0.1-50μs). Whereas, a positive tool polarity is normally recommended for pulse generators yielding smaller current amplitudes (1-1000A) and longer pulse durations (1-2000μs).

Although pulse energy and duration largely determine the machining rate, the efficiency of erosion depends on the pulse shape. In subsequent studies it has been reported that rectangular pulses are not the optimal shapes for maximum metal removal from point of view. Trapezoidal pulses with negative slopes have been found to yield higher metal removal rates [26, 42]. This has been confirmed theoretically also. However, in these experiments, high machining rate was associated with increasing tool wear, which may be undesirable in most of the practical machining situations.

2.4.3 Electrode Shape

The machining rate has also been reported to depend upon the sparking area, overall shape of the cavity to be produced, and the machining depth. It is understandable that a large machining surface would offer more possibilities of producing spark at various places. However, too large machining areas, with complicated geometry of the electrodes, or greater machining depths may reduce current densities and/ or offer resistance to efficient dielectric circulation and flushing and can sometimes lead to a drop in machining rates [42, 58].

2.4.4 Dielectric Fluids

The dielectric fluids are used to flush away the eroded particles from the gap between electrode and work piece, otherwise they can form bridges, which may cause short circuits. Such arcs can burn big holes in the work piece and the electrode. Modern spark erosion plants therefore have a built in power adaptive control system, which increases pulse spacing as soon as this happens and reduces or shuts off the power supply completely. The more thin dielectric fluid with lower surface tension can provide better ability to meet flushing requirements.

The dielectric medium greatly influences the process of electro sparking and the metal removal. Discharges in gaseous medium generate less energy and exhibit several secondary craters. Moreover, material eroded from the anode tends to adhere to the cathode. This

effect is, therefore, used for building up of worn parts and as a means of surface hardening [27, 28] On the other hand, liquid dielectrics confine the spark into a narrow channel, which helps to achieve higher current density and hence increases the erosion rate of the work material [48]. Apart from facilitating the plasma channel formation and providing insulation to the electrodes till the next discharge occurs, the dielectric also removes the heat from the electrodes and keep proper machining conditions by carrying the products of discharge (debris) away from the machining zone.

Although most of the commercially available hydrocarbons, siloxanes, alcohols and ordinary water possess the properties of a good dielectric to a greater extent but, kerosene has found widest application for fine and medium fine machining. During machining, the dielectric temperature rises and it gets contaminated with erosion debris. This may consist of re-solidified metal particles from electrodes, together with carbon rich solid particles produced due to the breakdown of the dielectric fluid during the spark. If kerosene is cooled and the solid debris is removed by settling or filtration it may be reused over a long period of time without any appreciable loss in machining efficiency [37].

2.4.5 Gap Flushing

Forced circulation of the dielectric through the discharge gap has an important influence on the efficiency of the process, particularly at greater depths of penetration where accumulation of the erosion debris and gases lead to highly irregular sparking and reduced MRR. This could also distort the work profile being produced and sometimes result into extensive damage to the workpiece and tool. Investigations indicate that optimum material removal rate strongly depends on the dielectric flow velocity and in general this should have a low value [47, 58]. Willey [58] has reported that by choosing a suitable flow velocity of dielectric fluid it is possible in some cases to have desired electrode wear and surface roughness values. On the other hand, large static pressure can lead to an increase in machining rate especially with long pulse durations.

The mode of dielectric flushing also influences the EDM performance. Greene [48] has reported some experimental results of the influence of continuous, alternate, and combined flushing methods on work piece and tool geometry and claimed that alternate flushing results in a small improvement. Others [77] have investigated the effects of pressure or suction flushing on degree of edge rounding, as well as the angle of inclination of the machined surface and reported that greater edge wear and taper occurs at the dielectric exit side. According to Heuvelman [37] under identical machining conditions, suction flushing during

finishing would be more beneficial. Experiments with vibrating tool electrodes have also been conducted by some investigators. This would mainly facilitate the gap cleaning. In such cases, for optimum MMR, the frequency of vibration should be high or alternatively the vibration amplitude should be small.

Pressure Flushing

Next to open flushing, pressure flushing is the most important mode. The dielectric is either pushed through a flushing hole in the electrode from above, or through a flushing hole in the work piece from below. The amount of dielectric flowing through is more important for effectivity than the pressure of flushing. When calculating the smaller than specified dimension of the electrode, it must be remembered that in this type of flushing particles rising up through the lateral gap are continuously causing additional erosion [31].

Suction Flushing

In suction flushing, the eroded particles are sucked out of the gap between electrode and work piece. This type of flushing is best in those cases, where a fine finish and parallel walls are required in the work piece. When using this method with narrow gaps and small amounts of dielectric flowing through, care must be taken that enough dielectric gets into the spark gap, so that the spark erosion process will remain stable [78]. In very complex jobs both suction and pressure flushing is practised.

Interval Flushing

In interval flushing, the erosion process is interrupted for a while and the electrode is retracted. This improves the flushing out of the eroded particles. The retraction and return of the electrode has the additional effect of suction and pumping respectively, which improves the effectiveness of the flushing process. This method is particularly suitable, when deep depressions or thin electrodes are involved, and also during finishing work.

Efficient flushing is a very critical factor in the entire spark machining process because the properties of the dielectric will rapidly deteriorate by progressive soiling [79]. This results in a marked decrease of the stock removal rate accompanied by an increased proneness to arcing and thus to interruptions of the machining process. This makes it imperative to provide not only for the supply of clean dielectric and the removal of the eroded particles but also for good filtration of the dielectric. Even an optimum generator setting will not produce satisfactory eroding results if the flushing conditions in the spark gap are inadequate. It should be noted in this respect, that poor flushing might also cause distortions, for example if sparking occurs on top of the debris, It is required to know about the flash point, dielectric

strength, viscosity, specific gravity, colour and odour of the dielectric fluid used.

2.5 Tool Electrode

The EDM is basically a copying process and therefore the shape and accuracy of the machined part would largely depend upon the shape and accuracy of the cutting tool electrode. Unfortunately, electrodes for discharge machining are highly expendable because each erosive spark removes a certain amount of the material from the tool electrode as well [80-84]. Thus, as machining progresses, the electrode shape may degenerate considerably which can influence the accuracy of machining. In some cases, a series of slightly differing tool shapes may have to be used to achieve the desired result. This obviously increases the machining cost. Consequently, materials that are cheap, easy to fabricate, and give high cutting rate with minimum self erosion are preferred for tool electrode manufacturing.

2.6 Machining of Tungsten Carbide

High-dimensional accuracy combined with complex geometries are frequent requirements in application involving WC-Co cemented carbides, materials also commonly referred to as hard materials. WC-Co are extensively used as tool materials in machining and forming of metals and alloys, as they display an exceptional combination of superior wear resistance and excellent toughness. However, some of their attractive properties may deteriorate as a result of extremely high cutting temperatures induced by frictional heating particularly, in case of insufficient machining fluid. Temperature measurements were conducted on the WC-Co test samples. Scanning electron micrographs of the tested samples revealed the occurrence of temperature dependent wear mechanisms, including binder phase modification.

The term Technical Ceramics or Advanced Ceramics is a relatively new term, which is applied to a range of various materials generally obtained from inorganic primary materials with a high grade of purity. These primary materials are subjected to typical processes in powder metallurgy technology, and afterward, to high temperature sintering processes. With this, it is possible to obtain high-density material that also processes good technical features related to hardness, mechanical resistance, wear and corrosion at high temperatures. Among the most important applications of these materials, resistance to wear and corrosion, are medical and dental prosthetics, ball bearing, cutting tools and extrusion dies, that require mechanical resistance at high temperatures, include gas turbines, heat exchangers and adiabatic steel engines, and space shuttles, electronic and magnetic applications.

Tool applications usually imply service conditions involving extreme mechanical and wear demands at the surface or sub surface regions. On the other hand, machining of hard and brittle materials is well known to introduce near surface damage. From the perspective of performance, the nature and severity of this damage may be quite important because it could dictate the fracture characteristics of the manufactured tool. For instance, traditional grinding of ceramics induces flaws that are often found to be responsible for the rapture of the material instead of other defects intrinsic to the processing stages. Because the finish of the machined surface is given by the demanded end use and this, in turn, directs the type of machining operation to follow. The foregoing ideas allow one to suggest a direct correlation between mechanical parameters and machining processes through surface integrity, for the referred materials [85]. The elevated hardness, and even more important, the intrinsic brittleness that cemented carbides and cermets exhibit, results in significant inconvenience and high cost for ensuring close tolerances and surface finish under traditional grinding techniques. Electrical discharge machining (EDM) turns out to be a very good alternative for shaping cemented carbides, cermets and metal matrix composites because it is a thermal mechanical process, i.e. it does not involve any physical contact between the processed material and the electrode. EDM of WC-Co has proven to be a satisfactory technique in terms of machining performance indexes, such as material removal rate or surface roughness. On the other hand, EDM is also known to yield a thermally affected zone just beneath the shaped surface, with poor surface properties such as unfavorable residual stresses, cracks and craters [86]. In recent years, this shortcoming has been drastically reduced by the implementation of multi-step sequential EDM and post-EDM surface treatments. Considering that these material systems are widely used in applications involving extreme mechanical contacts, such knowledge is decisive for their effective implementation as tools, wear resistant parts and structural components. Sometimes, due to extreme physical and mechanical properties, shaping of the required tungsten carbide parts is possible only by the state of art spark erosion methods (EDM), which introduce micro structural defects into tungsten carbide and are rather cost intensive.

2.7 Research Gap and Problem Formulation

From the ongoing discussion it appears from literature that limited work has been done on machining of WC-Co composite. The basic problem in machining of WC-Co composite with EDM is due to differences in melting and evaporation points of the binder Co and WC. Co has high electrical conductivity as compared to WC. Co melts at 1320^0C and evaporates at

2700^0C whereas WC melts at 2800^0C and evaporates at 6000^0C. During machining energy of discharge will melt and evaporates Co binder, making the WC in unbounded form. This may further cause problem when the molten mass gets re-solidifies which may lead to instability in machining process. In order to understand the mechanism of material removal the current problem is taken.

Testing Procedure;

One grade of WC-Co material has been selected for this work. WC-Co containing 8% Co will be machined at different machining conditions (Using Taguchi design of experiment). Attempt will be made to draw conclusion from these experiments. However, if need may arise few more experiment will be done. In order to use the energy properly, a suitable model will be developed using the experimental data. The reason for crack formation will be searched by analysing the microstructure of machined specimen.

Chapter 3

MACHINING OF WC-CO AND EFFECT OF PROCESSING PARAMETERS ON STRUCTURAL FEATURES

Overview

Tungsten Carbide (WC) is an extremely hard material which is extensively used in the manufacturing of tools and dies. In the presence of cobalt, as a, binder its machining becomes a tedious task because of interfacial bonding. In the EDM process, where electrical energy is used in the form of intermittent impulses for the machining of the substance, the heat generated due to the plasma is responsible for removal of stock material at the interface. The heat generated is conducted differentially because of the composite structure of the tungsten carbide cermets. In order to improve the technological performance it is essential to understand the morphological features of tungsten carbide after machining. The studies have been conducted using different machining parameters. The objective of this study is to analyze the impact of machining parameters on the morphology of tungsten carbide, suitable to withstand impact load on press forging of small components during the operation. Experiments have been performed with the specially designed fixtures using proper flushing arrangements to avoid arcing during the process. WC of P20 grade which is one of the most suitable grades to withstand load after EDM, has been used as work piece material in the entire study. Copper, graphite and copper-tungsten have been used as electrode material. The morphological features were studied with the help of the scanning electron microscope (SEM). It was observed that structural features varied with variation in electrode under similar experimental conditions. Phenomenon of such structures is discussed at length. The reason for formations of cracks on the machined surface of WC has also been studied and highlighted. In the present study experimental results were also validated by suitable mathematical models.

3.1 Introduction

The increasing demand for machining of hard and tough components requiring high accuracy for exact fitting and good surface finish has resulted in the development of a number of non- traditional machining processes [1]. Electric discharge machining (EDM) is one of the most accepted processes for such materials [89]. It is a high precision metal removal process that uses thermal energy from a fine, accurately controlled electrical discharge (spark) to erode (vaporize) metal. The impact of hardness is not a hindrance for machining. The only required parameter is that the workpiece material should be conductive in nature. There is no direct contact between the cutting tool and the work piece. The process is suitable to machine even thin sections as there is no deformation. However, due to generation of rapid heat with sudden quenching, the surface may undergo sudden changes leading to variation in the structure of parent material of the machined component [90]. Though this variation in structure may be beneficial in some cases but it may lead to formation of certain defects such as voids, cracks, induced stresses etc. which may cause overall deterioration of the mechanical properties of the components like abrasion and erosion resistance [42,91].

Tungsten carbide is used as an important tool and dies material in industries on account of its high hardness, strength and wear resistance over a wide range of temperatures But, it is difficult to process by conventional machining techniques. EDM has been found to be quite suitable for machining this material. Lot of work has been done to establish the relationship between processing parameters and machining parameters for steel, aluminium and titanium [29, 31, 92, 93 and 94]. But very few reports exist on machining of tungsten carbide (WC) by EDM [26]. Lee and Li [3, 20] have studied the effect of machining parameters and machining characteristics in EDM of tungsten carbide. In their study, they have optimised over a large range of peak current and pulse duration. But, in all practical applications a higher MRR is required using low current. Further structural analysis carried out by them could not establish the cause of crack formation [3].

Considering the above observations it is felt that some more work has to be done to optimize the processing parameters and understand the structural variations. In this present work, experiments were performed for higher pulse duration to obtain higher machining rate. Structural analysis of the machined component has been done to understand the basic cause of crack formation.

3.2 Experimental Work

In the present investigation, all the experiments were performed on a die sinking vertical EDM machine (Model Electroplus R50) where tungsten carbide of P20 grade and size 20 mm × 5 mm length was taken as workpiece material for all the experiments. For machining of the workpiece material CuW, Cu and graphite were used as electrode material, whose composition is given in table 3.1.

Table 3.1: Chemical composition (wt %) of workpiece

Element → / Material ↓	W%	Cu %	Al %	Ni%	Sn%	Zn%	Si%	Fe%	Cr%	Co%	C%
Tungsten Carbide	93.36	-	-	-	-	-	-	1.41	0.34	4.89	-
Copper Tungsten	1.21	81.09	14.07	1.61	0.11	1.01	0.88	0.02	-	-	-
Copper	-	99.97	-	0.03	-	-	-	-	-	-	-
Graphite	-	-	-	-	-	-	0.05	-	-	-	99.95

Finally polished and cleaned samples of the workpiece material were placed under SEM to analyse their composition by energy dispersive X-ray analyses at a probe current of 1×10^{-9} amp and the acceleration voltage of 23 kV which is shown in figure 3.1 and table 3.1. The structural analysis of the workpiece material was done with the help of the optical and scanning electron microscope. The analysis indicates that cobalt acts as a binder. The crystal structure was determined by the X-ray diffraction technique. Experiments have been conducted using specially designed fixtures and proper flushing arrangements to avoid arcing during the process.

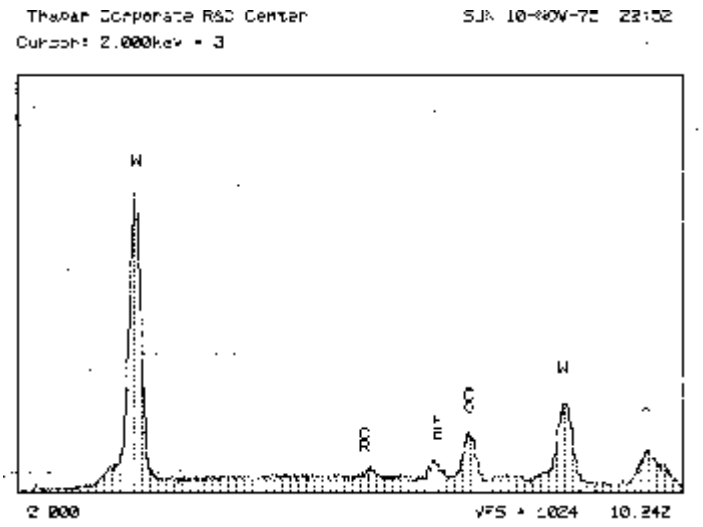

Fig. 3.1: Energy dispersive spectrogram showing the characteristics spectra of W, Cr, Co and Fe of un-machined workpiece

The morphological features of the EDMed workpiece material were analysed under SEM (Model GEOL 840x) at different magnifications. The machining parameters selected for this study were discharge current, electrode material, pulse duration and type of flushing as variable parameter as shown in table 3.2.

Table 3.2: Variable Parameters

Discharge Current	Electrode
10	Graphite, Copper Tungsten, and Copper
12	
14	
16	
18	
20	

The fixed parameters for the experiment are work piece material, input voltage and polarity these are shown in table 3.3.

Table 3.3: Fixed Parameters

1	Work Material	Tungsten Carbide
2	Input Voltage	30V
3	Polarity	Electrode = +Ve Work material = -Ve
4	Dielectric	Kerosene

In order to optimize the number of experiments with different levels orthogonal array design was followed which is given in table 3.4.

Table 3.4: Factor Level for EDM Orthogonal Array

Experiment No.	Electrode	Discharge current	Pulse Duration	Flushing
1	Gr	10	100	Side
2	Gr	12	100	Side
3	Gr	14	100	Side
4	Gr	16	100	Side
5	Gr	18	100	Side
6	Gr	20	100	Side

Experiment No.	Electrode	Discharge current	Pulse Duration	Flushing
1	CuW	10	100	Side
2	CuW	12	100	Side
3	CuW	14	100	Side
4	CuW	16	100	Side
5	CuW	18	100	Side
6	CuW	20	100	Side

Experiment No.	Electrode	Discharge current	Pulse Duration	Flushing
1	Cu	10	100	Side
2	Cu	12	100	Side
3	Cu	14	100	Side
4	Cu	16	100	Side
5	Cu	18	100	Side
6	Cu	20	100	Side

3.3 Results and discussion

3.3.1 Material removal rate (MRR) and Surface roughness (R_a)

MRR and R_a values are interdependent parameters as both are energetically derived processes. The results of the experiments performed at different processing parameters are given in table 3.5, 3.6 and 3.7.

Table 3.5: Effect of graphite electrode on surface roughness (R_a) and material removal rate (MRR)

Discharge current (Amp)	R_a (μm)	MRR (mm^3 /min)
10	3.31	6.8
12	3.94	7.45
14	4.59	8.31
16	5.2	9.44
18	5.84	10.83
20	6.44	12.4

Table 3.6: Effect of copper tungsten electrode on surface roughness (R_a) and material removal rate (MRR)

Discharge current (Amp)	R_a (μm)	MRR (mm^3 /min)
10	2.81	5.6
12	2.74	6.06
14	2.78	6.54
16	2.99	7.1
18	3.41	7.8
20	3.91	8.5

Table 3.7: Effect of copper electrode on surface roughness (R_a) and material removal rate (MRR)

Discharge current (Amp)	R_a (μm)	MRR (mm^3 /min)
10	0.94	5.1
12	1.49	5.58
14	1.94	6.02
16	2.21	6.36
18	2.34	6.77
20	2.32	7.25

The workpiece specially designed for proper suction and pressure flushing in Fig. 3.2

Fig. 3.2: Workpiece and electrode holder

The variations of MRR and R_a with variation in current for different electrodes are shown in Fig. 3.3 to 3.15.The important features observed in these figures are that both MRR and R_a values increases with increase in discharge current for all the three electrodes used in the experiments. However, the increase is linear for the graphite electrode, when the discharge current is increased from 10 amp to 20 amp. In the case of copper tungsten electrode variation in MRR is almost linear where as the surface roughness was nearly constant at lower currents i.e. 10 amp and 15 amp. However, the value of R_a increases when the discharge current is increased from 15amp to 20 amp. This increase in surface roughness indicates that material is not removed uniformly from the workpiece as the current is increased from 15 amp to 20 amp indicating that the material is being removed from the workpiece in the form of patches. The result indicates that higher the current it may lead to expansion of the plasma channel because of this the size of crater may increase [3,14]. The basic cause for these are the non uniform distribution of heat throughout

the material and because of the composite structure, low melting point substance (cobalt) is being flushed out at a higher rate as compared to the tungsten carbide.

Analysis of experimental results for Material Removal Rate (MRR):

EDM is a complex process. It will be of interest to find any theoretical model which can be appropriately fitted to the experimental results obtained by us. An exponential curve to the type $y = ae^{bx}$ for a power curve of the type $y = ax^b$ can be fitted using method of least square (we have not tried quadratic curve of the type $y = a + bx + cx^2$ as it was expected to be included in exponential type of curve $y = ae^{bx}$ since $(e^x = 1 + x + \frac{x^2}{2} \ldots\ldots)$

Validation of Material Removal Rate (MRR) for Graphite Electrode material

We have fitted two types of curves (power model and exponential model) to the data points given in table 3.8 taking x as current and y as material removal rate (MRR) using method of least square and have obtained the curves as $y = 3.619\ e^{0.61x}$ in the exponential case and $y = 0.879\ x^{0.867}$. These curves have been plotted and shown in Fig 3.3 along with data points. A comparison of the actual data with the curve corresponding points obtained using these two equations of the curve have also been presented in table 3.8.1.

Table 3.8.1 Comparison between $y = a\ x^b$ (power) model and $y = a\ e^{bx}$ (exponential) model

Current (Amp)	MRR (mm3/min)	Calculated value (power model)	% difference	Calculated value (exponential model)	% difference
10	6.80	6.471	**4.834**	6.594	3.026
12	7.45	7.579	-1.738	7.435	0.201
14	8.31	8.663	-4.251	8.383	-0.878
16	9.44	9.727	-3.036	9.452	-0.124
18	10.83	10.772	0.532	10.657	1.599
20	12.40	11.803	4.817	12.016	**3.101**

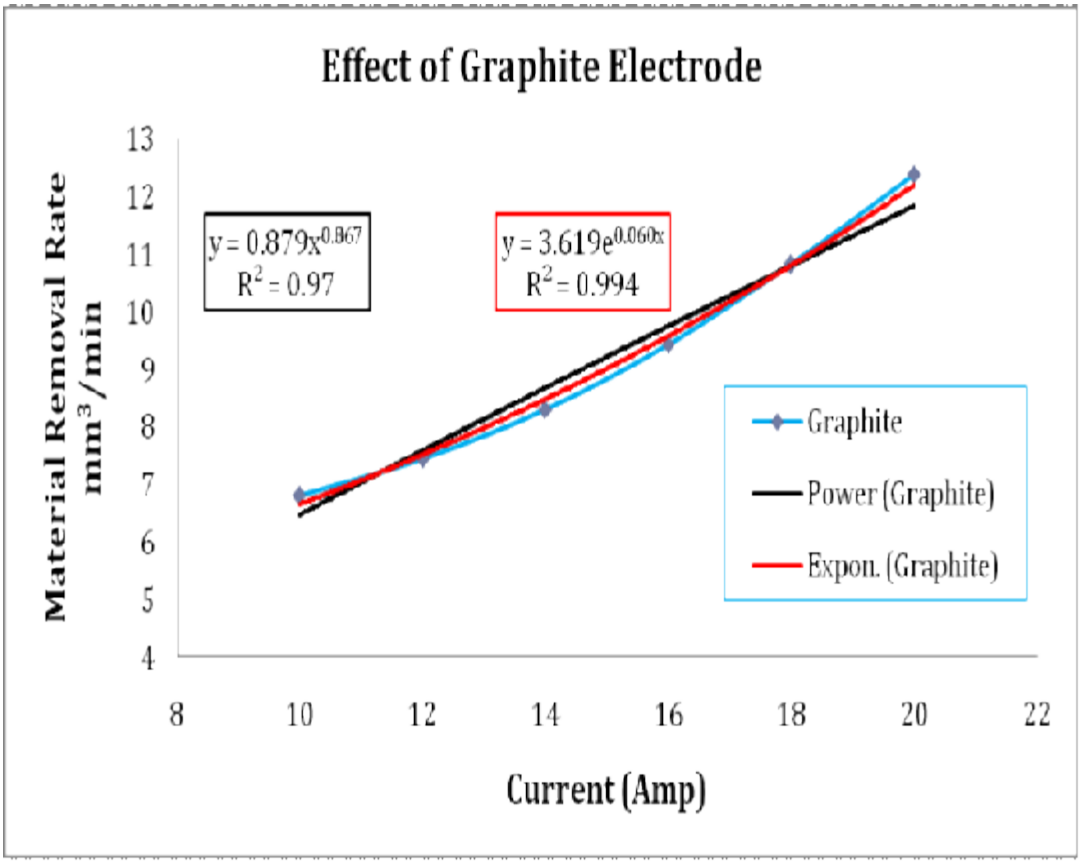

Fig. 3.3: Graphical presentation of power and exponential models obtained from the data observed and shown in Table 3.8.1.

Our results show that exponential model gives relatively a better fit to the experimental data than the power model because maximum difference between the experimental results and computed model is **3.101%** in the case of exponential and **4.834%** in case of power model.

We have also tried to see whether the analytical expression can be used for interpolation and extrapolation within reasonable limits. For this we tried to derive equations for both type of curves by first excluding points in the middle of the data (x=14 amp) and than by excluding extreme left point (x=10 amp) and extreme right point (x=20 amp). We than tried to observe the difference between experimental value of MRR and value of MRR for these points as obtained using set of remaining 5 points. These results are presented in table 3.8.2, 3.8.3, 3.8.4. These are also shown in figure 3.4, 3.5 and 3.6 respectively.

Table 3.8.2 Comparison between observed and calculated values for 10Amp current

Current (Amp)	MRR (mm^3/min)	Calculated value power model	% difference	Calculated value exponential model	% difference
10	6.80	6.036	11.234	6.469	4.869
12	7.45	7.242	2.792	7.352	1.312
14	8.31	8.448	-1.657	8.356	-0.556
16	9.44	9.653	-2.258	9.497	-0.607
18	10.83	10.859	-0.264	10.794	0.331
20	12.40	12.064	2.711	12.268	1.063

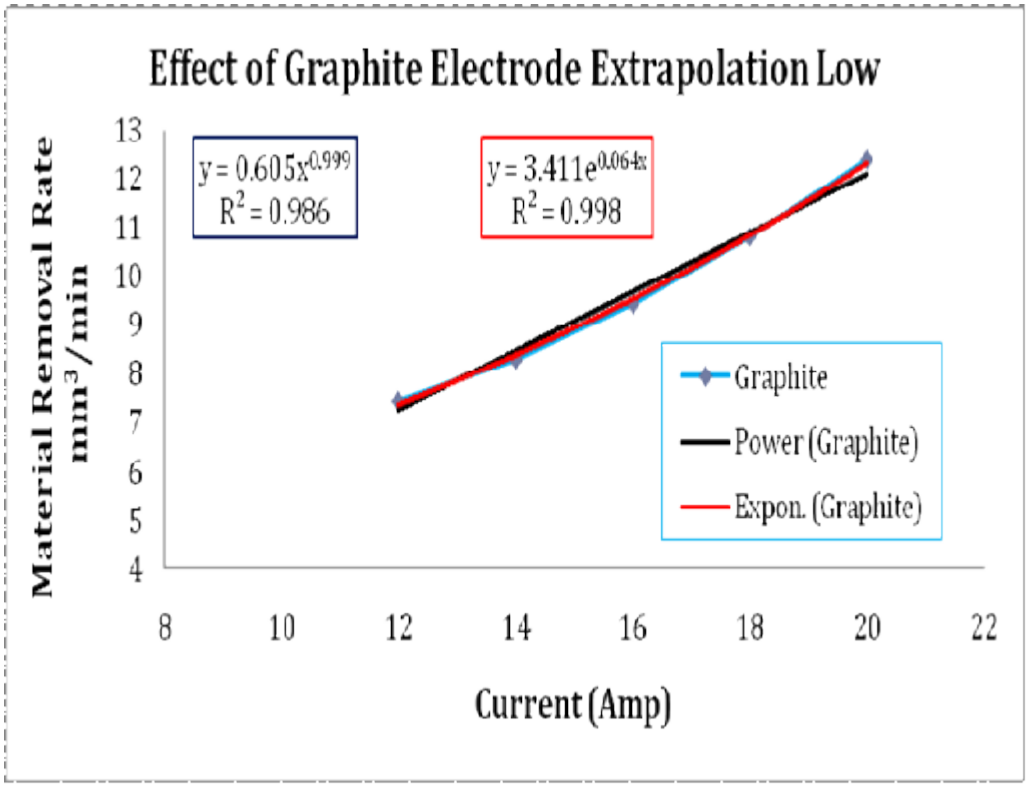

Fig. 3.4: Graphical presentation of power and exponential models obtained from the data observed from 12Amp to 20 Amp shown in Table 3.8.2.

Table 3.8.3 Showing comparisons between observed and calculated values for 14Amp current

Current (Amp)	MRR (mm^3/min)	Calculated value power model	% difference	Calculated value exponential model	% difference
10	6.80	6.557	3.577	6.656	2.115
12	7.45	7.671	-2.969	7.505	-0.736
16	9.44	9.827	-4.103	9.541	-1.065
18	10.83	10.876	-0.427	10.757	0.675
20	12.40	11.909	3.960	12.128	2.190
14	8.31	8.760	-5.415	8.462	-1.825

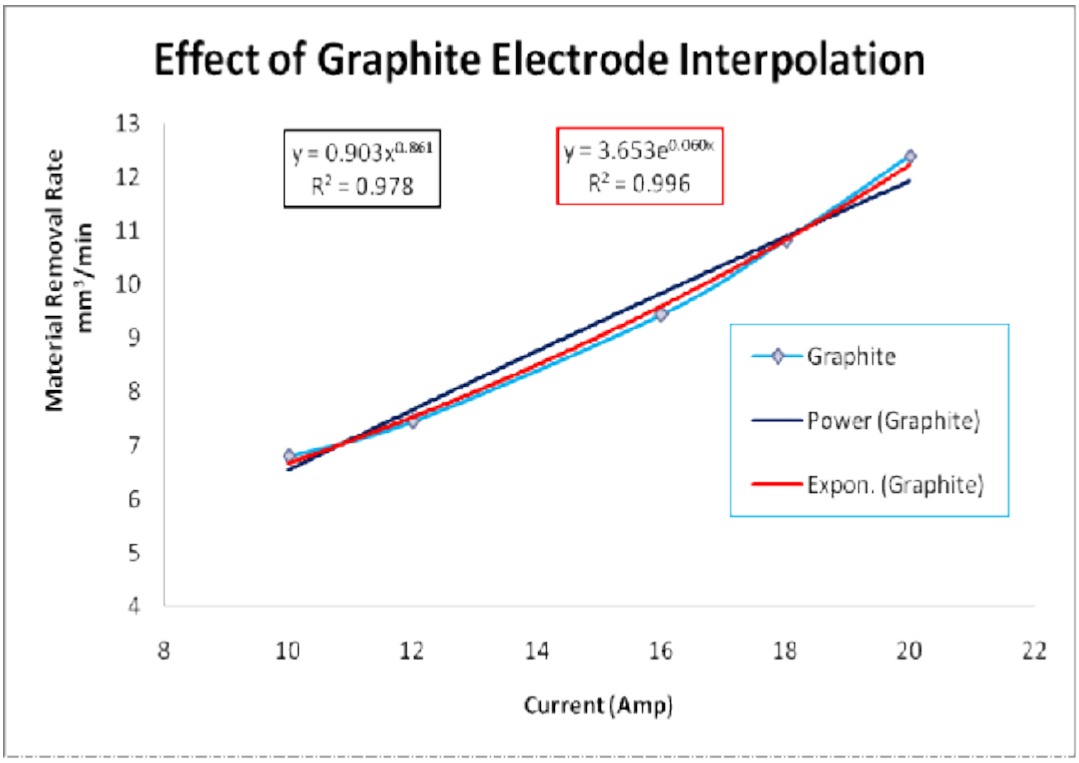

Fig. 3.5: Graphical presentation of power and exponential models obtained from the data observed from 10 Amp to 20 Amp shown in Table 3.8.2.

Table 3.8.4 Showing comparisons between observed and calculated values for 20Amp current

Current (Amp)	MRR (mm^3/min)	Calculated value power model	% difference	Calculated value exponential model	% difference
10	6.80	6.586	3.148	6.664	2.004
12	7.45	7.601	-2.023	7.483	-0.447
14	8.31	8.580	-3.246	8.404	-1.128
16	9.44	9.529	-0.945	9.437	0.028
18	10.83	10.454	3.476	10.598	2.141
20	12.40	11.356	8.419	11.902	4.019

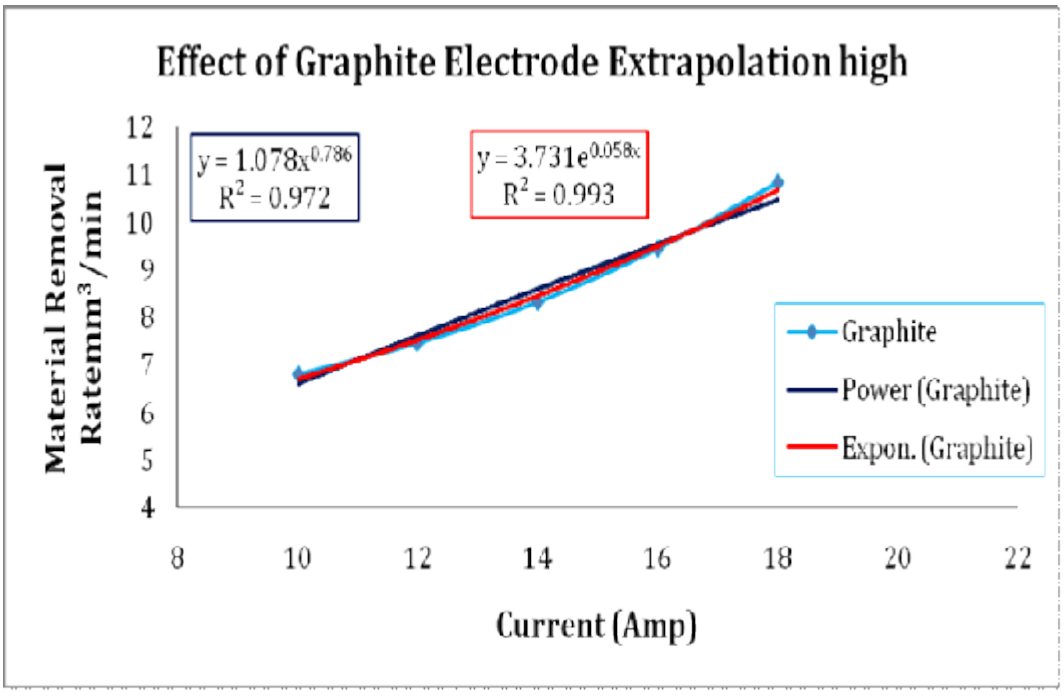

Fig. 3.6: Graphical presentation of power and exponential models obtained from the data observed from 10 Amp to 18 Amp shown in Table 3.8.3

Our results again confirm that exponential model is more appropriate for the present set of experimental results.

Validation of Material Removal Rate (MRR) for copper tungsten as Electrode

Similarly we have fitted these two types of curves to the data point given in table 3.9 taking x as current and y as material removal rate (MRR) using method of least square and have obtained the curves as $y = 3.666\, e^{0.41x}$ in the exponential case and $y = 1.376\, x^{0.699}$ Again in this case also our results show that exponential model gives results with maximum deviation of 2.075%. We have also tried to see whether the analytical expression can be used for interpolation and extrapolation within reasonable limits. Our results show that difference in observed value and computed values for interpolation is 0.184%, extrapolation lower side 2.610% and extrapolation higher side is 1.166%. Hence it can be concluded that $y = 3.666\, e^{0.41x}$ for copper tungsten electrode within reasonable limits.

Validation of Material Removal Rate (MRR) for copper tungsten Electrode

Also we have fitted these two types of curves to the data point given in table 3.9 taking x as current and y as material removal rate (MRR) using method of least square and have obtained the curves as $y - 3.675\, e^{0.034x}$ in the exponential case and $y = 1.626\, x^{0.495}$. Again in this case also our results indicate that exponential model gives result with maximum deviation of 1.738%. We have also tried to see whether the analytical expression can be used for interpolation and extrapolation within reasonable limits. Our results show that difference in observed value and computed values for interpolation is 2.433%, extrapolation lower side 2.988% and extrapolation higher side is 2.594%. Hence it can be concluded that the equation $y = 3.675\, e^{0.034x}$ for copper electrode gives better results within reasonable limits.

R^2 value in each case is also computed. It is observed that the value is within reasonable limit and is close to 1 as acceptable value.

Table 3.9.1 Comparison between $y = a\,x^{b}$ (power) model and $y = a\,e^{bx}$ (exponential) model

Current (Amp)	MRR (mm^3/min)	Calculated value power model	% difference	Calculated value exponential model	% difference
10	5.60	5.465	2.404	5.524	1.357
12	6.06	6.096	-0.595	5.996	1.055
14	6.54	6.686	-2.228	6.508	0.482
16	7.10	7.242	-2.007	7.065	0.498
18	7.80	7.772	0.360	7.668	1.688
20	8.50	8.278	2.610	8.324	2.075

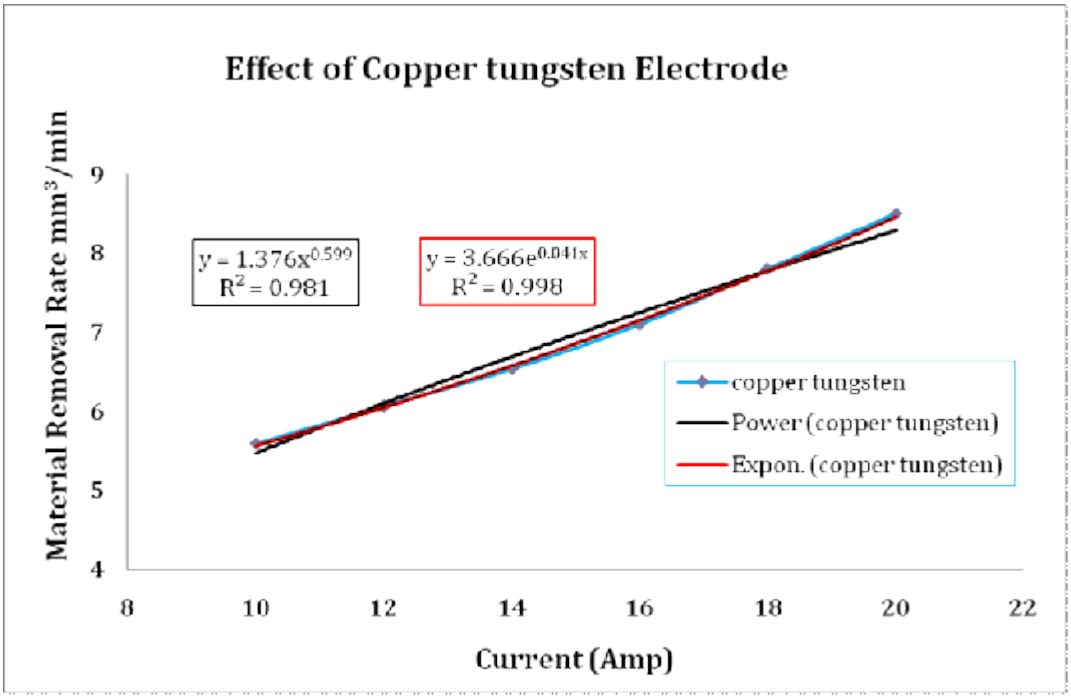

Fig 3.7: Showing the effect of Current on Material Removal Rate (MRR)

Table 3.9.2 Computing the % difference after interpolation

Current (Amp)	MRR (mm^3/min)	Calculated value power model	% difference	Calculated value exponential model	% difference
10	5.60	5.490	1.964	5.541	1.061
12	6.06	6.119	-0.975	6.014	0.758
16	7.10	7.261	-2.274	7.086	0.200
18	7.80	7.789	0.146	7.691	1.393
20	8.50	8.293	2.441	8.349	1.781
14	6.54	6.707	-2.552	6.528	0.184

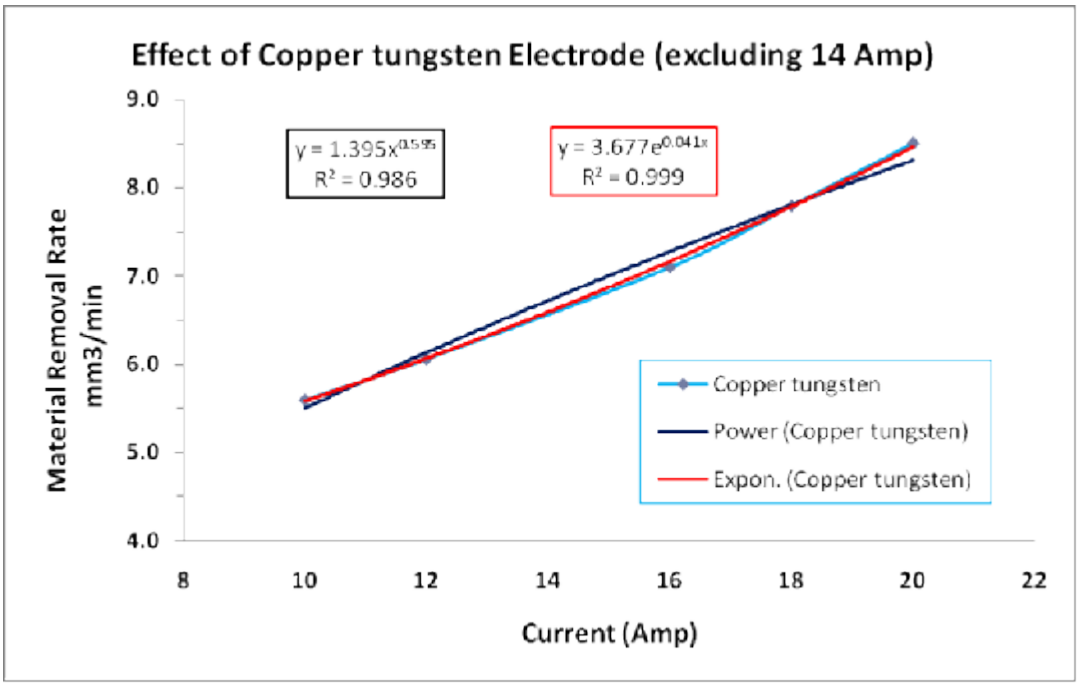

Fig 3.8: Showing Effect of Interpolation on suggested model with CuW electrode

Table 3.9.3 Computing the % difference after extrapolation low

Current (Amp)	MRR (mm^3/min)	Calculated value power model	% difference	Calculated value exponential model	% difference
10	5.60	5.277	**5.759**	5.497	**1.833**
12	6.06	5.957	1.705	5.979	1.336
14	6.54	6.599	-0.897	6.503	**0.566**
16	7.10	7.210	-1.555	7.073	0.383
18	7.80	7.797	0.039	7.693	1.377
20	8.50	8.362	**1.624**	8.367	1.568

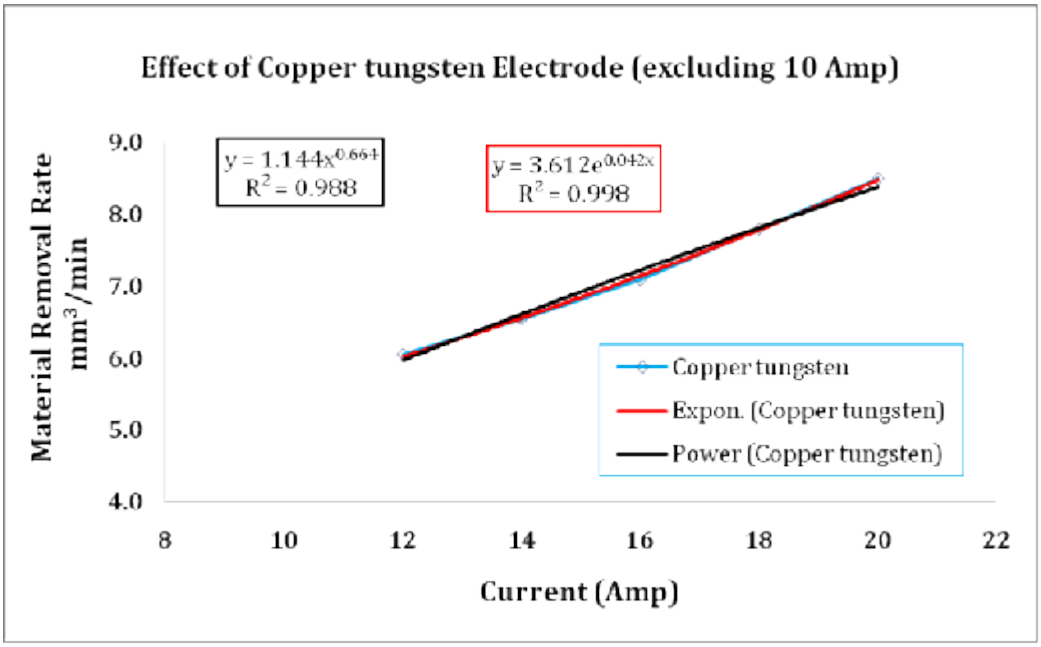

Fig 3.9: Effect of Extrapolation low on suggested model with CuW electrode

Table 3.9.4 Computing the % difference after extrapolation high

Current (Amp)	MRR (mm^3/min)	Calculated value power model	% difference	Calculated value exponential model	% difference
10	5.60	3.948	29.498	5.575	0.442
12	6.06	4.255	29.793	6.052	0.138
14	6.54	4.532	30.701	6.569	-0.441
16	7.10	4.787	32.575	7.130	-0.425
18	7.80	5.024	35.589	7.739	0.776
20	8.50	5.246	38.284	8.401	1.166

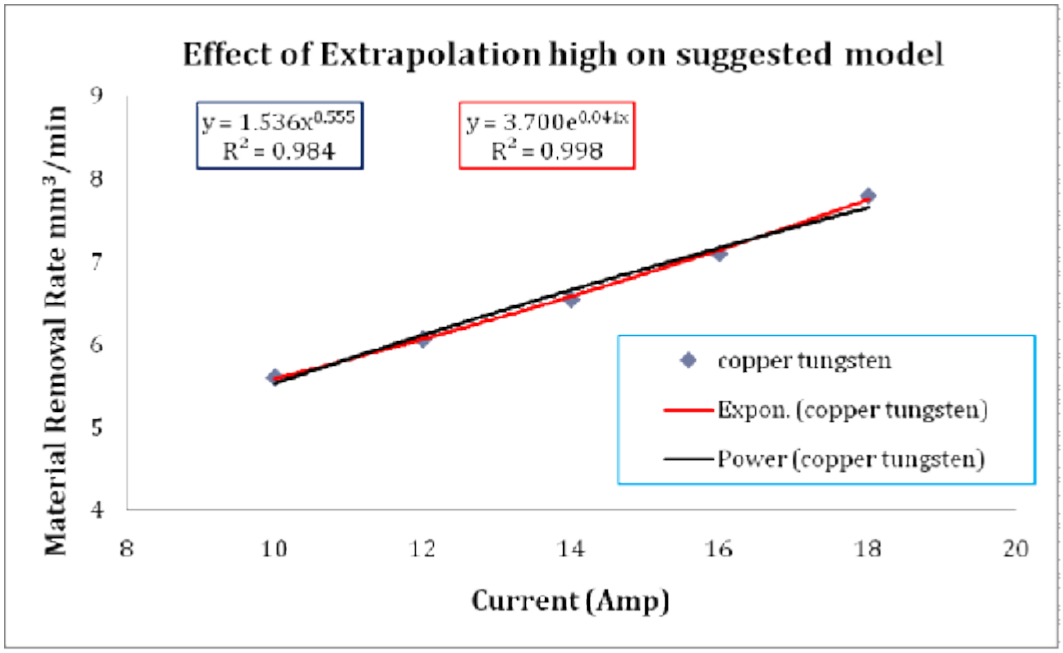

Fig 3.10: Effect of Extrapolation high on suggested model with CuW electrode

Table 3.10.1 Comparison between $y = a\,x^b$ (power) model and $y = a\,e^{bx}$ (exponential) model

Current (Amp)	MRR (mm^3/min)	Calculated value power model	% difference	Calculated value exponential model	% difference
10	5.10	5.083	0.333	5.163	-1.239
12	5.58	5.563	0.303	5.526	0.959
14	6.02	6.004	0.263	5.915	1.738
16	6.36	6.414	-0.856	6.332	0.447
18	6.77	6.800	-0.437	6.777	-0.105
20	7.25	7.164	1.192	7.254	-0.055

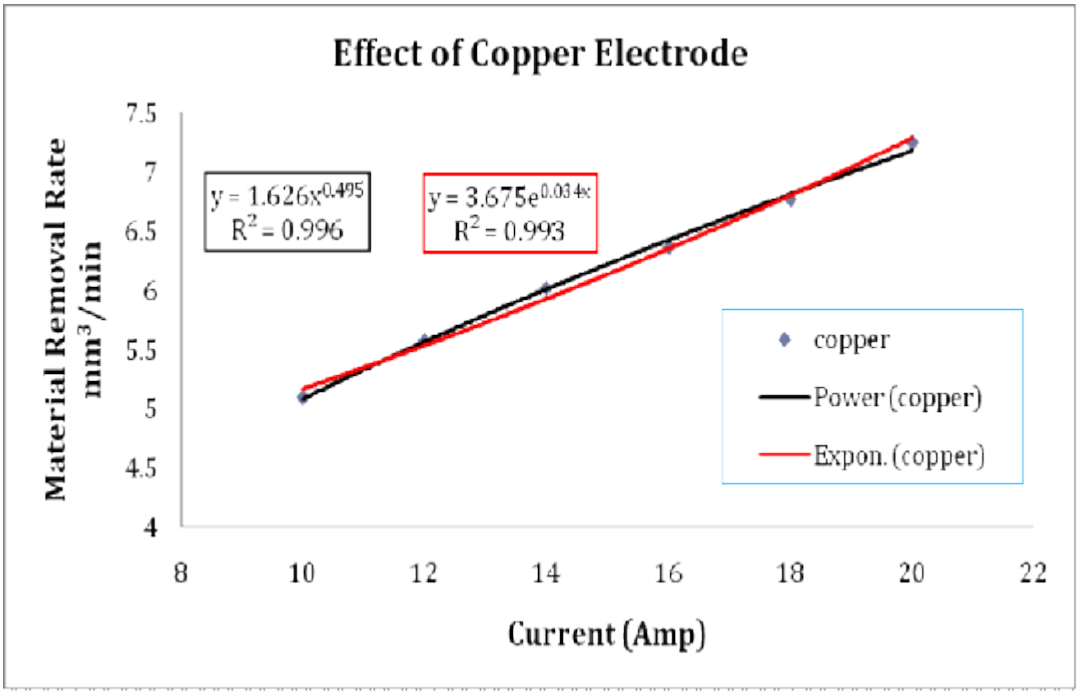

Fig 3.11: Showing the effect of Current on Material Removal Rate (MRR)

Table 3.10.2 Computing the % difference after interpolation

Current (Amp)	MRR (mm^3/min)	Calculated value power model	% difference	Calculated value exponential model	% difference
10	5.10	5.080	0.395	5.127	-0.523
12	5.58	5.560	0.365	5.487	1.660
16	6.36	6.411	-0.794	6.287	1.151
18	6.77	6.795	-0.375	6.729	0.603
20	7.25	7.159	1.253	7.203	0.653
14	6.02	6.000	0.324	5.874	2.433

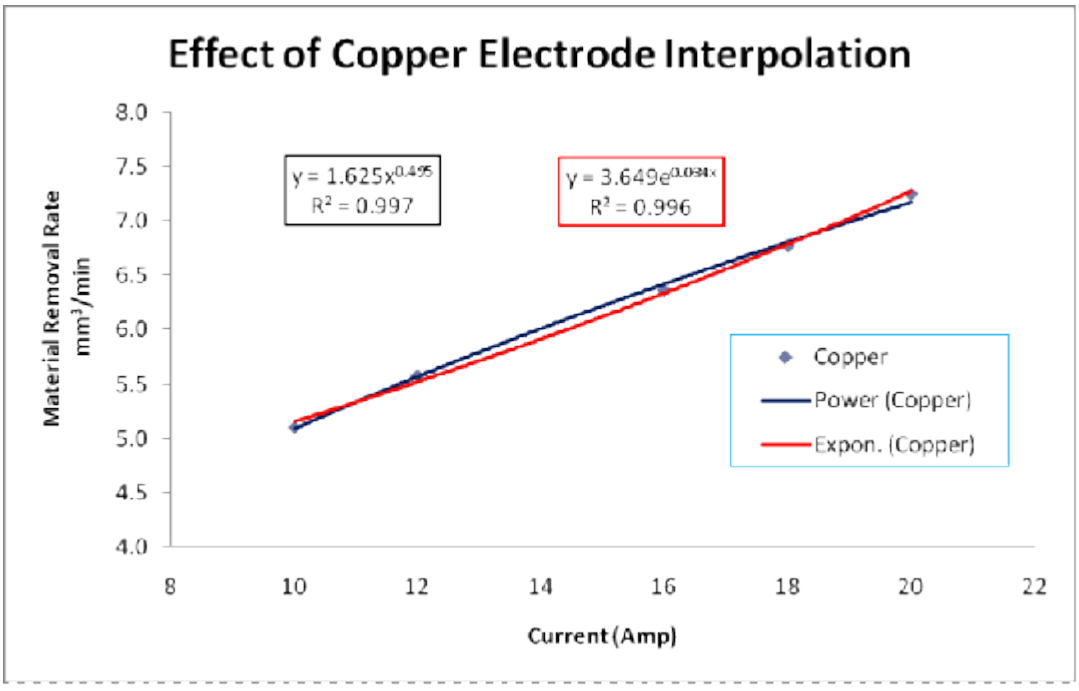

Fig 3.12: Showing Effect of Interpolation on suggested model with Cu electrode

Table 3.10.3 Computing the % difference after extrapolation (low)

Current (Amp)	MRR (mm^3/min)	Calculated value power model	% difference	Calculated value exponential model	% difference
12	5.58	5.553	0.486	5.600	-0.350
14	6.02	5.999	0.353	5.970	0.837
16	6.36	6.414	-0.845	6.364	-0.065
18	6.77	6.804	-0.497	6.785	-0.218
20	7.25	7.172	1.070	7.233	0.232
10	5.10	5.068	0.625	5.252	-2.988

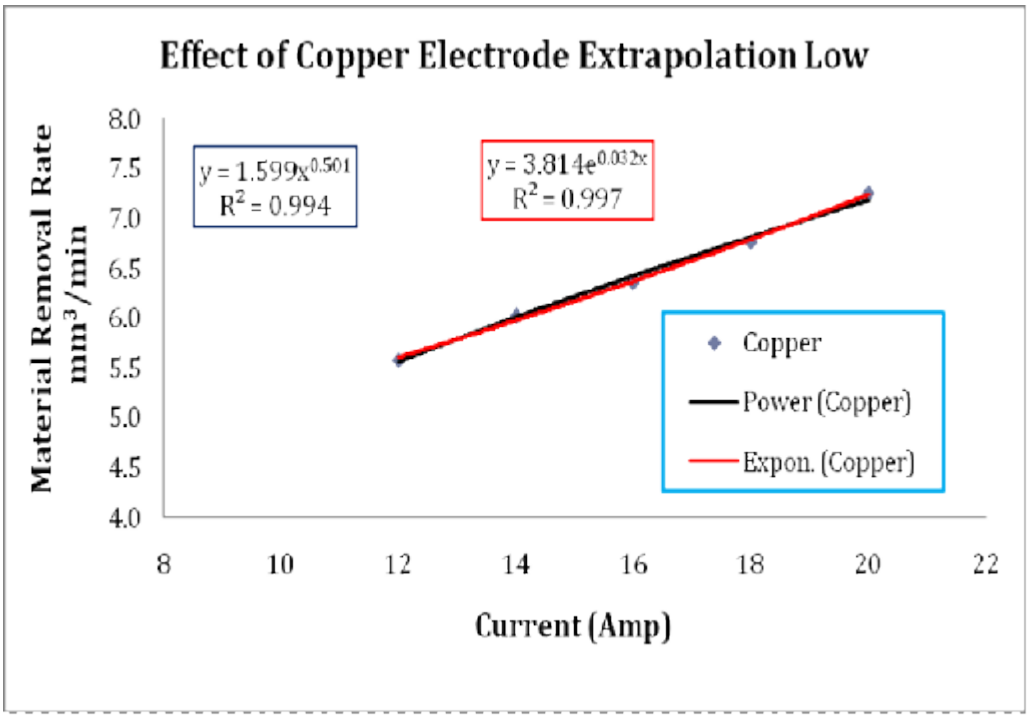

Fig 3.13: Effect of Extrapolation low on suggested model with CuW electrode

Table 3.10.4 Computing the % difference after extrapolation (high)

Current (Amp)	MRR (mm^3/min)	Calculated value power model	% difference	Calculated value exponential model	% difference
10	5.10	5.096	0.082	5.118	-0.357
12	5.58	5.558	0.397	5.478	1.821
14	6.02	5.981	0.648	5.864	2.594
16	6.36	6.373	-0.212	6.276	1.313
18	6.77	6.741	0.428	6.718	0.766
20	7.25	7.088	2.239	7.191	0.816

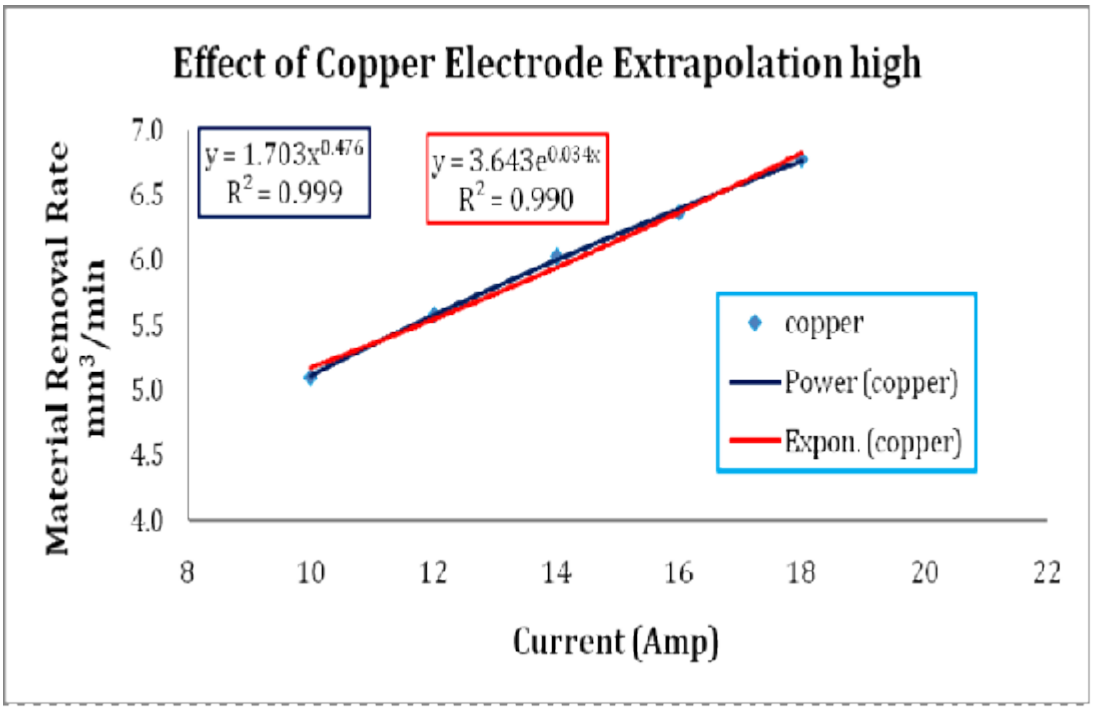

Fig 3.14: Effect of Extrapolation high on suggested model with CuW electrode

Analysis of experimental results for Surface Roughness:

An exponential curve of the type $y = ae^{bx}$, power curve of the type $y = ax^{b}$ and quadratic curve of the type $y = a + bx + cx^2$ can be fitted using method of least square. In this case for any electrode or work piece has to have some surface finish at the initial stage, hence exponential curves and quadratic curves have been compared for study and analysis.

Validation of Surface Roughness (R_a) for graphite as Electrode material

We have fitted these two types of curve to the data point given in table 3.11 taking x-axis, as current and y-axis, as surface roughness (R_a) using method of least square and have obtained the curves equations as $y = 1.765\ e^{0.66x}$ in the exponential model and $y = 0.000\ x^2 + 0.339\ x$ in the quadratic model. These curves have been plotted in Fig 3.15 along with data points. A comparison of the actual data with the curve corresponding to points obtained using these two equations of the curve have also been presented in table 3.11. The maximum difference found is only 0.368% when compared with the experimental results. This result is compared with the exponential model where the difference found is 6.607%. Both of the models were compared using interpolation i.e. excluding 14 Amp current as shown in Fig. 3.17 and table 3..12.2 where difference found is only 2.2%. In case of extrapolation (low) i.e. excluding 10 Amp current as shown in Fig. 3.18 and table 3.12.3, the percentage difference observed is 1.408% and in case of exponential model the difference is 6.572%. Also extrapolation (high) i.e. excluding 20 Amp current as shown in Fig. 3.19 and table 3.12.4 and the maximum difference found is 4.219%. It shows that the model obtained with quadratic equation $y = 0.000\ x^2 + 0.339\ x$ is within the acceptable limit of around 5%.

Validation of Surface Roughness (R_a) for copper tungsten as Electrode material

We have also fitted these two types of curve to the data points given in table 3.13 taking x as current and y as surface roughness (R_a) using method of least square and have obtained the curves as $y = 1.849\ e^{3.034x}$ in the exponential model and $y = 0.019\ x^2 - 0.475\ x + 5.614$ in the quadratic model. These curves have been plotted in Fig 3.20 along with data point. A comparison of the actual data with the curve corresponding to points obtained using these two equations of the curve have also been presented in table 3.13.1. The maximum difference found is only 5.277% when compared with the experimental results. This result is compared with the exponential model where the difference found is 8.171%. Both of the models were

compared using interpolation i.e. excluding 14 Amp current as shown in Fig. 3.21 and table 3.13.2 where difference found is only 3.302%. In case of extrapolation (low) i.e. excluding 10 Amp current as shown in Fig. 3.22 and table 3.13.3, the maximum percentage difference observed is 8.056% and in case of exponential model the difference is 6.572%. Also extrapolation (high) i.e. excluding 20 Amp current and the maximum difference found is 2.464% and in case of exponential model the maximum difference is 3.709% which is shown in Fig. 3.23 and table 3.13.4. It shows that the model obtained with quadratic equation $y = 0.019\,x^2 - 0.475\,x + 5.614$ is within the acceptable limit of around 5%.

Validation of Surface Roughness (R_a) for copper as Electrode material

We have fitted these two types of curve to the data point given in table 3.14 taking x as current and y as surface roughness (R_a) using method of least square and have obtained the curves as $y = 0.456\,e^{0.088x}$ in the exponential model and $y = -0.018\,x^2 + 0.692\,x - 4.142$ in the quadratic model. These curves have been plotted in Fig 3.24 along with data points. A comparison of the actual data with the curve corresponding points obtained using these two equations of the curve have also been presented in table 3.14.1. The maximum difference found is only 7.126% when compared with the experimental results. This result is compared with the exponential model where the difference found is 19.714%. Both of the models were compared using interpolation i.e. excluding 14 Amp current as shown in Fig. 3.25 and table 3.14.2 where difference found is only 2.766%. In case of extrapolation (low) i.e. excluding 10 Amp current as shown in Fig. 3.26 and table 3.14.3, the maximum percentage difference observed is maximum 4.527% and in case of exponential model the difference is 35.739%. Also extrapolation (high) i.e. excluding 20 Amp current and the maximum difference found is 3.974% and in case of exponential model the maximum difference is 28.395% as shown in Fig. 3.27 and table 3.14.4. It shows that the model obtained with quadratic equation $y - -0.018\,x^2 + 0.692\,x - 4.142$ is within the acceptable limit of around 5%.

Table 3.11 Comparison between $y = a\,x^{b}$ (power) model, $y = a\,e^{bx}$ (exponential) model and polynomial model

Discharge current (Amp)	R_a (µm)	calculated value power model	% difference in calculated and observed	calculated value exponential model	% difference in calculated and observed	calculated value polynomial model	% difference in calculated and observed
10	0.94	1.094	14.092	1.164	**19.221**	0.937	-0.309
12	1.49	1.386	-7.540	1.381	-7.875	1.512	**1.422**
14	1.94	1.692	**-14.684**	1.639	-18.330	1.939	-0.067
16	2.21	2.011	-9.902	1.946	-13.566	2.219	0.392
18	2.34	2.342	0.093	2.310	-1.306	2.352	0.489
20	2.32	2.685	13.579	2.742	15.381	2.337	0.732

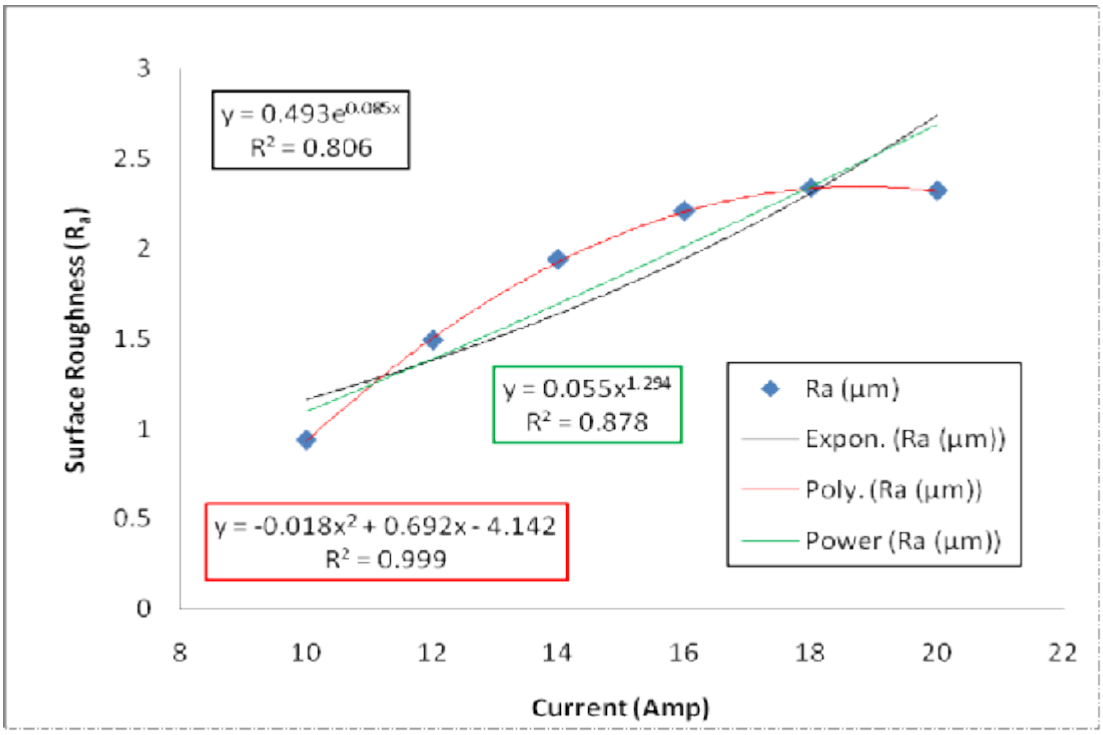

Fig 3.15: Effect of current on surface finish with copper electrode

Table 3.12.1 Comparison between exponential and quadratic models in case of graphite electrode

Discharge current (Amp)	R_a (µm)	Exponential Model		Quadratic Model	
		calculated value (exponential model)	% difference in calculated and actual	calculated value polynomial model	% difference in calculated and observed
10	3.31	3.415	3.072	3.310	0.000
12	3.94	3.897	-1.109	3.953	0.324
14	4.59	4.447	-3.224	4.589	-0.017
16	5.2	5.074	-2.481	5.219	0.368
18	5.84	5.790	-0.862	5.843	0.048
20	6.44	6.607	2.530	6.460	0.310

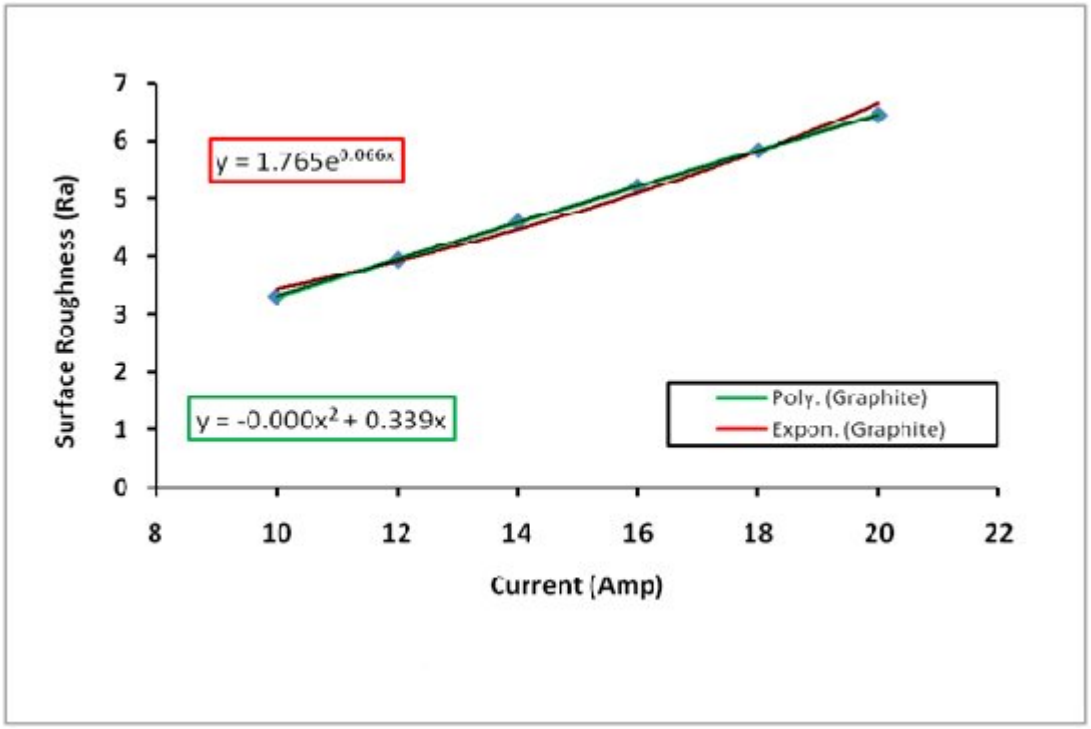

Fig. 3.16: Effect of current on surface finish in case of graphite electrode (comparison of computed and observed results)

Table 3.12.2 Comparison between exponential and quadratic models in case of graphite electrode (excluding 14amp)

Discharge current (Amp)	R_a (µm)	Exponential Model		Quadratic	
		calculated value (exponential model)	% difference in calculated and actual	calculated value polynomial model	% difference in calculated and observed
10	3.31	3.370	1.792	3.240	-2.160
12	3.94	3.846	-2.444	3.869	-1.840
16	5.2	5.008	-3.834	5.107	-1.817
18	5.84	5.715	-2.193	5.717	-2.155
20	6.44	6.521	1.243	6.320	-1.899
14	4.59	4.389	-4.587	4.491	-2.200

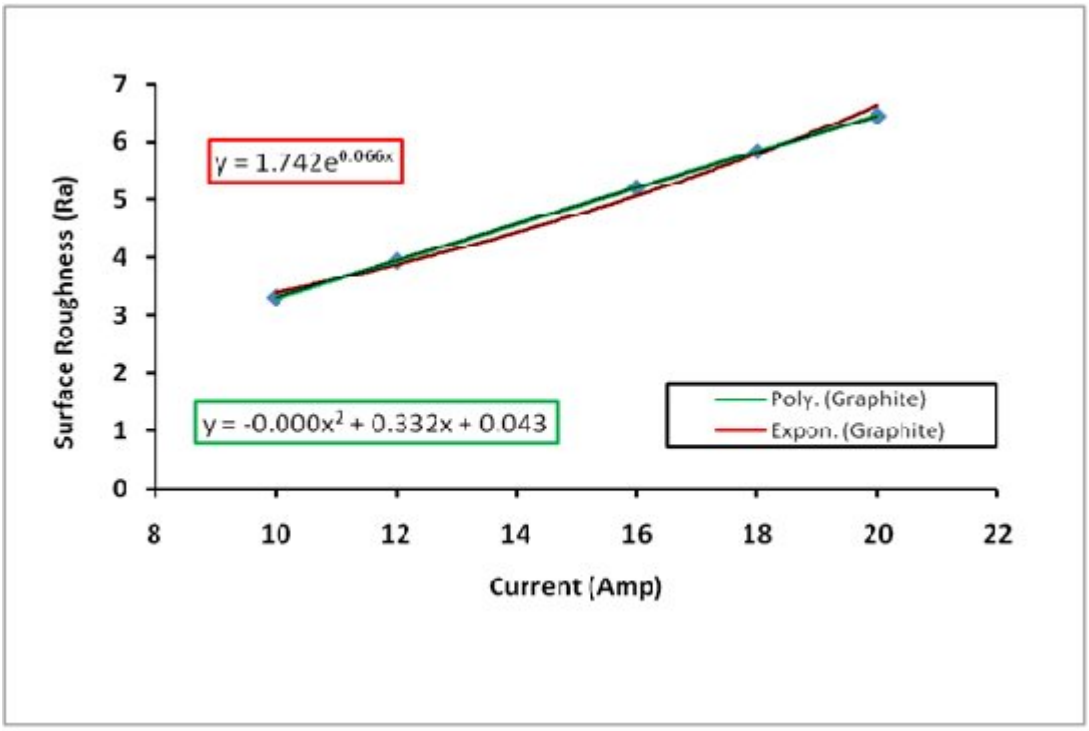

Fig. 3.17: Effect of current on surface finish in case of graphite electrode (excluding 14 Amp)

Table 3.12.3 Comparison between exponential and quadratic models in case of graphite electrode (excluding 10amp)

Discharge current (Amp)	R_a (µm)	Exponential Model		Quadratic Model	
		calculated value (exponential model)	% difference in calculated and actual	calculated value polynomial model	% difference in calculated and observed
12	3.94	4.003	1.562	3.972	0.806
14	4.59	4.522	-1.507	4.624	0.735
16	5.2	5.109	-1.789	5.268	1.291
18	5.84	5.771	-1.187	5.904	1.084
20	6.44	6.520	1.232	6.532	1.408
10	3.31	3.543	6.572	3.312	0.060

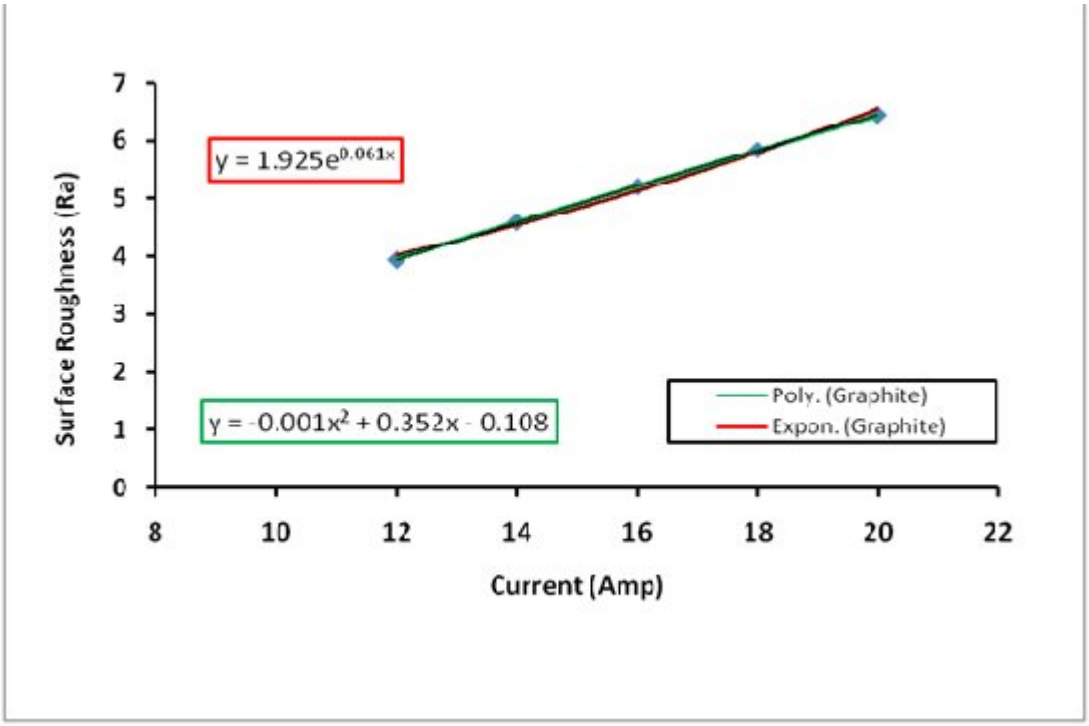

Fig. 3.18: Effect of current on surface finish in case of graphite electrode (excluding 10 Amp)

Table 3.12.4 Comparison between exponential and quadratic models in case of graphite electrode (excluding 20 Amp)

Discharge current (Amp)	R_a (µm)	Exponential Model		Quadratic Model	
		calculated value (exponential model)	% difference in calculated and actual	calculated value polynomial model	% difference in calculated and observed
10	3.31	3.359	1.457	3.176	-4.219
12	3.94	3.864	-1.975	3.828	-2.926
14	4.59	4.444	-3.278	4.480	-2.455
16	5.2	5.112	-1.718	5.132	-1.325
18	5.84	5.880	0.687	5.784	-0.968
20	6.44	6.764	4.791	6.436	-0.062

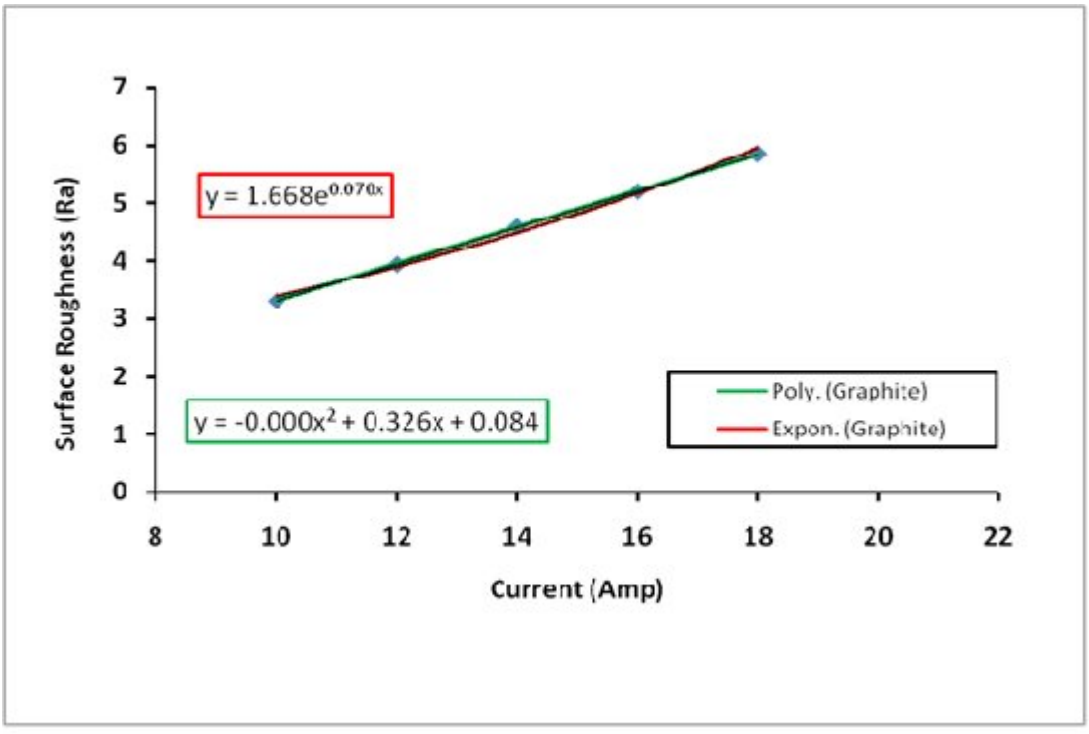

Fig. 3.19: Effect of current on surface finish in case of graphite electrode (excluding 20 Amp)

Table 3.13.1 Comparison between exponential and polynomial models with copper tungsten electrode

Discharge current (Amp)	R_a (μm)	Exponential Model		Quadratic Model	
		calculated value (exponential model)	% difference in calculated and actual	calculated value polynomial model	% difference in calculated and observed
10	2.81	2.598	-8.171	2.764	-1.664
12	2.74	2.781	1.458	2.650	-3.396
14	2.78	2.976	6.592	2.688	-3.423
16	2.99	3.186	6.141	2.878	-3.892
18	3.41	3.410	-0.007	3.220	-5.901
20	3.91	3.650	-7.132	3.714	-5.277

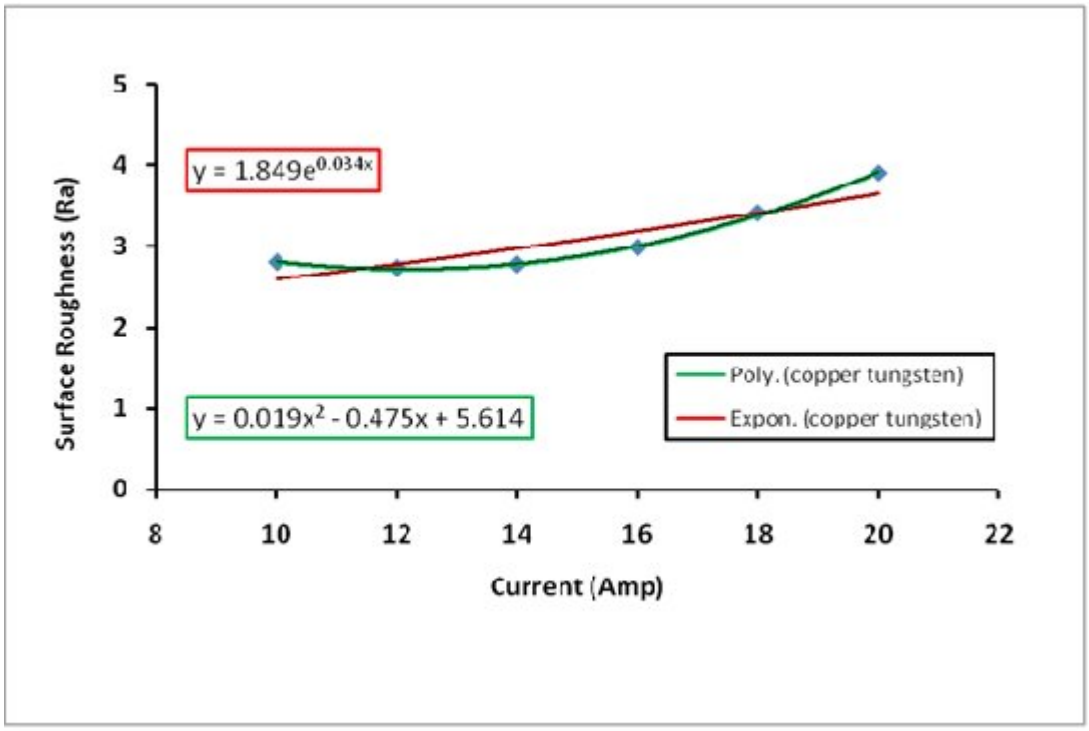

Fig. 3.20: Effect of current on surface finish in case of graphite electrode (comparison of computed and observed results)

Table 3.13.2 Comparison between exponential and polynomial models

(Interpolation i.e. 14 Amp excluded)

Discharge current (Amp)	R_a (µm)	Exponential Model		Quadratic Model	
		calculated value (exponential model)	% difference in calculated and actual	calculated value polynomial model	% difference in calculated and observed
10	2.81	2.628	-6.943	2.789	-0.753
12	2.74	2.801	2.186	2.689	-1.897
16	2.99	3.184	6.085	2.945	-1.528
18	3.41	3.394	-0.467	3.301	-3.302
20	3.91	3.618	-8.056	3.809	-2.652
14	2.78	2.986	6.910	2.741	-1.423

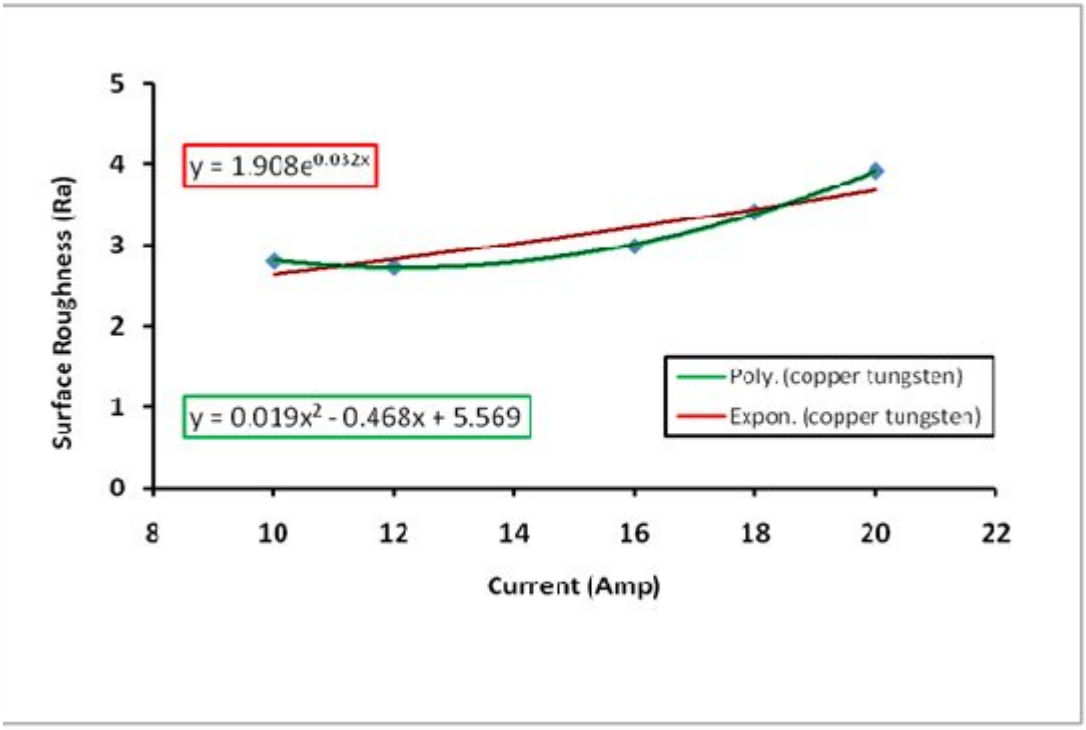

Fig. 3.21: Effect of current on surface finish in case of copper tungsten electrode (excluding 14 Amp)

Table 3.13.3 Comparison between exponential and polynomial models

(Extrapolation low i.e. 10 Amp excluded)

Discharge current (Amp)	R_a (µm)	Exponential Model		Quadratic Model	
		calculated value (exponential model)	% difference in calculated and actual	calculated value polynomial model	% difference in calculated and observed
12	2.74	2.588	-5.884	2.710	-1.107
14	2.78	2.831	1.817	2.756	-0.871
16	2.99	3.098	3.489	2.962	-0.945
18	3.41	3.390	-0.595	3.328	-2.464
20	3.91	3.709	-5.417	3.854	-1.453
10	2.81	2.365	-18.815	2.824	0.496

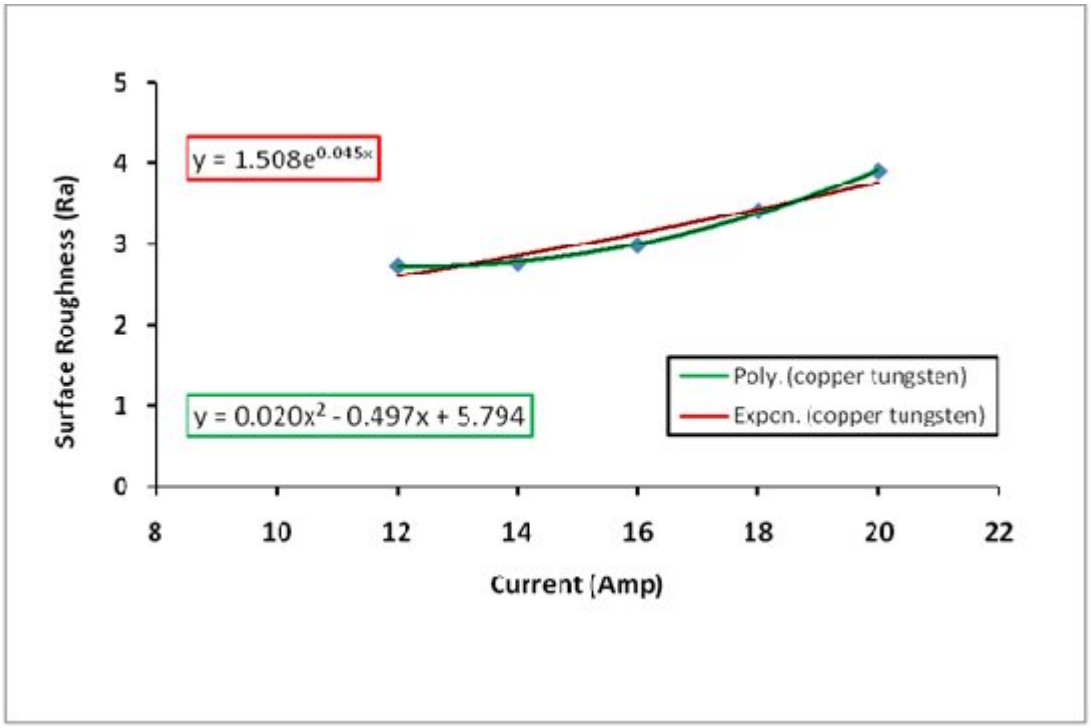

Fig. 3.22: Effect of current on surface finish in case of copper tungsten electrode (excluding 10 Amp)

Table 3.13.4 Comparison between exponential and polynomial models (excluding20 Amp)

Discharge current (Amp)	R_a (µm)	Exponential Model		Quadratic Model	
		calculated value (exponential model)	% difference in calculated and actual	calculated value polynomial model	% difference in calculated and observed
10	2.81	2.365	-18.815	2.824	0.496
12	2.74	2.588	-5.884	2.710	-1.107
14	2.78	2.831	1.817	2.756	-0.871
16	2.99	3.098	3.489	2.962	-0.945
18	3.41	3.390	-0.595	3.328	-2.464
20	3.91	3.709	-5.417	3.854	-1.453

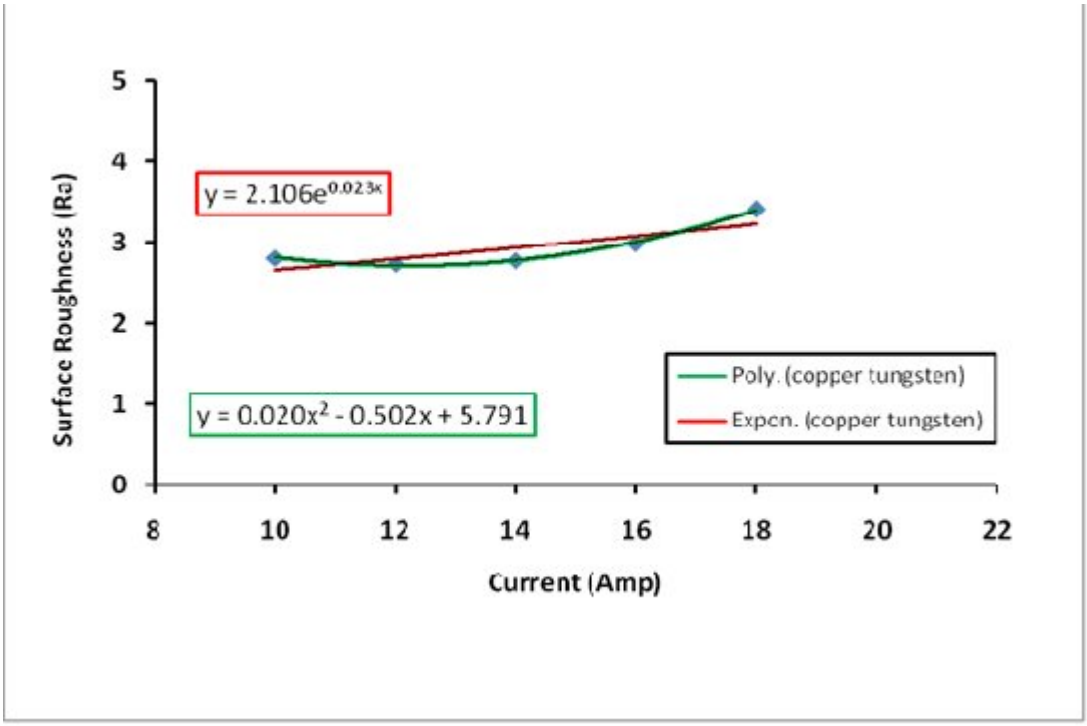

Fig. 3.23: Effect of current on surface finish in case of copper tungsten electrode (excluding 20 Amp)

Table 3.14.1 Comparison between exponential and polynomial models with copper electrode					
Discharge current (Amp)	**R_a (µm)**	**Exponential Model**		**Quadratic Model**	
		calculated value (exponential model)	**% difference in calculated and actual**	**calculated value polynomial model**	**% difference in calculated and observed**
10	0.94	1.153	18.505	0.978	3.885
12	1.49	1.367	-8.983	1.570	5.096
14	1.94	1.621	-19.714	2.018	3.865
16	2.21	1.921	-15.055	2.322	4.823
18	2.34	2.277	-2.778	2.482	5.721
20	2.32	2.699	14.031	2.498	7.126

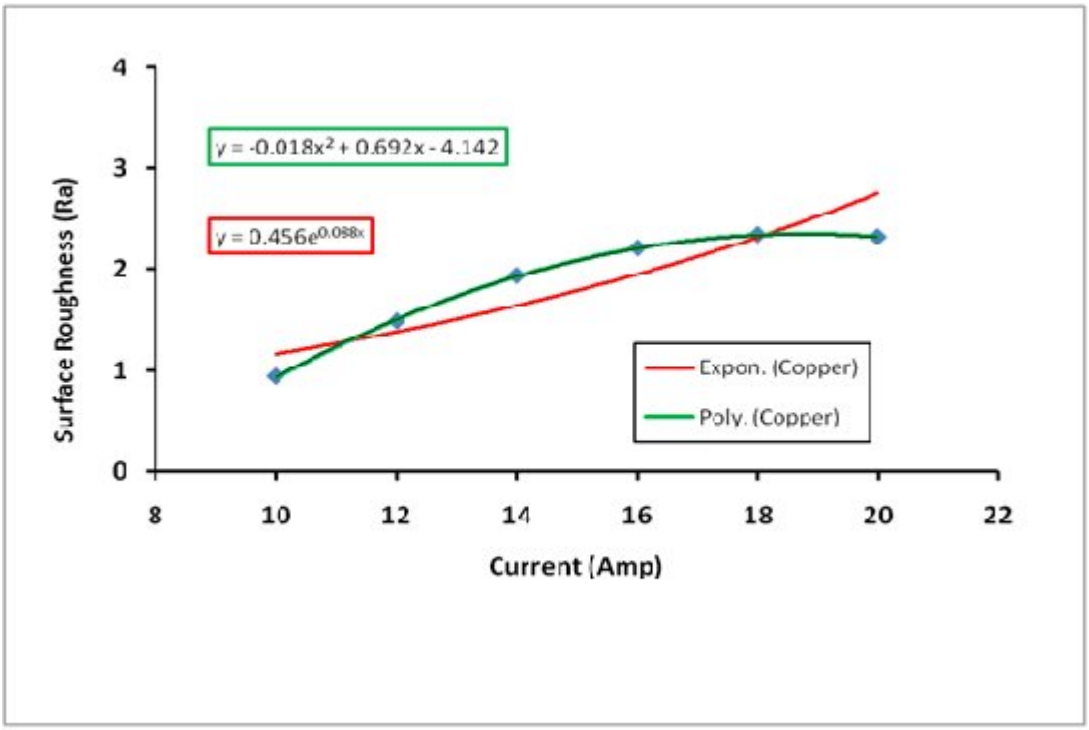

Fig. 3.24: Effect of current on surface finish in case of copper tungsten electrode (comparison of computed and observed results)

Table 3.14.2 Comparison between exponential and polynomial models

(Interpolation i.e. 14 Amp excluded)

Discharge current (Amp)	R_a (µm)	Exponential Model		Quadratic Model	
		calculated value (exponential model)	% difference in calculated and actual	calculated value polynomial model	% difference in calculated and observed
10	0.94	1.099	14.497	0.946	0.634
12	1.49	1.311	-13.660	1.522	2.102
16	2.21	1.864	-18.561	2.242	1.427
18	2.34	2.223	-5.276	2.386	1.928
20	2.32	2.650	12.468	2.386	2.766
14	1.94	1.563	-24.104	1.954	0.716

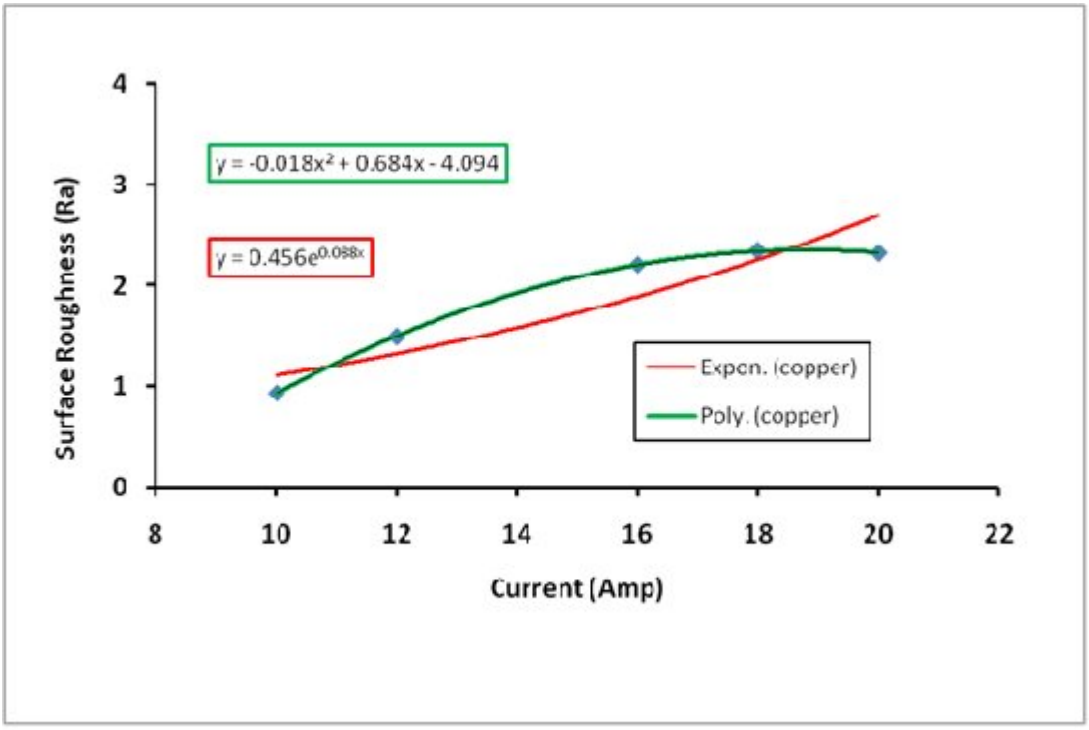

Fig. 3.25: Comparison of computed and observed results 14 Amp excluded

Table 3.14.3 Comparison between exponential and polynomial models
(Extrapolation low i.e. 10 Amp excluded)

Discharge current (Amp)	R_a (µm)	Exponential Model		Quadratic Model	
		calculated value (exponential model)	% difference in calculated and actual	calculated value polynomial model	% difference in calculated and observed
12	1.49	1.626	8.384	1.534	2.868
14	1.94	1.808	-7.288	1.986	2.316
16	2.21	2.010	-9.928	2.286	3.325
18	2.34	2.235	-4.688	2.434	3.862
20	2.32	2.485	6.646	2.430	4.527
10	0.94	1.463	35.739	0.930	-1.075

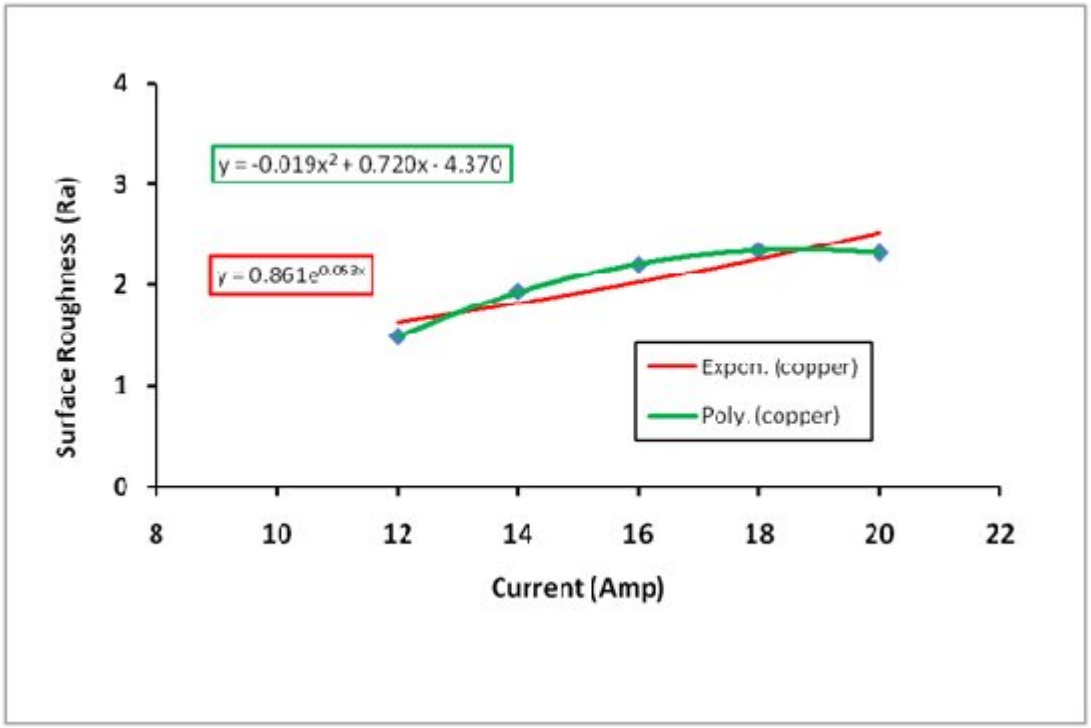

Fig. 3.26: Comparison of computed and observed results 10 Amp excluded

Table 3.14.4 Comparison between exponential and polynomial models when 20 Amp excluded

Discharge current (Amp)	R_a (µm)	Exponential Model		Quadratic Model	
		calculated value (exponential model)	% difference in calculated and actual	calculated value polynomial model	% difference in calculated and observed
10	0.94	1.078	12.842	0.956	1.674
12	1.49	1.344	-10.872	1.536	2.995
14	1.94	1.675	-15.849	1.972	1.623
16	2.21	2.087	-5.911	2.264	2.385
18	2.34	2.600	10.005	2.412	2.985
20	2.32	3.240	28.395	2.416	3.974

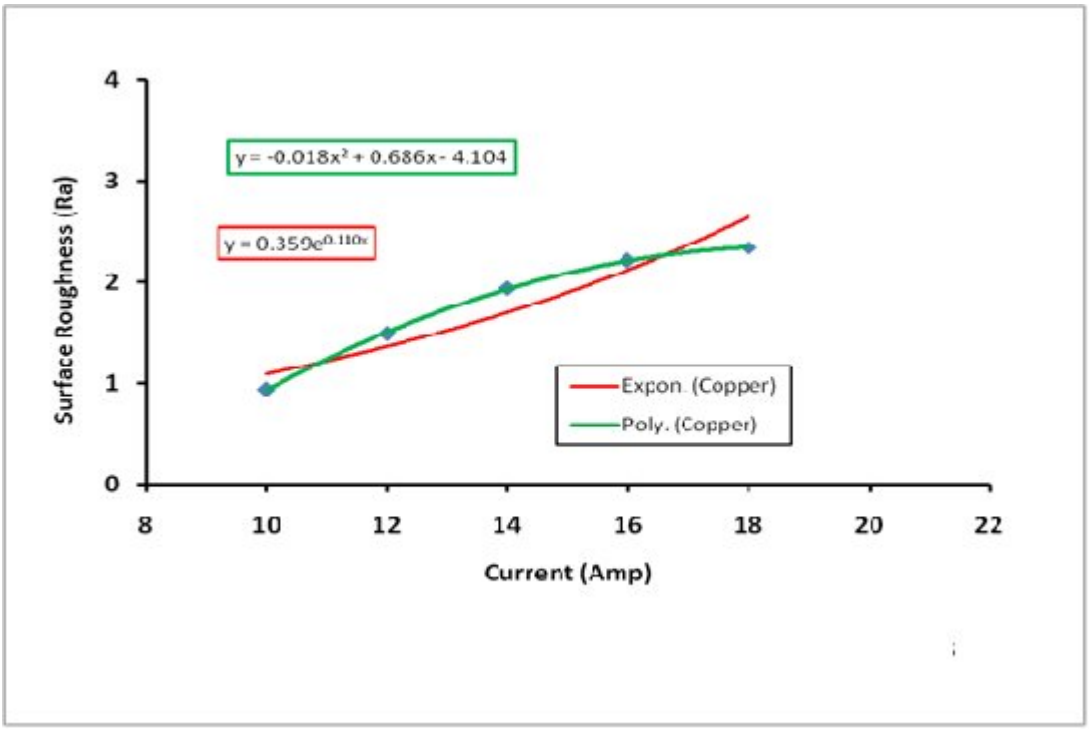

Fig. 3.27: Comparison of computed and observed results 20 Amp excluded

3.3.2 Structural Analysis

The work piece material, before EDM, exhibits the presence of WC phase indicating that it is pure tungsten carbide. It does not show any peaks of W_2C. However, presence of Fe and Co was also noticed as shown in the X-ray diffractrogram (Fig. 3.28). Further, the presence of these elements was detected by Energy Dispersive Spectroscope (EDX) as already shown in Fig. 3.1.

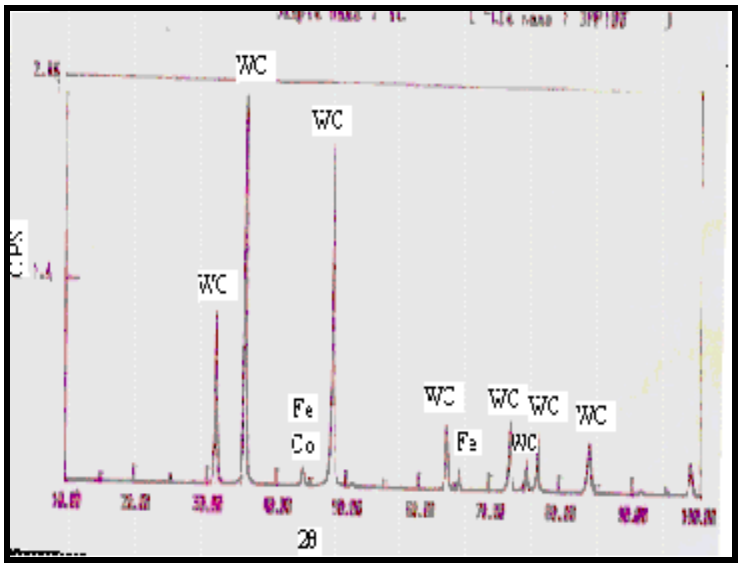

Fig. 3.28: XRD Pattern of WC workpiece

In order to verify the homogeneity of the material, the tungsten carbide work piece was analysed under the optical microscope after mechanical polishing and etching. The structural features observed are shown in Fig. 3.29.

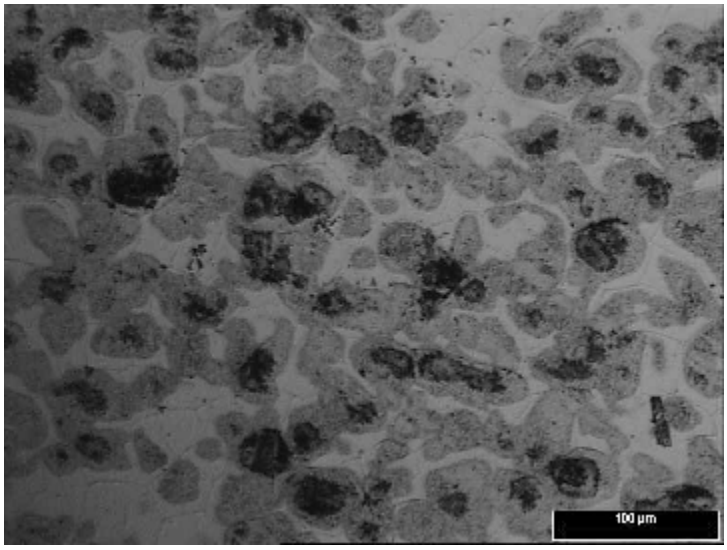

Fig. 3.29: Polished and Unmachined sample of WC

It can be visualised from the micrograph that WC is uniformly distributed throughout the material in the matrix of cobalt. The substance does not exhibit any porosity indicating that it is a well compacted and sintered substance, as can be seen in the higher magnification micrograph (Fig. 3.30) where the grains can be easily distinguished. The average grain size of the workpiece material is 40 µm.

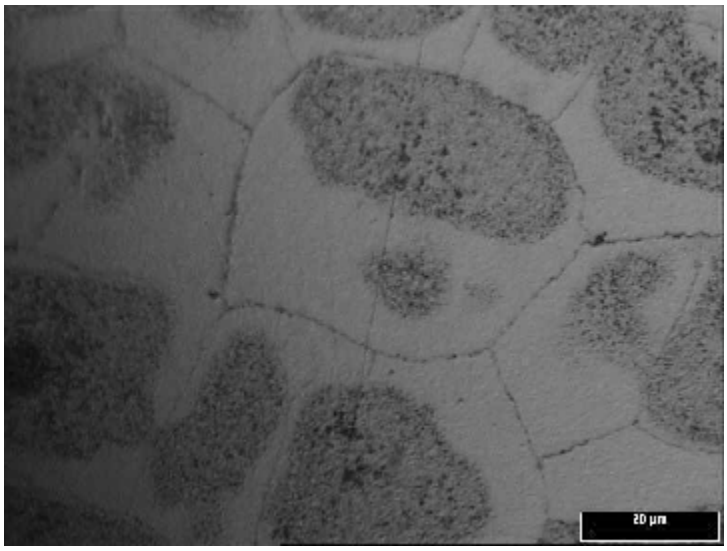

Fig. 3.30: Unmachined sample of WC

While analysing the machining parameters it was observed that MRR of the workpiece material increases linearly with an increase in pulse current what so ever the pulse duration persists. However, the R_a factor was observed to vary non-linearly. In order to understand

this variation the structural features of the workpiece material after machining was studied under SEM.

Though the structural analysis was done for each set of experiments performed, in the present investigation only a few select cases with prominent features are being presented here. While analysing the structure of the workpiece material, certain parameters were kept in mind. Included peak current (15 Amp) with and type of flushing involved i.e. suction, pressure and side.

Fig. 3.8 represents the micrograph of the tungsten carbide workpiece material machined using a graphite electrode at 15 amp current, 50 µs pulse duration with pressure flushing. Microstructure reveals the existence of different sizes of craters along the micro-cracks throughout the work piece. During the course of machining the sudden heating leads to the loosening of the substance all along the grain boundary. Since grain boundaries are the weak points, the grains chip out from the material. The higher magnification micrograph (Fig. 3.31) clearly indicates that there are patches of bigger size of the crater here and there observed in the structure.

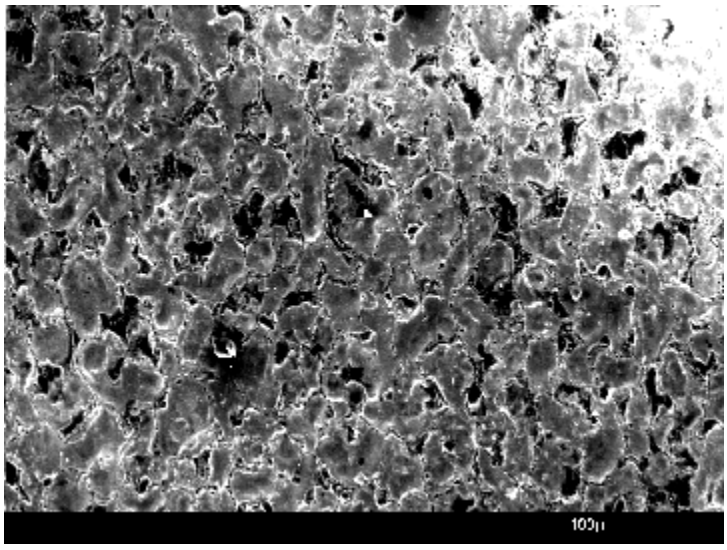

Fig. 3.31: Machined sample of WC6, Magnification 100x

The depth of the crater formed looks to be deeper. The formation of cracks appears to be due to thermal stress. The low melting point constituent like cobalt (which is a network structure as observed in the blank sample before EDM) starts melting first, thus making the grain very loose and under the influence of high temperature, grain boundary sliding takes place, thus providing a path for chipping out of entire grain. Because of these reasons, the value of the surface roughness is higher as compared to the experiments performed with

other electrodes under similar conditions. The chipping off phenomenon under the influence of grain boundary sliding supports the fact that the formation of contour can be seen from the nearby area from where the substance has chipped out (Fig. 3.31).

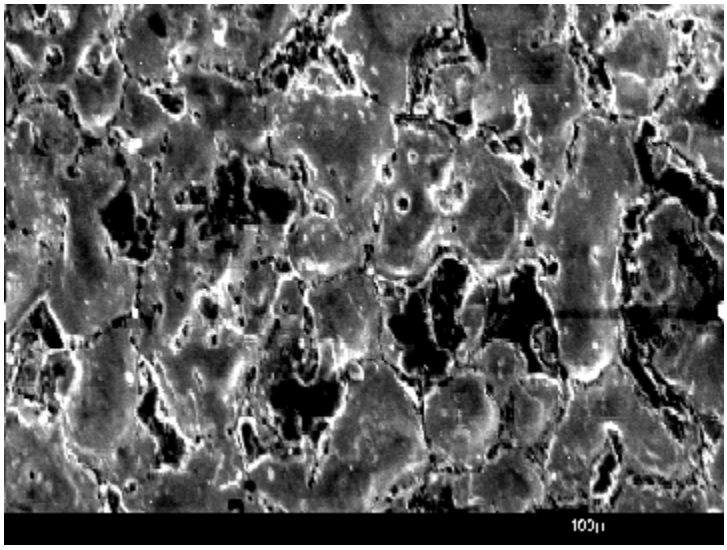

Fig. 3.32: Machined sample of WC6, Magnification 250x

In order to establish the loosening mechanism of the grain, the compositional analysis was done at the centre of the crater as well as at periphery of the grain, which is represented in Fig. 3.32 and 3.33 respectively. The amount of cobalt within the crater was found to be more (6.07%) as compared to the other area where it was nearly 5% (4.97%). Though this variation is very less but it clearly indicates that at first a partial melting of cobalt has occurred, which at a later stage gets evaporated. The loss of cobalt which acts as a binder exposes the fresh surface of tungsten carbide which provides a path for loosening of the grain. Because of this phenomenon thermal stresses are developed leading to formation of cracks which are intergranular in nature as exhibited by the microstructure.

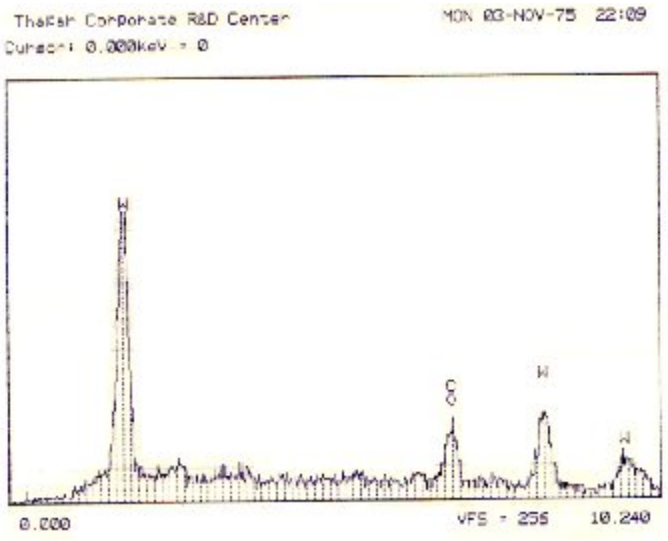

Fig. 3.33: Chemical Compositional Analysis of WC6 Black Phase

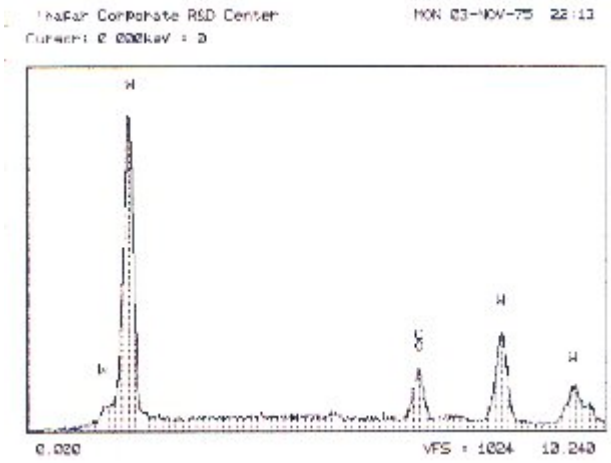

Fig. 3.34: Chemical Compositional Analysis of WC6 Grey Phase

Fig. 3.34 represents the micrograph of the workpiece material where the machining has been done using the copper electrode at 15 amp peak current with 200 µs pulse duration and under suction flushing. The structure appears to be wavy in nature. The existence of smaller to bigger size of the crater is evident. The structure reveals the presence of a white layer to a greater extent, indicating that the phenomenon of resolidification is dominating one. The structure gives the appearance of a river bed pattern which is characteristic of erosion phenomena [19].

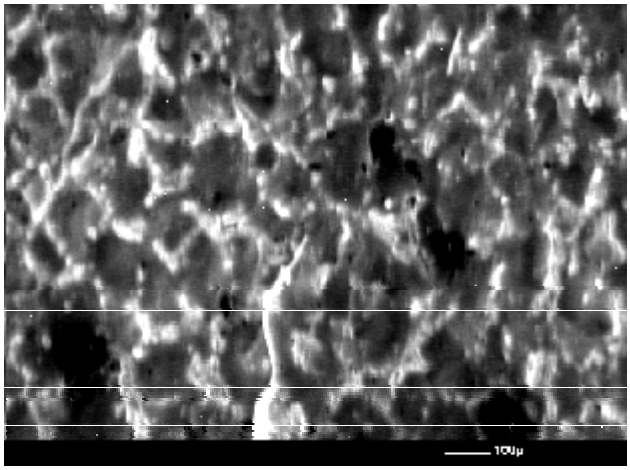

Fig. 3.35: Machined sample of WC4, Magnification 50x

Fig. 3.35 presents the view of micrograph of the tungsten carbide workpiece using the copper tungsten electrode when machining parameters were 15 amp current, 100 μs pulse duration and with side flushing condition. The structure gives the appearance of three types of areas. These are dark, grey and white.

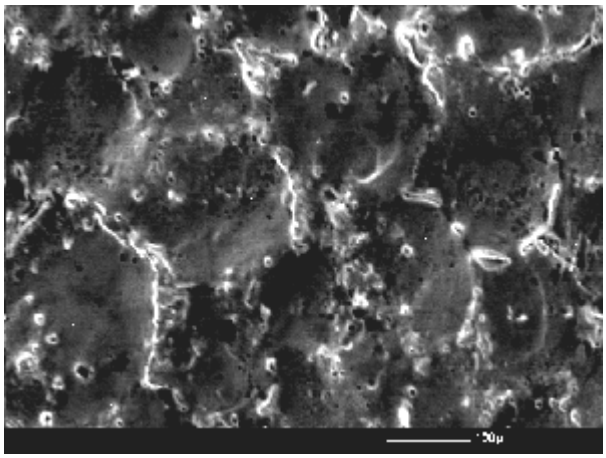

Fig. 3.36: Machined sample of WC4, Magnification 100x

The dark area represents the existence of deep craters, the grey area represents the shallow craters with heat affected zone and the white phase represents a resolidified layer. The structural features observed in the work piece material where machining was done using the copper tungsten electrode in all the experiments were similar. The structure obtained is fascinating one as it gives a minimum R_a value as compared to the workpiece material where the other two electrodes were used. The analysis of structure indicates that the erosion phenomenon is more uniform and craters formed are shallow in nature. Further, there are

certain areas where deep small craters existed from where the substance has chipped off, these appear as black areas. The structure reveals that the loss of material takes place by the phenomenon of melting and evaporation, both occuring simultaneously. The network of the white layer observed corresponds to the resolidified layer. The presence of cracks all along these networks indicates that the mechanism of crack formation is due to mechanical stresses which is evident more clearly in higher magnification micrograph (Fig. 3.36).

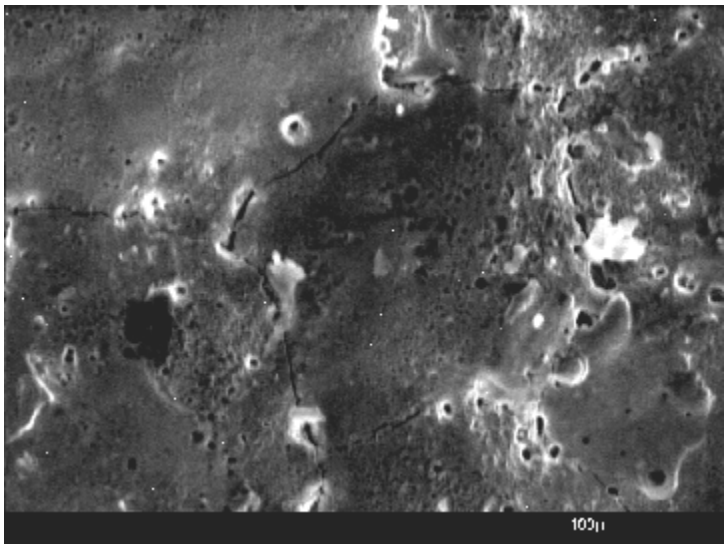

Fig. 3.37: Machined sample of WC4, Magnification 250x

The flow pattern observed all along these materials indicates that the side flushing was involved. The presence of projected smooth, molten layer all along the crater, in which small size volcanic eruptions are, indicates that material beneath this white layer was still in the liquid state.

Figure 3.37 shows the micrograph taken from the area near the junction of two cracks. The structural features indicate that a tearing phenomenon which is typical of tensile stress has occurred.

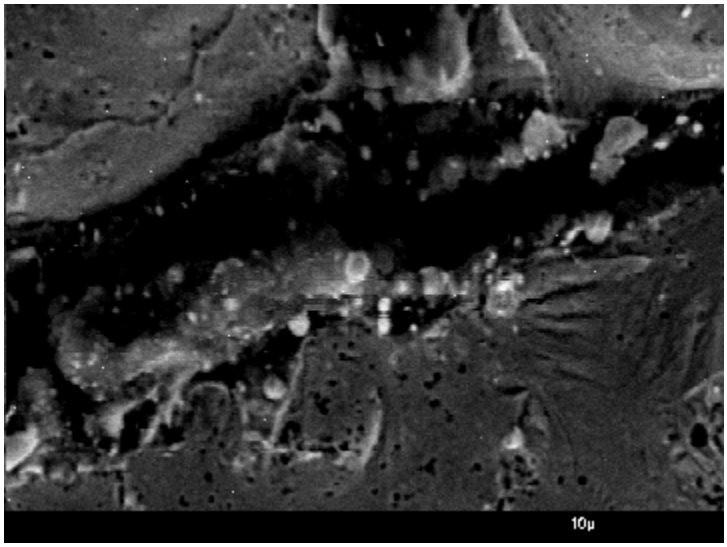

Fig. 3.38: Micrograph showing junction of two cracks, Magnification 6000x

The loss of material is because of melting followed by its evaporation that can be observed from the features existing at the interface of the crack. The presence of grain boundary (top left side corner) indicates that the initiation of crack has not occurred from the grain boundary; instead it has started from the area where the resolidified layer exists. The compositional analysis was done from the dark phase (deep crater), the grey phase (shallow craters) and the white phase as given in Table 3.15.

Table 3.15: Chemical composition of black phase, Grey phase, white phase for work piece WC4 and WC6

Workpiece	Phase	W %	Co %	Cu %
WC4	Black Phase	89.23	7.41	3.36
WC4	Grey Phase	95.78	4.22	Nil
WC4	White Phase	94.90	5.10	Nil
WC6	Black Phase	93.93	6.07	Nil
WC6	Grey Phase	95.03	4.97	Nil
WC6	White Phase	94.90	5.10	Nil

The most important feature observed was that percentages of cobalt in the dark areas were observed to be more as compared to the other two areas. The presence of copper in the deep crater indicates that melting of electrode has occurred. This has led to the deposition of copper while in molten stage inside the crater (Fig. 3.39). The analysis carried out from the grey phase indicated the presence of lower cobalt content indicating that loss of cobalt is more (Fig. 3.40). This is true for the white layer where Co content is 5.1% (Fig. 3.41). The

amount of contents was observed to vary from 7.41% deep craters to 4.22% (shallow craters) 5.10% in white zone (deposited layer).

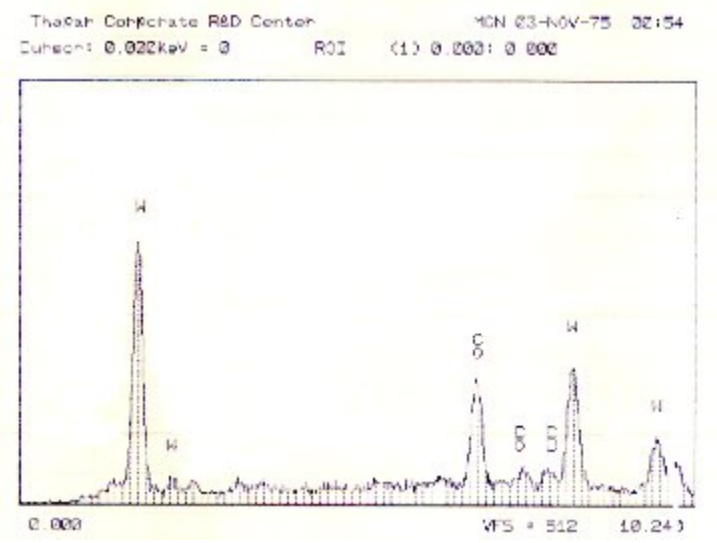

Fig. 3.39: Chemical Compositional Analysis of WC4 Black Phase

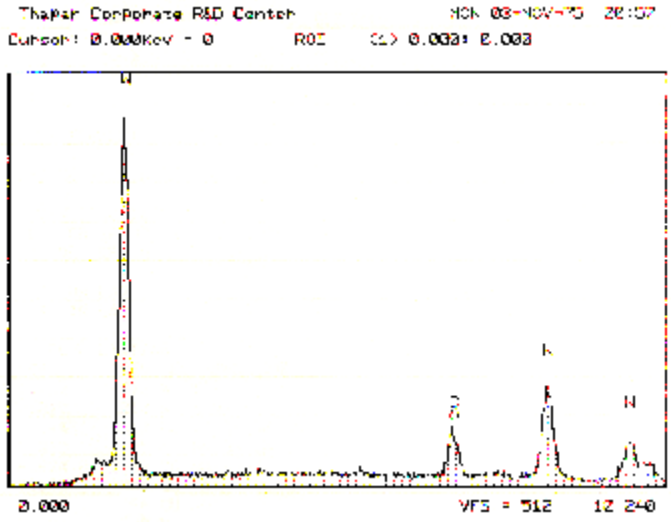

Fig. 3.40: Chemical Compositional Analysis of WC 4 Grey Phase

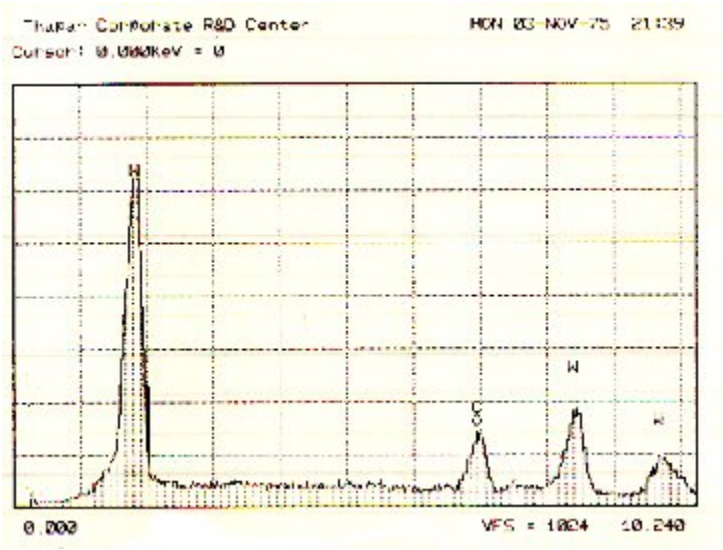

Fig. 3.41: Chemical Compositional Analysis of WC4 White Phase

After analysing the surface it was observed that certain area are rich in Co. Apart from this there is a continuous variation in W content in the entire segment, whatsoever variation in contrast is observed on the surface of the EDMed piece. It is obvious from this variation in chemical composition that there may be structural transformations which are causing the formation in cracks in the material. It is also possible that as the input energy is increased, possibility of continuous phase transformation may occur. Considering these factors a detailed study for the reason of the formation of cracks has been done which is described in next chapter.

Chapter 4

STUDY OF SURFACE CRACKS ON EDMED TUNGSTEN CARBIDE CERMET

Overview

The investigation on machining of WC-Co composite revealed that surface topography keeps on changing as the machining conditions are varied. It was also observed that the nature of cracks also varies with the variation in machining conditions are changed. In order to improve the performance of EDM process it is essential to understand the mechanism of formation of cracks, their size and distribution for each material machined at different machining conditions. An experimental study was conducted separately to study the formation of cracks and their morphology on EDMed tungsten carbide cermets under high current load. The reason for selecting high current was to improve machining performance. The copper tungsten electrode has been used for this study. Current and pulse duration have been selected as variable parameters. The objective of this investigation has been to study the phenomenon of formation of micro cracks at different energy input levels. It was observed that minimum cracks are formed at low pulse energy per unit surface area. The details of this study have been presented in this chapter.

4.1 Introduction

WC cermet is one of the materials in which cobalt is used as a binder to sinter WC particles. The amount of cobalt, which varies from 6% to 15%, determines the hardness and toughness of the carbide. The electrical conductivity of cobalt (conductor) is more than that of tungsten carbide (insulator). This helps to machine the surface by EDM process. If the machining conditions are not optimized it may lead to development of cracks [3, 9, 27, 28, 53 and 103]. Formation of these cracks is due to high tensile and compressive stresses that build up at the interface of the WC and Co binder. EDM induces metallurgical, mechanical and geometrical modifications leading to surface tensile stresses, micro cracks and roughness which can reduce the lifetime of a workpiece material [57]. The phenomenon of crack formation is related to the EDM parameters.

Work piece surface deterioration caused by the thermal effects of EDM operations can be controlled by setting the process parameters. Modern power supplies which offer a precise control over current, voltage, on-time and duty cycle may be programmed for roughing, semi-finishing or finishing work, as required by the desired results. However, there are number of problems that are being encountered during machining which require a effective control to achieve good surface finish. The most difficult task is to set specific machining parameter which varies from material to material, for avoiding surface cracks. The first major type of cracking which may be encountered during machining is the result of thermal stress. Carbide (such as tungsten carbide or silicon carbide) is particularly susceptible to this problem [31, 35]. These stresses can lead to formation of cracks which propagate further during each spark discharge. Thermal stress cracking is as deep as the reach of the pulse energy [15, 42, 47, and 80]. The work done so far on machining of WC-Co is limited [36, 39, 44, 55 and 67]. Moreover, in these published works, the machining conditions opted are also different. In order to maintain surface integrity along with high machining rates the reasons underlying the occurrence of surface cracks has to be investigated.

Considering the above facts, the present study was planned to investigate the formation of cracks at different machining conditions in WC-Co composite which is extensively used in different dies and tool manufacturing industries.

4.2 Experimental Set-up

In this investigation, series of experiments were conducted on tungsten carbide cermet using Charmilles Technologies Roboform 40 EDM Die-Sinking Machine, energized by a 64A pulse generator. The tool electrodes were made of copper tungsten.

The dielectric fluid used was Total EDM 22 with a viscosity of 3.4 cst (mm^2/s) at 20 ^0C and density of 812 kg/mm^3. Fresh dielectric fluid was provided to the tool/work piece interface via an adjustable nozzle using lateral sweep flushing. The schematic diagram of EDM process is shown in Fig. 4.1 and chemical composition of work piece and electrode is already given in Table 3.1 and part of its segment required in present study is reperesented in Table 4.1. The work piece and tool had same cross-sectional area of 20mm diameter.

Table 4.1: Chemical composition (wt %) of workpiece and electrode materials

Element→ Material↓	W%	Cu%	Al %	Ni %	Sn %	Zn %	Si %	Fe %	Cr %	Co %	C %
Tungsten Carbide	93.37	-	-	-	-	-	-	1.41	0.34	4.89	-
Copper Tungsten	1.11	81.09	14.07	1.61	0.11	1.01	0.88	0.03	-	-	-

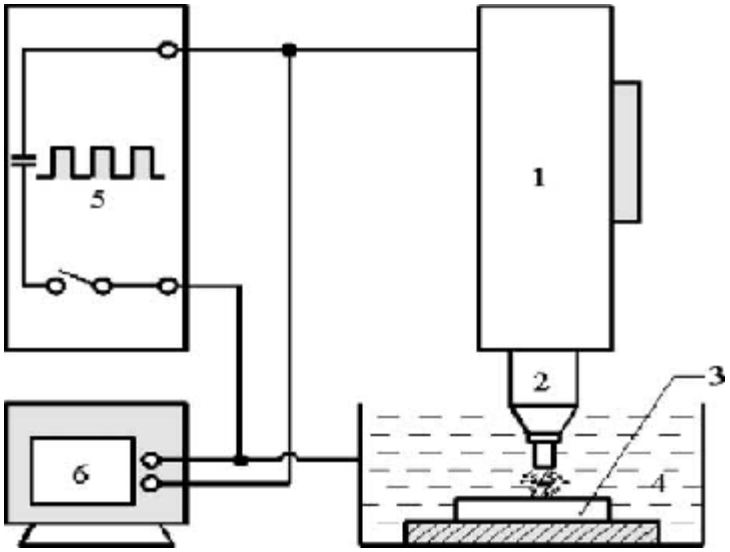

Fig. 4.1: Schematic diagram of the EDM process (1: servo-control; 2: electrode; 3: specimen; 4: dielectric fluid; 5: pulsed generator; 6: oscilloscope).

The work piece material, after mechanical polishing, was analysed under microscope. The microstructural analysis of the workpiece material was done with the help of the optical microscope (model Nikon100, Japan). For this, the samples were mechanically polished and etched with Murakami reagent (solution of 10gm potassium ferricynide and 10gm sodium

hydroxide in 100 ml water). The morphological features of EDMed workpiece material were analyzed under SEM (Model GEOL 840x). The crystal structure of phases present in the material was determined by the X-ray diffractogram (Rigaku model-Geiger) with Cu K_α radiation.

After EDM operations, the machined work piece surfaces were examined, and then the work pieces were cut into halves perpendicular to the EDMed surface with a wire cut EDM, so that the section of the EDMed surface could be revealed. The cut surfaces were then polished with emery papers and diamond paste of reducing grain sizes. This was followed by polishing with alumina (Al_2O_3) solution and etching with Murakami reagent. The polished and etched surface was examined under optical microscope at different magnifications to determine the size and shape of the cracks generated by EDM.

4.3 Process Parameters

The range of parameters have been selected (by trial and error method and previous references) whereby the experiments could be conducted without facing the hindrance of arcing [26, 60 and 92]. The fixed parameters which are kept constant during all the experiments and variable parameters, which were varied with every experiment, are given in table 4.2 and table 4.3 respectively.

Table 4.2: Fixed Parameters

Voltage(V)	60
Flushing	Side Flushing
Duty Factor	0.8-0.9
Polarity	Straight or Positive polarity: Work piece - Anode (positive) Electrode – Cathode (negative)

Table 4.3: Variable Parameters

Discharge Current (Amp)	5	10	15	20	25	30	35	40
Pulse Duration (μs)	100	100	100	100	100	100	100	100
	50	50	50	50	50	50	50	50

4.4 Analysis of experimental results for pulse duration:

In chapter 3, a detailed analysis of observed results has been done. Here in the present chapter, the range of processing variables has been enlarged from 5 Amp to 40 Amp. Now the results so obtained are analysed for the quadratic or exponential models and is discussed briefly. An exponential curve of the type $y = ae^{bx}$ or power curve of the type $y = ax^{xb}$ or a curve of the type $y = a + bx + cx^2$ can be fitted to the experimental results using method of least square. We have not tried the quadratic curve of the type $y = a + bx + cx^2$ as it was expected to be included in exponential type of curve $y = ae^{bx}$ since $(e^x = 1 + x + \frac{x^2}{2} \ldots \ldots)$.

Validation of Material Removal Rate (MRR) for copper tungsten electrode at 50 & 100 µs Pulse Duration:

We have fitted two types of curves (power model and exponential model) to the data points given in table 4.4 taking x-axis as current and y-axis as material removal rate (MRR) using method of least square and have obtained the curve as a $y = 3.528\, e^{0.050x}$ in the exponential case and $y = 0.995\, x^{0.804}$ as power curve. These curves have been plotted and shown in Fig 4.2 along with data points. A comparison of the actual data with the curve corresponding points obtained using these two equations of the curve have also been presented in table 4.4.1.

Our results show that exponential model gives relatively a better fit to the experimental data than the power model because maximum difference between the experimental results and computed model is **16.169%** in the case of exponential and **20.593%** in case of power model.

We have also tried to see whether the analytical expression can be used for interpolation and extrapolation within reasonable limits. For this we tried to derive equations for both type of curves by first excluding points in the middle of the data (x=20 amp) and than by excluding extreme left point (x=5 amp) and extreme right point (x=40 amp). We than tried to observe the difference between experimental value of MRR and value of MRR for these points as obtained using set of remaining 7 points. These results are presented in table 4.4.2, 4.4.3 and 4.4.4. These are also shown in figure 4.3, 4.4 and 4.5 respectively.

EDM being complex machining process it is observed that due to long range of experimentation from 5 Amp to 40 Amp at the steps of 5Amp each the % difference in experiment data and the computed data from this long range shows the % difference from 0.364 to 25.852. It was interesting to find out the effect of % age variation if the lowest and highest range is removed and than once again the exercise is repeated. The results revealed that considerable % difference has reduced and these results are in the range of 0.529% to 7.859%. Detailed results are presented in table 4.4.1 to 4.4.4 and graphical presented in fig 4.2 to 4.5

Table 4.4.1 Comparison between exponential and quadratic models in case of 100µs pulse duration					
Discharge current (Amp)	**MRR (mm3/min)**	**Quadratic Model**		**Exponential Model**	
		calculated value (quadratic) model	**% difference in calculated and actual**	**calculated value (exponential) model**	**% difference in calculated and observed**
5	3.875	3.512	-10.339	4.622	16.169
10	6.055	6.333	4.387	5.897	-2.683
15	8.456	8.941	5.423	7.523	-12.408
20	10.867	11.420	4.840	9.597	-13.238
25	12.451	13.807	9.818	12.242	-1.703
30	15.561	16.123	3.484	15.618	0.364
35	19.157	18.382	-4.219	19.924	3.848
40	**23.914**	**20.593**	**-16.130**	**25.417**	**5.913**

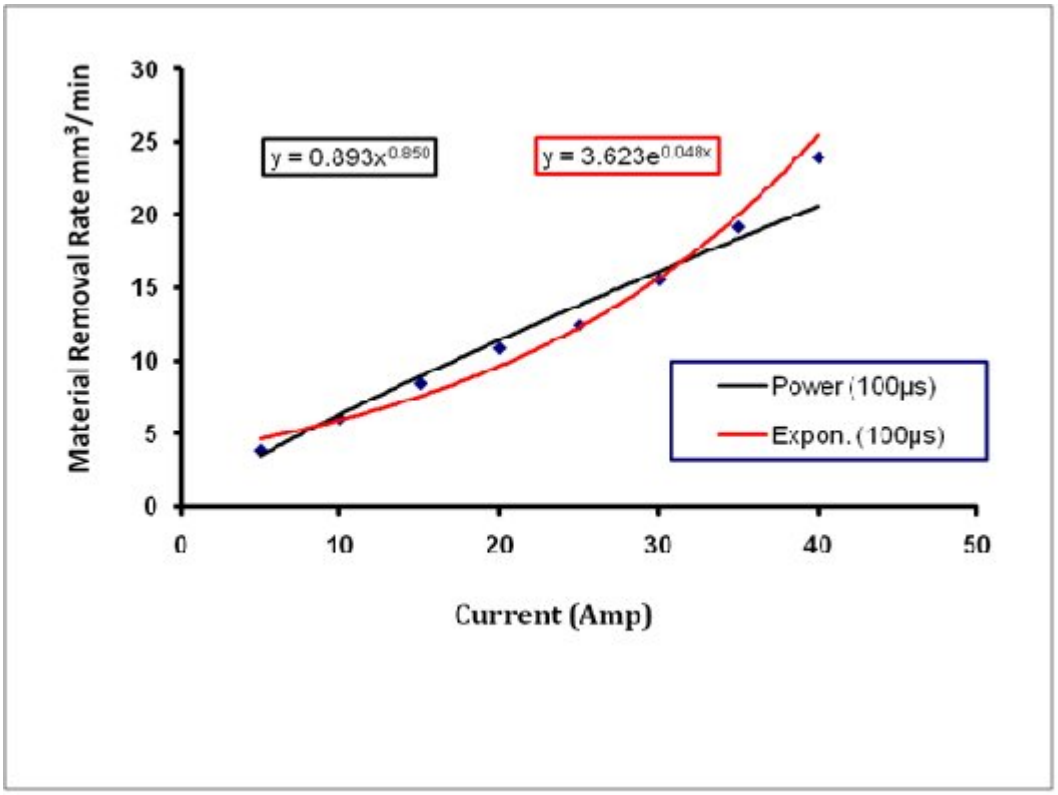

Fig. 4.2: Effect of 100µs Pulse Duration on MRR (comparison of computed and observed results)

Table 4.4.2 Comparison between exponential and quadratic models in case of 100µs pulse duration (20 Amp excluded)					
Discharge current (Amp)	**MRR (mm3/min)**	**Quadratic Model**		**Exponential Model**	
		calculated value (quadratic) model	**% difference in calculated and actual**	**calculated value (exponential) model**	**% difference in calculated and observed**
5	3.875	3.512	-10.339	4.622	16.169
10	6.055	6.333	4.387	5.897	-2.683
15	8.456	8.941	5.423	7.523	-12.408
25	12.451	13.807	9.818	12.242	-1.703
30	15.561	16.123	3.484	15.618	0.364
35	19.157	18.382	-4.219	19.924	3.848
40	23.914	20.593	-16.130	25.417	5.913
20	**10.867**	**11.420**	**4.840**	**9.597**	**-13.238**

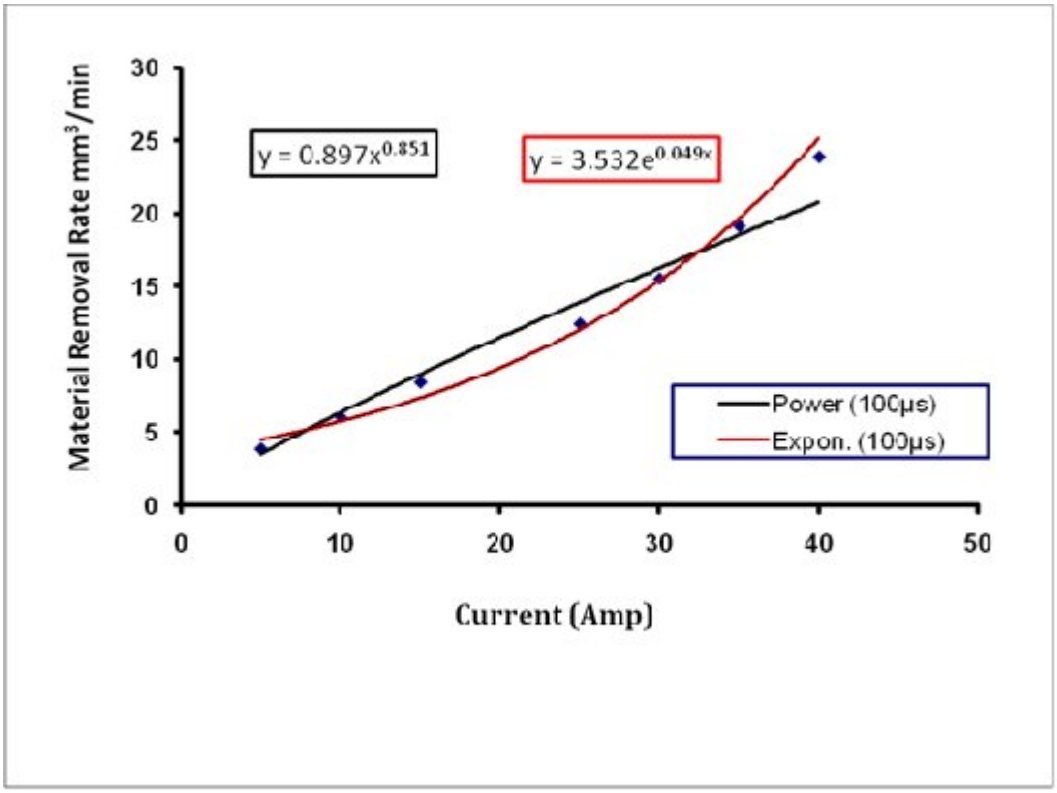

Fig. 4.3: Effect of 100µs Pulse Duration on MRR (excluding 20 Amp)

Table 4.4.3 Comparison between exponential and quadratic models in case of 100µs pulse duration (5 Amp excluded)					
Discharge current (Amp)	**MRR (mm3/min)**	**Quadratic Model**		**Exponential Model**	
		calculated value (quadratic) model	**% difference in calculated and actual**	**calculated value (exponential) model**	**% difference in calculated and observed**
10	6.055	5.735	-5.588	6.480	6.552
15	8.456	8.439	-0.196	8.034	-5.256
20	10.867	11.102	2.113	9.961	-9.099
25	12.451	13.732	9.329	12.350	-0.818
30	15.561	16.338	4.755	15.312	-1.625
35	19.157	18.923	-1.235	18.985	-0.906
40	23.914	21.491	-11.273	23.539	-1.594
5	**3.875**	**2.962**	**-30.813**	**5.226**	**25.852**

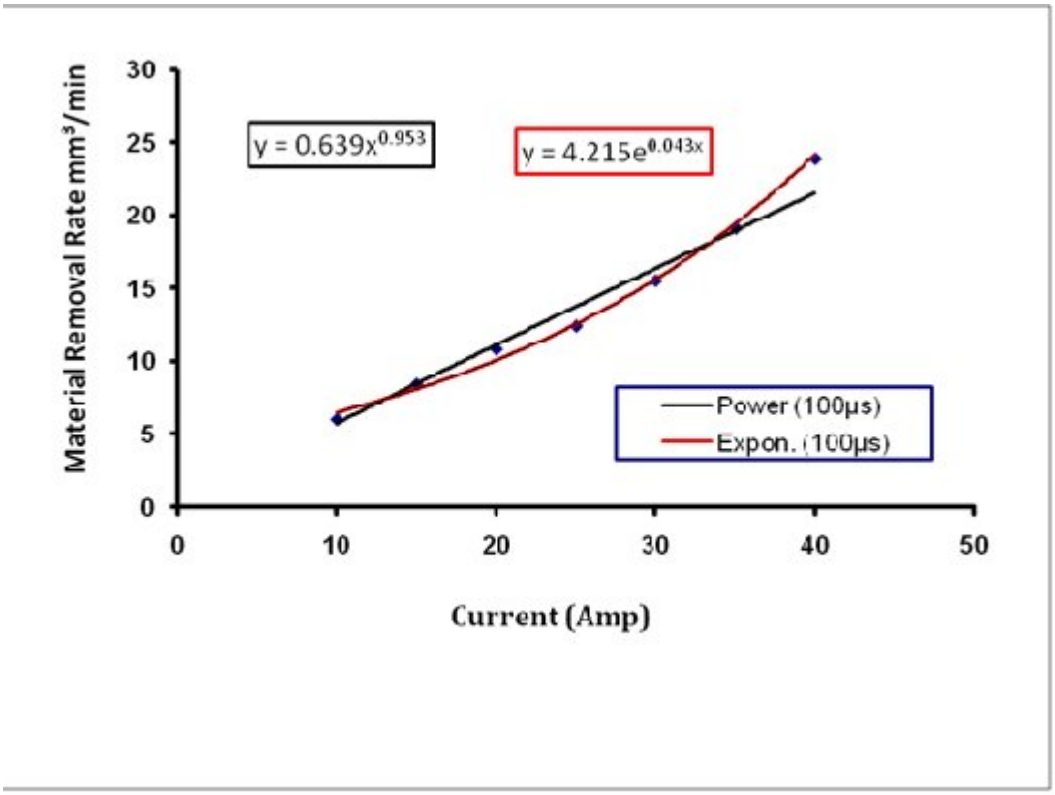

Fig. 4.4: Effect of 100µs Pulse Duration on MRR (excluding 5 Amp)

Table 4.4.4 Comparison between exponential and quadratic models in case of 100µs pulse duration (40 Amp excluded)					
Discharge current (Amp)	**MRR (mm3/min)**	**Quadratic Model**		**Exponential Model**	
		calculated value (quadratic) model	**% difference in calculated and actual**	**calculated value (exponential) model**	**% difference in calculated and observed**
5	3.875	3.629	-6.777	4.530	14.460
10	6.055	6.336	4.437	5.817	-4.097
15	8.456	8.778	3.669	7.469	-13.218
20	10.867	11.062	1.767	9.590	-13.315
25	12.451	13.236	5.933	12.314	-1.113
30	15.561	15.326	-1.533	15.811	1.584
35	19.157	17.348	-10.427	20.302	5.641
40	**23.914**	**19.314**	**-23.815**	**26.069**	**8.265**

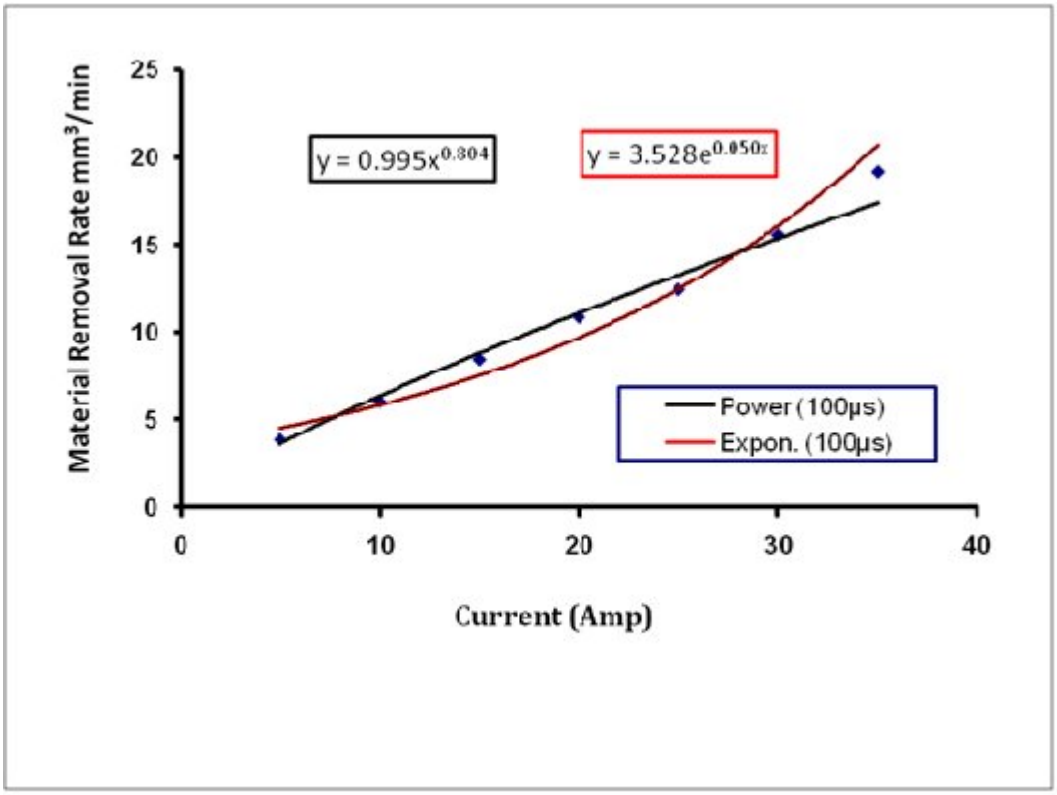

Fig. 4.5: Effect of 100µs Pulse Duration on MRR (excluding 40 Amp)

Table 4.4.5 Effect of 100µs pulse duration on MRR (comparison of computed and observation results)

Discharge current (Amp)	MRR (mm3/min)	Quadratic Model		Exponential Model	
		calculated value (quadratic) model	% difference in calculated and actual	calculated value (exponential) model	% difference in calculated and observed
10	6.055	5.896	-2.705	6.489	6.685
15	8.456	8.451	-0.063	8.085	-4.582
20	10.867	10.910	0.397	10.075	-7.859
25	12.451	13.301	6.393	12.554	0.824
30	15.561	15.639	0.499	15.644	0.529
35	19.157	17.933	-6.824	19.493	1.725

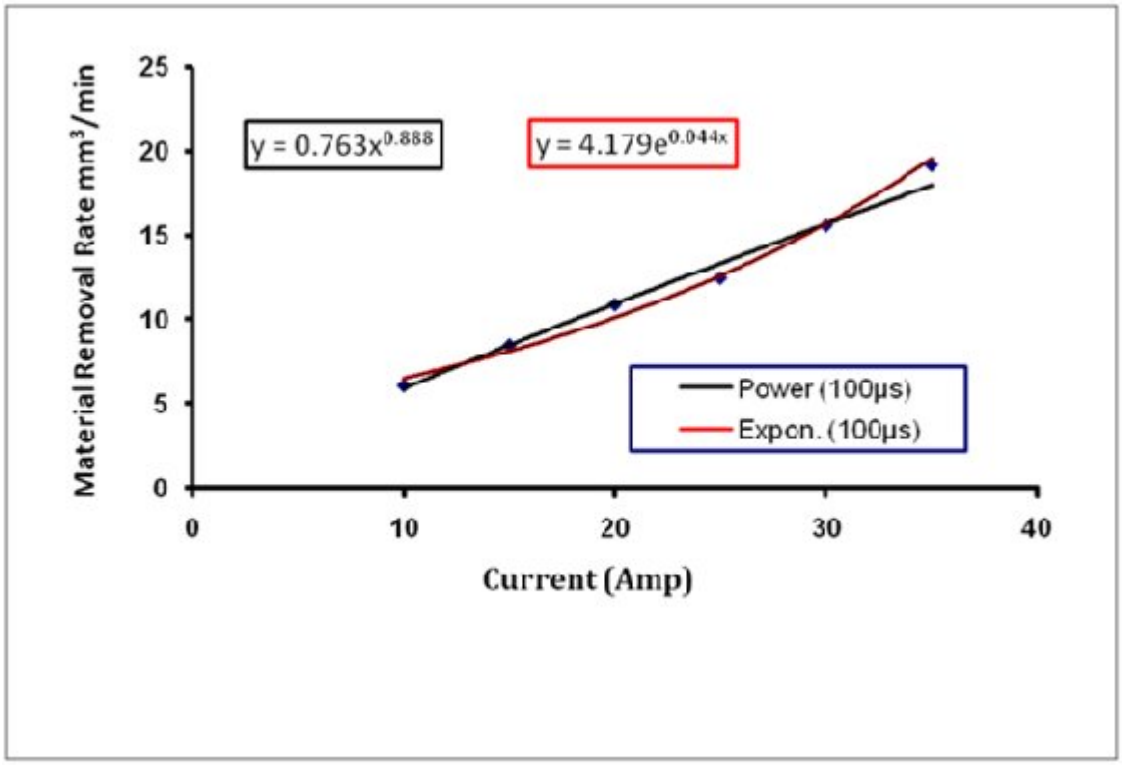

Fig. 4.6: Effect of 100µs Pulse Duration on MRR (comparison of computed and observed results)

Table 4.4.6 Comparison between exponential and quadratic models in case of 100µs pulse duration (20 Amp excluded)					
Discharge current (Amp)	**MRR (mm3/min)**	**Quadratic Model**		**Exponential Model**	
		calculated value (quadratic) model	**% difference in calculated and actual**	**calculated value (exponential) model**	**% difference in calculated and observed**
10	6.055	5.911	-2.436	6.321	4.209
15	8.456	8.473	0.199	7.877	-7.357
25	12.451	13.336	6.638	12.230	-1.807
30	15.561	15.680	0.759	15.239	-2.110
35	19.157	17.980	-6.545	18.990	-0.882
20	**10.867**	**10.939**	**0.658**	**9.815**	**-10.721**

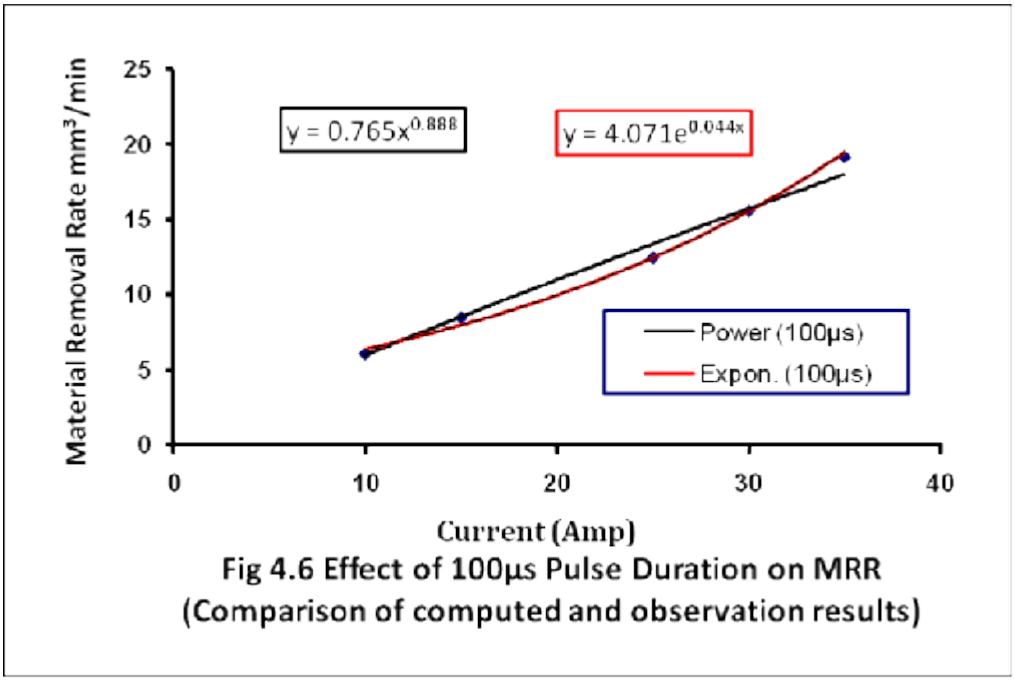

Fig. 4.7: Effect of 100µs Pulse Duration on MRR (comparison of computed and observed results)

Table 4.4.7 Comparison between exponential and quadratic models in case of 100µs pulse duration (10 Amp excluded)					
Discharge current (Amp)	**MRR (mm3/min)**	**Quadratic Model**		**Exponential Model**	
		calculated value (quadratic) model	**% difference in calculated and actual**	**calculated value (exponential) model**	**% difference in calculated and observed**
15	8.456	8.249	-2.510	8.591	1.575
20	10.867	10.798	-0.639	10.493	-3.560
25	12.451	13.306	6.426	12.817	2.853
30	15.561	15.782	1.401	15.654	0.596
35	19.157	18.232	-5.076	19.120	-0.192
10	**6.055**	**5.644**	**-7.284**	**7.034**	**13.918**

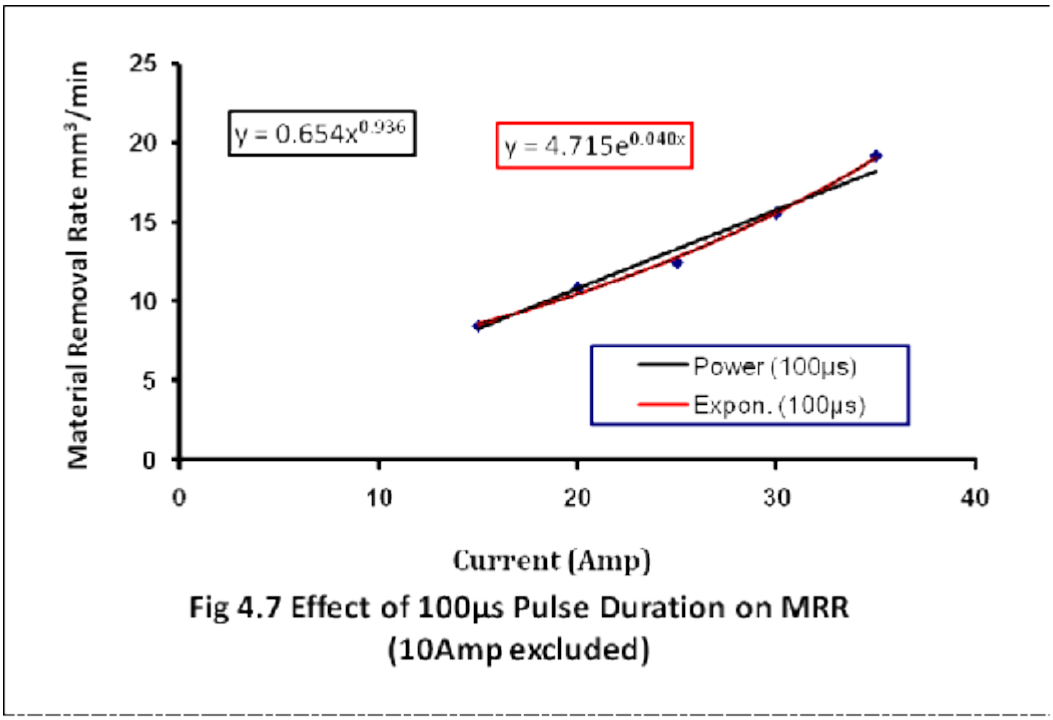

Fig. 4.8: Effect of 100µs Pulse Duration on MRR (excluding 10 Amp)

Table 4.4.8 Comparison between exponential and quadratic models in case of 100µs pulse duration (35 Amp excluded)

Discharge current (Amp)	MRR (mm3/min)	Quadratic Model		Exponential Model	
		calculated value (quadratic) model	% difference in calculated and actual	calculated value (exponential) model	% difference in calculated and observed
10	6.055	6.019	-0.605	6.408	5.511
15	8.456	8.447	-0.106	8.025	-5.370
20	10.867	10.744	-1.147	10.050	-8.130
25	12.451	12.947	3.832	12.586	1.071
30	15.561	15.079	-3.198	15.761	1.272
35	**19.157**	**17.153**	**-11.684**	**19.738**	**2.946**

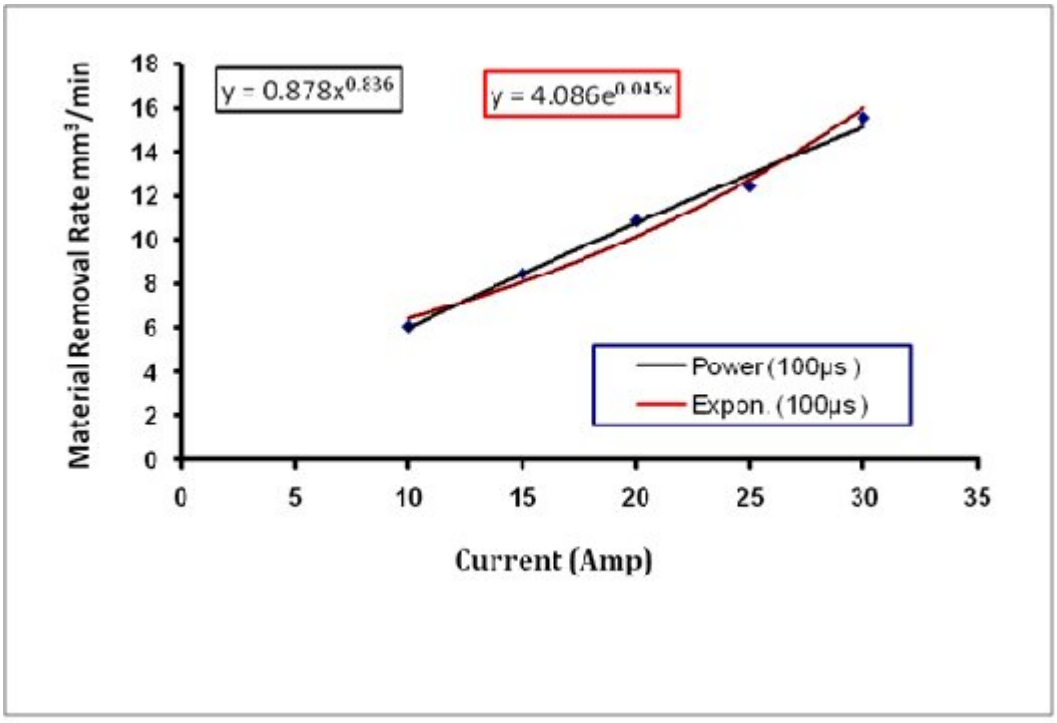

Fig. 4.9: Effect of 100µs Pulse Duration on MRR (excluding 35 Amp)

Table 4.4.9 Effect of 50µs Pulse Duration

Current (Amp)	MRR (mm3/min)	Power Model		Exponential Model	
		calculated value power model	% difference in calculated and observed	calculated value exponential model	% difference in calculated and observed
5	4.803	4.334	-10.827	5.515	**12.914**
10	7.535	7.406	-1.747	6.907	-9.095
15	9.0182	10.132	10.990	8.650	-4.261
20	11.635	12.655	8.059	10.832	-7.412
25	13.737	15.037	8.647	13.565	-1.266
30	16.438	17.313	5.055	16.988	3.238
35	20.465	19.504	-4.926	21.275	3.805
40	26.357	**21.625**	-21.882	26.643	1.072

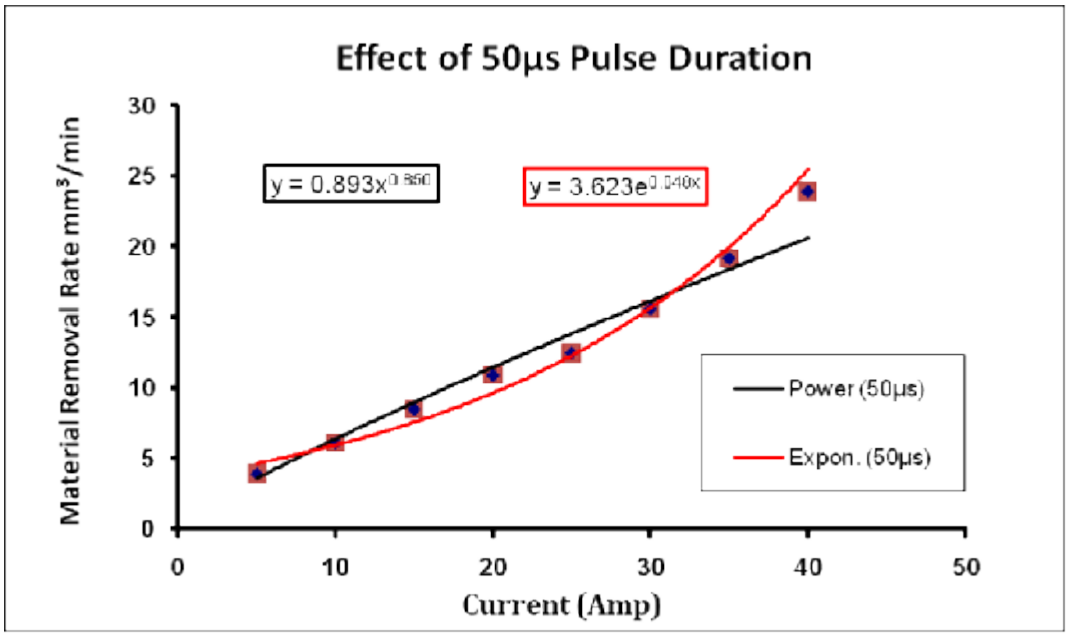

Fig 4.10: Graphical presentation of power and exponential models obtained from the data observed and shown in Table 4.4.9

Table 4.4.10 Effect of 50µs Pulse Duration					
Current (Amp)	**MRR (mm3/min)**	**Power Model**		**Exponential Model**	
		calculated value power model	**% difference in calculated and observed**	**calculated value exponential model**	**% difference in calculated and observed**
5	4.803	4.379	-9.681	5.434	**11.609**
10	7.535	7.493	-0.555	6.805	-10.729
15	9.0182	10.260	12.104	8.522	-5.823
25	13.737	15.243	9.883	13.365	-2.783
30	16.438	17.557	6.373	16.737	1.789
35	20.465	19.785	-3.438	20.961	2.364
40	26.357	21.942	-20.121	26.249	-0.410
20	**11.635**	**12.823**	**9.262**	**10.672**	**-9.021**

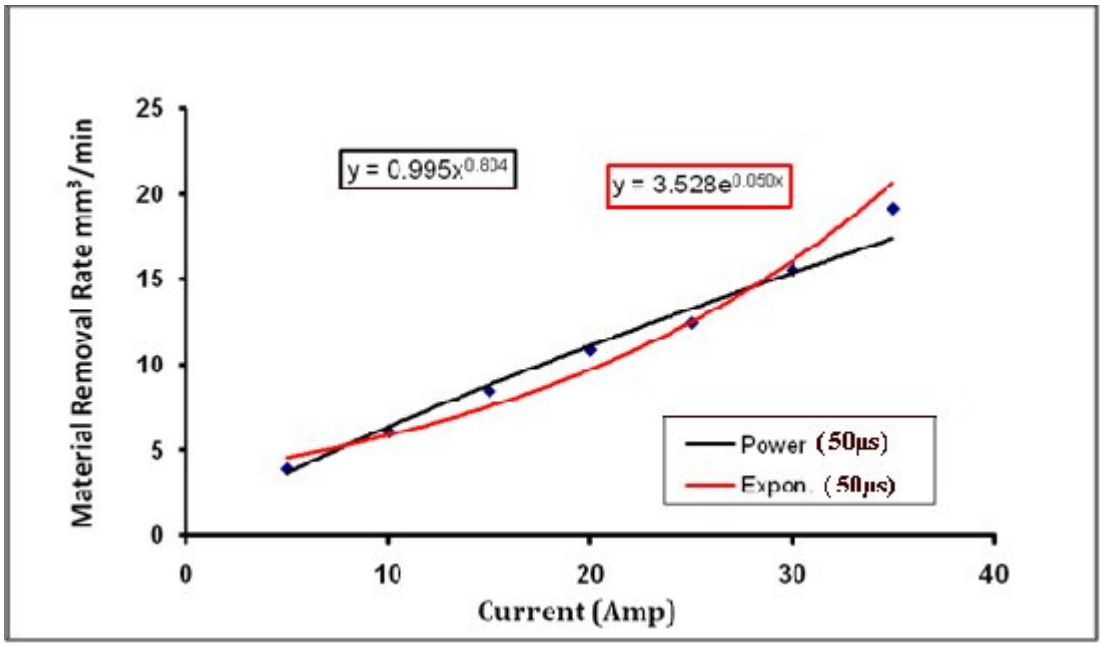

Fig 4.11: Effect of 50µs Pulse Duration Interpolation

Table 4.4.11 Effect of 50µs Pulse Duration

Current (Amp)	MRR (mm3/min)	Power Model		Exponential Model	
		calculated value power model	% difference in calculated and observed	calculated value exponential model	% difference in calculated and observed
5	**4.803**	**3.646**	**-31.730**	**6.085**	**21.066**
10	7.535	6.706	-12.370	7.469	-0.880
15	9.0182	9.577	5.832	9.169	1.642
20	11.635	12.332	5.653	11.255	-3.377
25	13.737	15.005	8.448	13.816	0.569
30	16.438	17.613	6.669	16.959	3.072
35	20.465	20.168	-1.471	20.818	1.694
40	26.357	22.680	**-16.212**	25.554	-3.142

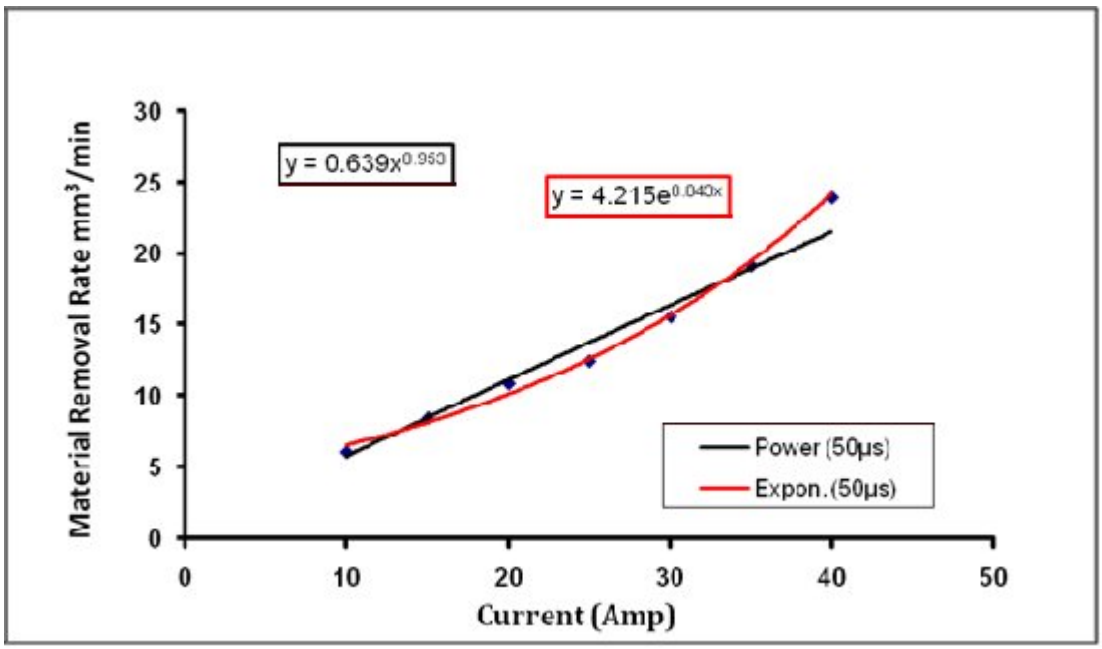

Fig 4.12: Effect of 50µs Pulse Duration Extrapolation Low

Table 4.4.12 Effect of 50µs Pulse Duration					
Current (Amp)	**MRR (mm3/min)**	**Power Model**		**Exponential Model**	
		calculated value power model	**% difference in calculated and observed**	**calculated value exponential model**	**% difference in calculated and observed**
5	3.875	2.962	**-30.813**	5.226	**25.852**
10	6.055	5.735	-5.588	6.480	6.552
15	8.456	8.439	-0.196	8.034	-5.256
20	10.867	11.102	2.113	9.961	-9.099
25	12.451	13.732	9.329	12.350	-0.818
30	15.561	16.338	4.755	15.312	-1.625
35	19.157	18.923	-1.235	18.985	-0.906
40	23.914	21.491	-11.273	23.539	-1.594

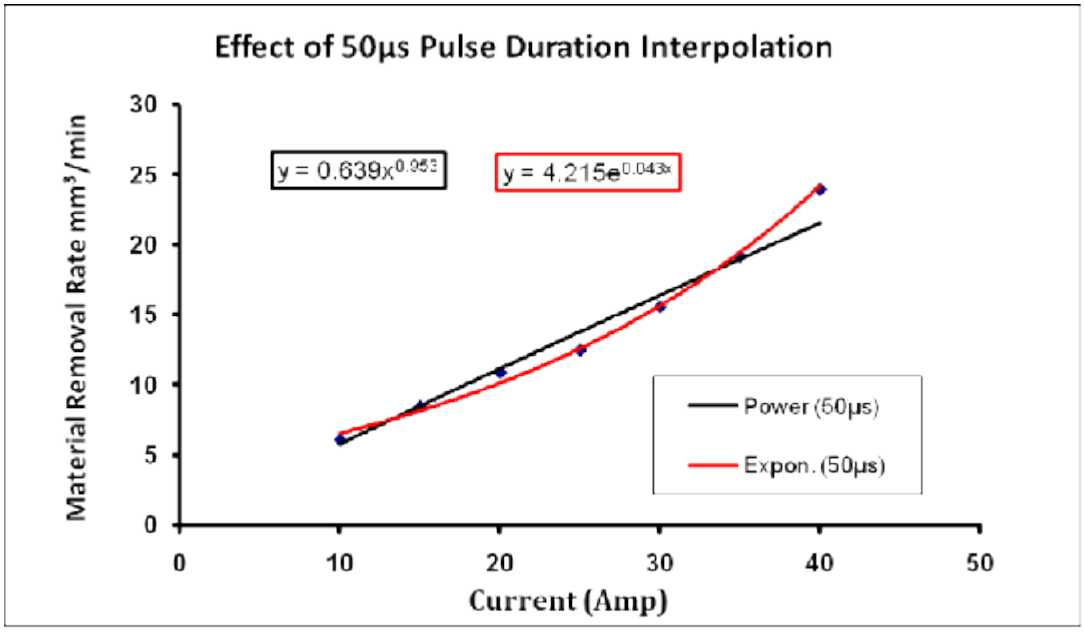

Fig 4.13: Graphical presentation of power and exponential models obtained from the data excluding 5 Amp and shown in Table 4.1.4

4.5 Results and Discussion

4.5.1 Structural Analysis of Unmachined WC

In order to verify the presence of different phases, X-ray diffraction study of un-machined surface of WC-Co cermets was done. The diffractrogram shows the presence of WC and Co peaks (Fig. 4.14). The intensity of WC peaks is much higher than Co peaks. However, it also indicates the presence of Fe. The diffraction pattern indicates that volume fraction of WC is more as compared to Co. Microstructure analysis also revealed the uniform distribution of WC in the matrix of Co.

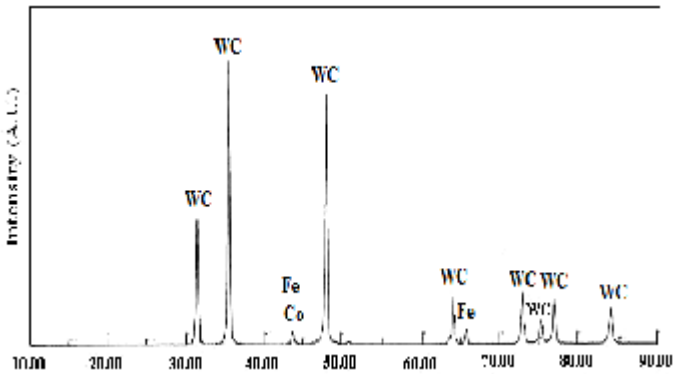

Fig. 4.14: XRD Pattern of WC workpiece

The WC-Co work piece material does not exhibit any porosity, indicating that it is well compacted and sintered substance as can be seen in higher magnification micrograph (Fig. 4.15) where the grains can be easily distinguished. The average grain size of the workpiece material is 60 μm. These analyses were done to ensure the homogeneity and existence of different phases in the system. After ensuring the characteristics of material, machining was done at different currents but for fixed on time duration (either 50μs or 100μs). In both cases the material removal rate (MRR) was monitored. The results obtained are given in table 4. 5 and are plotted in Fig. 4.16. It is observed that MRR increases linearly up to 25Amp current irrespective of pulse on time, after that it increases at higher rate and this increment becomes more at higher currents. Since duty time was nearly constant in these experiments, the nature of graph remains the same. However, MRR is relatively higher for 50μs pulse on time which is obvious as the debris flushing time is more per cycle of EDM spark (better duty factor).

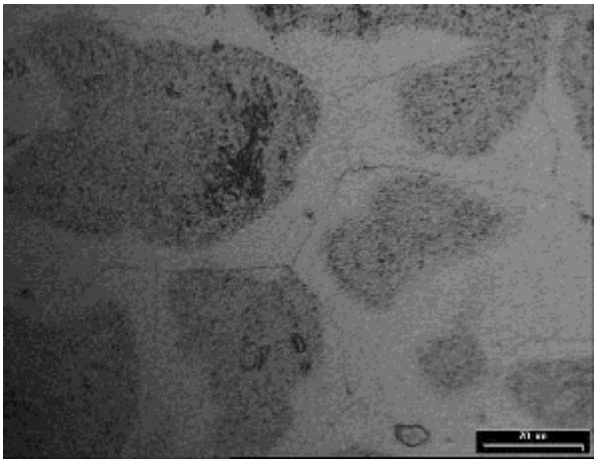

Fig. 4.15: Microstructure of un-machined sample of WC-Co composite

Table 4.5: Details of machining parameters

Experiment No.	Current (Amp)	On time (μs)	Off time (μs)	MRR (mm^3/min)
1	5	100	10	3.875
2	10	100	10	6.055
3	15	100	10	8.456
4	20	100	10	10.867
5	25	100	10	12.451
6	30	100	10	15.561
7	35	100	10	19.157
8	40	100	10	23.914
9	5	50	12	4.803
10	10	50	12	7.535
11	15	50	12	9.0182
12	20	50	12	11.635
13	25	50	12	13.737
14	30	50	12	16.438
15	35	50	12	20.465
16	40	50	12	26.357

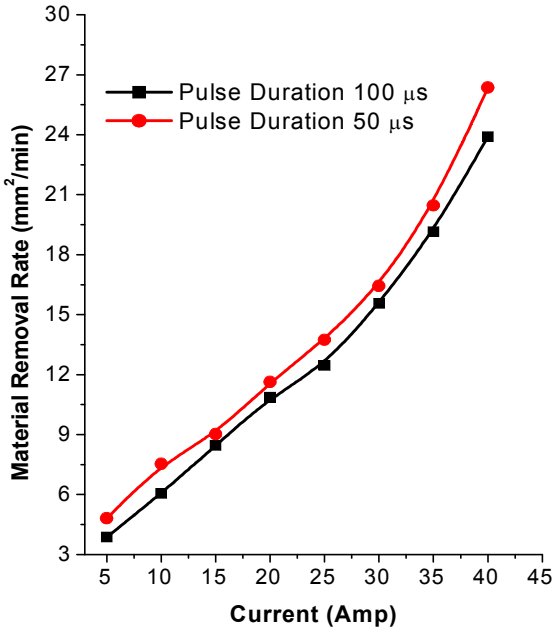

Fig. 4.16: Effect of current on material removal rate at different pulse durations

Considering this variation in MRR from linear to exponential, the surface analysis was divided into two parts. One corresponding to current values upto 25 Amp and another beyond this value. In order to analyse the surface morphology, the machined surface was analysed under SEM. It was observed that surface cracks are present on each machined sample irrespective of current at which machining was done.

Structural analysis of the EDMed surfaces of tungsten carbide workpiece has revealed several aspects. This includes formation of cracks as a continuous network as well as discontinuous pattern. These features have been recorded in the previous chapter and the corresponding micrograghs have also been discussed. The interesting feature observed was the formation of different size of craters. Normally, cracks were observed at each machining condition. Formation of cracks starts from the peripheries of the craters (Fig. 3.13). The nature of these craters varies from shallow to deep but most of the craters are observed in the resolidfied layer which is continuous in nature. When machining was done at higher current and larger duration of pulse on time (15 Amp and 100 μs) using Cu-W electrode, Figure 3.14 depicts this feature where continuous and interconnected cracks were observed.

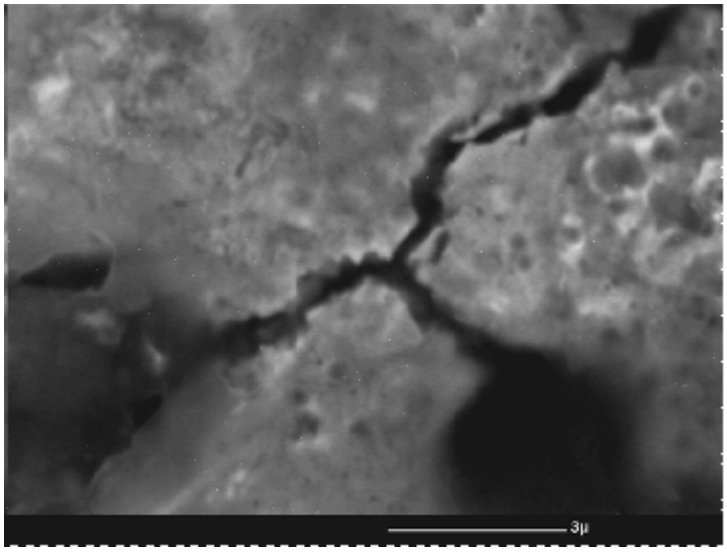

Fig. 4.17: Structure showing the tearing of grains

As the current is increased beyond 25Amp the nature of cracks alters. The surface cracks which were confined earlier to only some areas of resolidified layers are increased. Moreover, at higher current values tearing action indicating its deep panetration has been observed. Fig. 4.17 shows the features of surface cracks observed at 40 Amp current for 100µs pulse duration. The feature gives the appearance of propagation of shock waves inside the material [93, 104].

In a study on machining of WC, Lee and Li [3] have reported that at low current of 16 Amp there is no significant variation in microstructructures but their study was for 1.6µs pulse duration. However, as current was increased to 64 Amp, structure variation was observed and also formation of microcracks which are parallel and perpandicular to machined surface were observed. Ghanem et al. [55] have reported the formation of cracks at 5 Amp machining in chromium steel. However, when the current is increased to 25 Amp, severity of cracks increases. It became more severe at 50 Amp current. In the entire study of Ghanem et al. [55] the pulse duration was 5µs. Lee et al. [106] have observed the morphological behavier of cracks with variation in current and pulse on time for carbon steel. They have reported that the nature of cracks varies if either pulse duration or current is increased. For the machining of tungsten carbide with higher production rate (higher MRR) it is essential to machine it at higher current and higher pulse duration which has been followed in the present work. If the crack generated during the machining is confined to surface only, then these are not so dangerous. If their penetration is deep into the sample, this may cause failure of the machined component. The analysis of structural features of entire machined samples indicated two types of morphological features. One corresponding to cracks of discontineous

nature confined to only resolified layers and another of severe type, propagating deep inside the material. The observation of Lee and Li [106] on the machinng of WC indicate that these cracks are in abundance particularly when machining is done at higher current and pulse duration. In order to study the severity of cracks the transverse area of machined suface was analysed.

4.4.2 Analysis of Nature of Cracks

Analysis of transverse section of machined surface was done after polishing the surface carefully. The general morphology of cracks observed was of two types. One confined to surfaces only and other that penetrated deep inside the surface. The important feature of all these cracks was that these had originated from the machined surface and after propagating inside the sample, they got bent. As the heat flux is supplied over the surface, the low melting point constituent Co melts first. Since Co is occupying the grain boundary area so it provides path for loosening of the grain. Depending upon the amount of heat flux and its propagation inside the material, the loosening of grains causes detachment of the piece from rest of the mass.

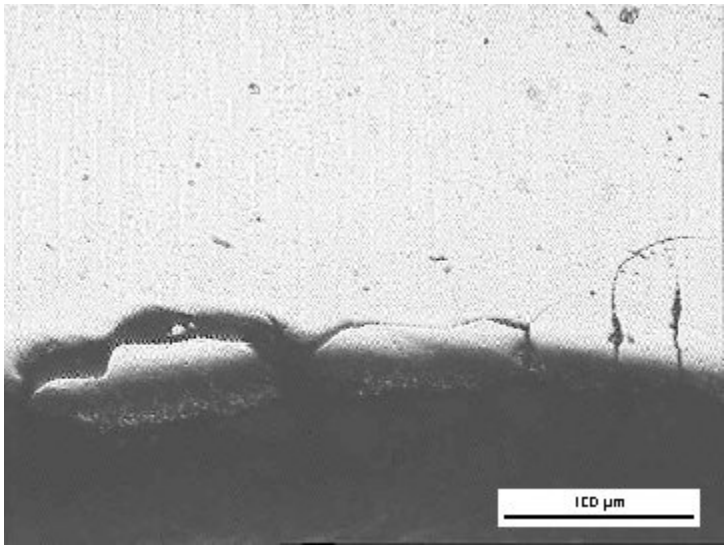

Fig. 4.18: Microstructure observed perpendicular to machined surface showing formation of cracks (5 Amp and 50µs)

Fig. 4.18 presents the microstructure of such a surface when machining was done at 5 Amp where cracks observed have propagated beyond the re-solidified layer. Since cracks formed are parallel to machined surface, they cause machining of the material by getting them

removed. The average size of the chunk is 100 to 200 μm. When etched, the structure gives clear visualization of such type of cracks.

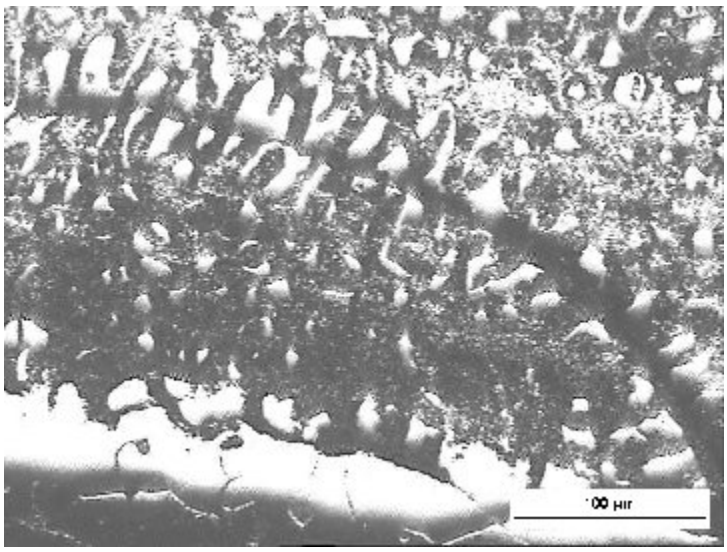

Fig. 4.19: Microstructure showing etched surface where crack is visible **(**5 Amp and 100μs)

Fig. 4.19 presents the section of etched surface of such a crack in which re-solidified layer and crack can be seen. The opening of grain boundaries clearly indicates the loss of cobalt from these areas. Such types of structural features were observed in all the samples machined at low to high currents. As the current was increased, the length of crack increase and it penetrates deeper inside the material. These cracks have similarity to the propagation of shock waves.

Fig. 4.20 presents such type of cracks for the material machined at 20 Amp current and 100μs pulse on time. One of the typical features observed at high current was formation of star type of crack, deep inside the material (Fig 4.21). Such types of crack are thermal cracks. However, at higher current such features acquire a wavy pattern as shown in Fig. 4.22. It has been observed that apart from formation of surface cracks, which do propagate as machining proceeds, there is a continuous opening of grain boundaries even deep inside the material (Fig. 4.23).

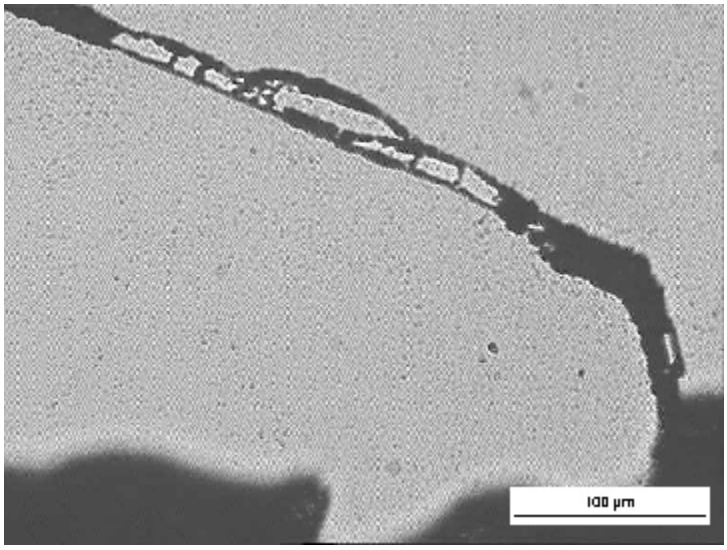

Fig. 4.20: Propagation of cracks along higher thermal stress areas where debris intact can be seen (20 Amp and 100µs)

The volume fraction of these openings is very high for materials machined at higher current. Such types of structural features are not possible if only loss of cobalt occurs. Some other phenomenon is also occurring apart from loss of cobalt which causes this type of structural variation.

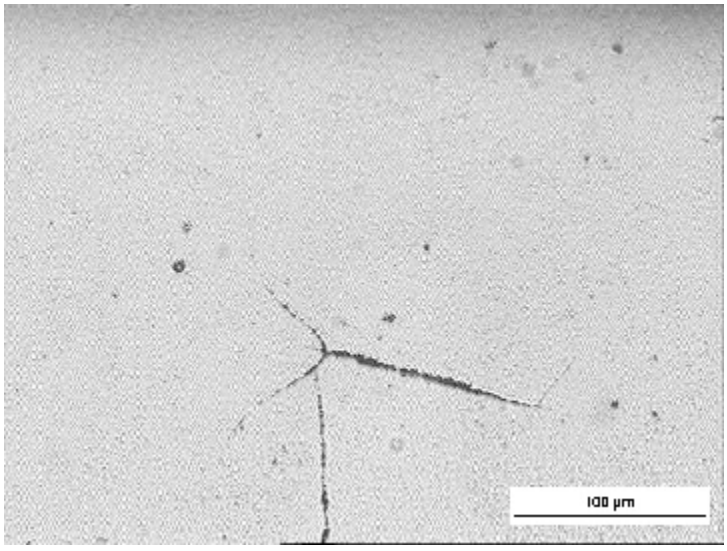

Fig. 4.21: Structure showing star like crack (brittle thermal failure mode) deep inside the material (30 Amp and 100µs)

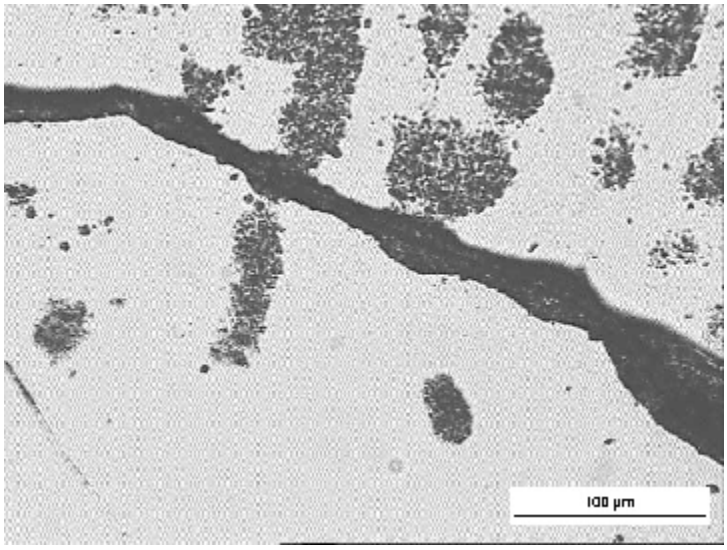

Fig. 4.22: Structure showing dumble shape crack (40 Amp and 100µs)

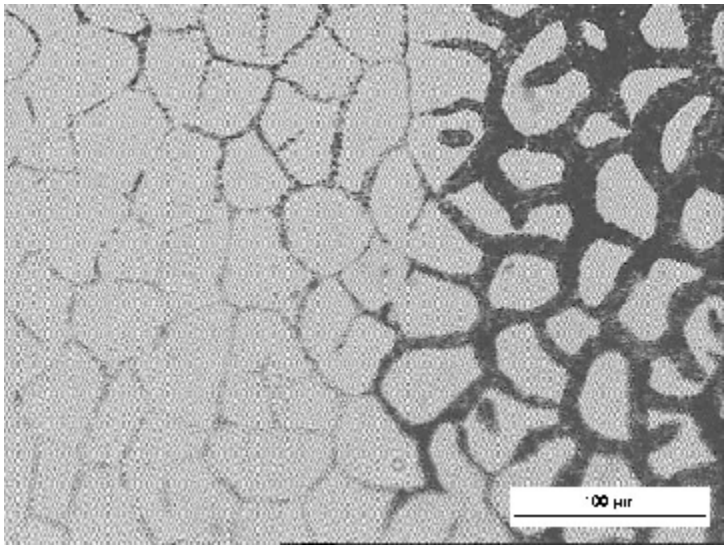

Fig. 4.23: Figure showing sequential movement and widening of cracks from surface (35 Amp and 50µs)

The overall analyses indicate that the majority of cracks have initiated at the surface and with higher input energy the thermal shocks created result in its propagation inside the material. Such types of cracks are observed in brittle materials. The tensile stresses are created at the surface of the material as a result of shrinkage of the re-solidified layer from where heat is extracted at a faster rate, making it solidify faster than the surface beneath it, causing the stress to build. This re-solidified layer develops cracks to relieve this stress. However, if this resolidified layer gets removed during course of machining, it exposes the WC grains.

The fracture toughness of ceramic material is lower than that of the metallic material. Any discontinuity on the surface of ceramic material, even shallow in nature, drastically reduces the load required for fracture. If the stress intensity (calculated by multiplying the crack length by stress on the part) exceeds the fracture toughness value, then the part breaks.

The investigations on the formation of cracks in EDMed sample indicates that the depth of the surface cracks increases with increasing discharge energy [107]. Due to the presence of carbon of the dielectric fluid, which becomes part of molten metal, the surface chemistry, becomes different than that of the parent material. When the stress in the surface exceeds the ultimate tensile strength of the material, cracks are formed [108]. The fast heat removal here may cause less cracks. Since the thermal conductivity of WC is less as compared to that of metals, it may develop more cracks with increase in current. However, the structural features of un- etched surface as observed in Fig. 4.23 indicate that material erosion mechanism is different for higher current machining. In order to verify it, X-ray diffraction study of the machined surface was done.

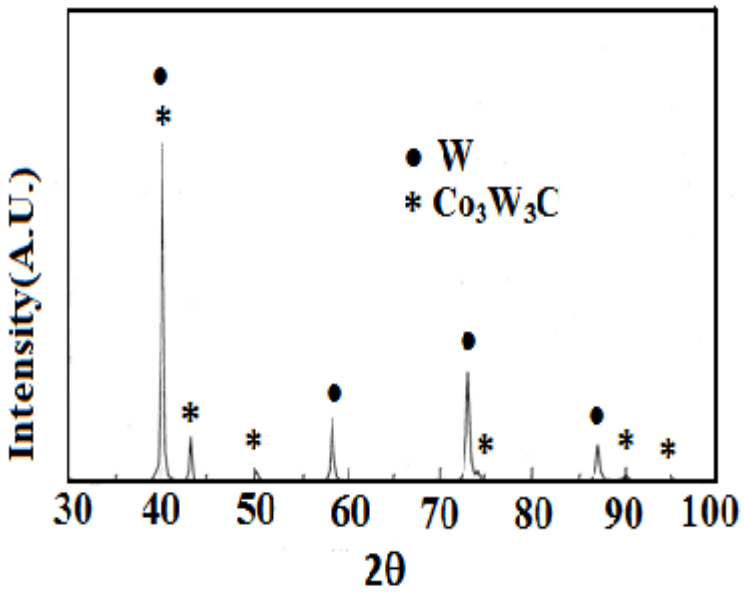

Fig. 4.24: Showing X-ray diffraction pattern (35 Amp current for 50µs pulse on time)

Fig. 4.24 presents the X-ray diffractrogram of machined surface in which machining was done at 35 Amp current for 50µs pulse on time. The phases present in the machined surface are W and a complex compound cobalt tungsten carbide (Co_3W_3C). Cobalt tungsten carbide phase is brittle, and is detrimental in nature. Formation of such a phase occurs because of decomposition of WC. The studies carried out on thermal spray of WC-Co coating have reported the formation of such complex carbide (Co_3W_3C) [33]. However, the origin of

nucleation of this has not been understood till date. Moreover, such type of phase formation has been reported in substances exposed to very high temperature which is also there in the present case. Because of loss of carbon from tungsten carbide the opening is more [108].

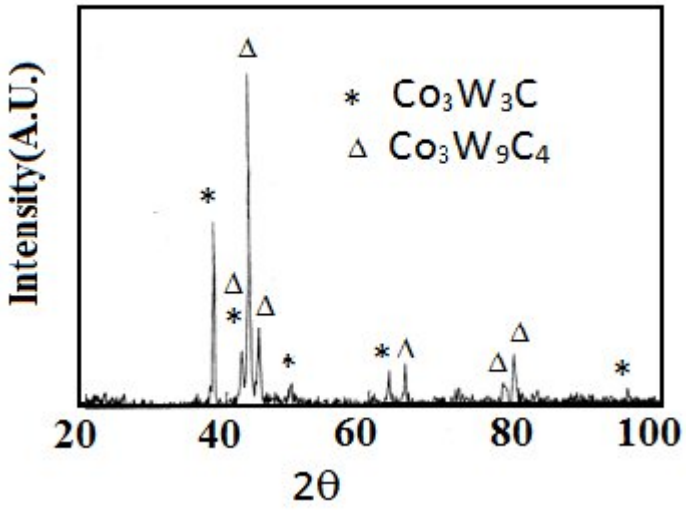

Fig. 4.25: Showing X-ray diffraction pattern (40 Amp current for 50μs pulse on time)

Fig. 4.25 shows the X-ray diffractogram of machined surface when machining was done at 40 amp current for 50 μs. The peaks of the phases present have been marked which correspond to Co_3W_3C and $Co_3W_9C_4$ phases. The interesting feature observed was the presence of ε-phase. The formations of such type of phases have been reported during thermal spray coating of WC-Co powders. At high temperature (Plasma spraying), the WC-Co phase tends to undergo a combination of decarburization, oxidation and reduction process [109]. The dissolution reaction between the WC and Co binder results in the formation of hard and brittle phases [110] such as W_2C, Co_3W_3C, Co_6W_6C, Co_2W_4C, $Co_3W_9C_4$ and even WO_3 and W. The reasons for formation of these phases have been discussed by other authors [111]. Formation of these phases may lead to loss of carbon upto 50% [113]. This loss causes the crack formation inside the material when machining is done at higher currents. One of the interesting features observed at the interior of the machined surface is agglomeration of carbides (Fig. 4.26).

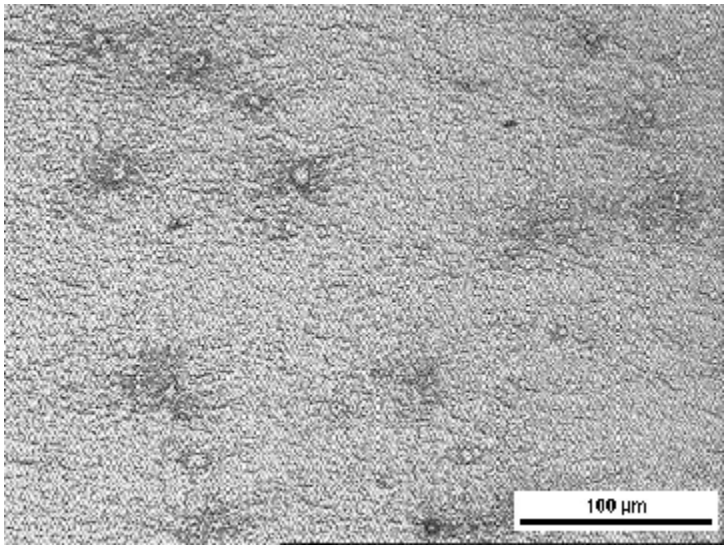

Fig. 4.26: Structure showing soft spot deep inside the material (10 Amp, 100µs)

This causes stresses inside the material. This type of features observed in the material gives rise to soft spots in the carbide. These soft spots lead to initiation of cracks inside the material. Fig. 4.27 presents the structure showing such type of structural features.

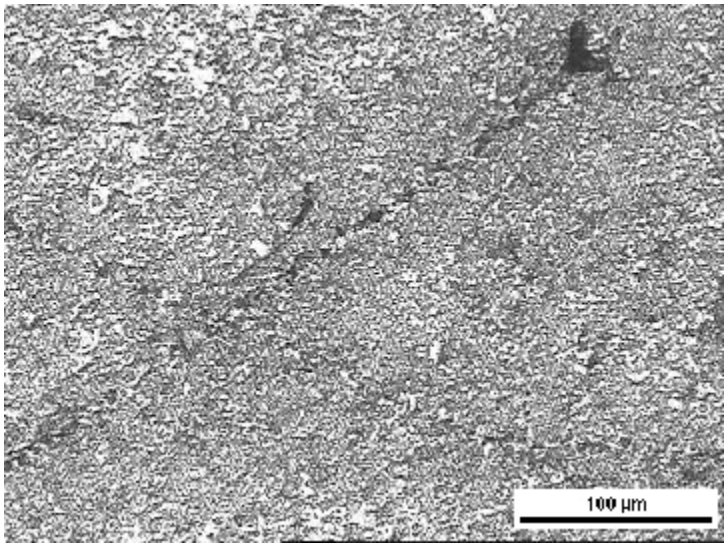

Fig. 4.27: Joining of cracks from soft spots (Current 10 Amp, pulse on time 100µs)

This provides soft path for the shock waves to propagate leading to deterioration of surface to a greater extent. Such features, observed inside the material, provide path for propagation of cracks deep inside the material. Fig. 4.28 presents the structural features observed at low current machining of WC-Co. One can see the presence of carbide clusters around the crack area. The carbide grain coarsening occurs when grain size and dispersion are not properly

controlled during machining. Due to this phenomenon, carbide grains tend to grow in size leading to occurrence of clustering. This causes internal stress fractures of parts under load or stress. This phenomenon occurring during machining is due to improper heat flow inside the material. Since pulse duration in the entire machining process was higher, the amount of heat provided on the surface penetrated deep inside the material causing such a type of structure variation inside the material.

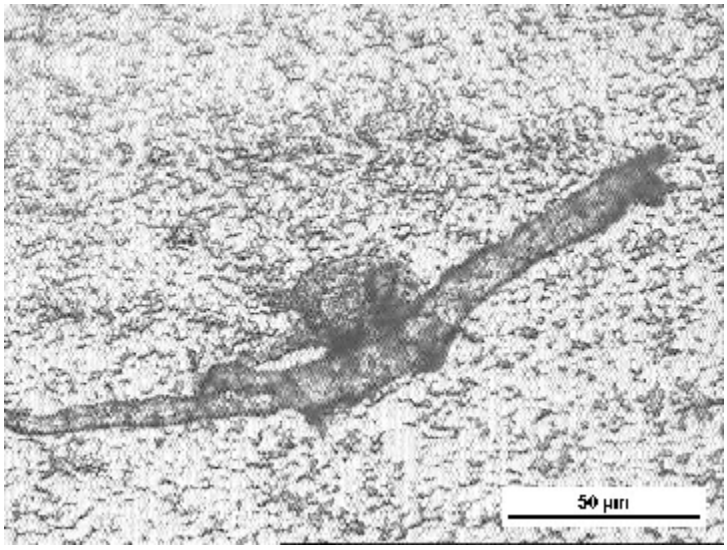

Fig. 4.28: Defect created due to thermal energy (Current 5 Amp, 100µs)

From the above studies it appears that the basic cause for the origin of crack and its propagation is the formation of complex carbide, as evident from X-ray diffraction studies. Since the plasma created between workpiece material and cathode generates tremendous amount of energy which in turn leads to material removal from the component, it is essential to understand the distribution of energy in the entire system of machining. The next chapter describes such an attempt to understand the amount of energy distributed among the different process elements ,during the machining process.

Chapter 5

ANALYSIS OF ENERGY DISTRIBUTION DURING ELECTRIC DISCHARGE MACHINING (EDM) OF TUNGSTEN CARBIDE

Overview

In this chapter experimental results have been validated/analysed using different heat equations to build theoretical model. It is well established fact that EDM is thermal erosion process. The amount of energy available for this process is generated through plasma. In order to understand the actual amount of energy utilized for machining of WC this work was planned. Experiments have been conducted in a planned sequence to take an account of the total energy input and to find the fraction of the energy utilized for the purpose of material removal or useful part and also the fraction of energy that goes as waste. This was done to optimize the process parameter so that maximum amount of energy is used for the useful purpose. Some theoretical work in literature has been reported but no evidence of experimental proof has been given. For this purpose special tanks to perform the experiments have been indigenously designed. Data collected in these experiments was used to calculate the amount of energies utilized by electrode and workpiece material with the help of heat transfer equations. It was observed that only 17% of total available energy is utilized for machining of WC.

Nomenclature:

c	specific heat
d	Diameter
E_y	component of primary energy distribution
f_p	pulse frequency
h	depth (of the dielectric fluid)
f_e	average discharge current
k_y	fraction of eroded material which is evaporated
k_{yz}	Coefficients
L	Length
L_z	percentage fraction of secondary energy distribution
M_y	percentage fraction of primary energy distribution
$q_{m,v}$	Heat sinks due to melting and evaporation
q	constant point heat source
q_t	component of the secondary energy distribution
r	Radius
R	latent heat of evaporation
R_{yz}	Coefficients
S	latent heat of melting
t	Time
t_i	pulse duration
$\bar{u}_e$	average discharge voltage
$\bar{u}_i$	open circuit voltage
$V_{W,E}$	erosion and wear volumetric rate
W_e	pulse energy
W_{in}	energy input

Greek Symbols:

Φ	Thermal diffusivity
A	Relative frequency
θ	Temperature
Λ	heat conductivity
T	heat source (total)
ρ	density
B	duty factor
Φ	temperature functions

Subscripts:

D	dielectric fluid
E	Tool
M	Melting
0	Initial
V	Evaporation
W	Workpiece

5.1 Introduction

The machining of WC-Co cermets is difficult because of the physical characteristics of workpiece material [18, 20, 25, 114, 115 and 116]. The work presented in previous chapters showed the variations in nature of cracks observed even under similar conditions of machining. This is because of the fact that the energy distribution inside the system is vibrant. Considering this fact this work has been undertaken to analyse the amount of energy distributed in different segments of the system during EDM process. Several investigators have shown that the energy distribution in the EDM process influences the material removal rate and accuracy to great extent [117, 118]. In general the material removal rate and machining characteristics during the EDM process depend upon the distribution of the energy supplied in between electrode and work piece by the electric current [22, 119]. The input energy supplied during machining is distributed to various components i.e. work piece, electrode, dielectric etc. Part of this input energy is utilized for machining and remaining goes as waste.

The effectiveness of the EDM process is evaluated in terms of the material removal rate (erosion of work piece per unit time), relative wear ratio and the surface roughness of the EDM machined surface. All these parameters depend upon the distribution of the energy supplied during the process [19, 120 and 121]. For a particular application and with given technical conditions Juhr [19] has studied the thermal load using different simulation conditions of different pulse wave forms. In many applications EDM of cemented carbide is restricted by the basic properties of this family of materials. The aim of the present study is to optimize the experimental conditions for an effective energy distribution which is available for electric discharge machining for tungsten carbide.

5.2 Experimental

In order to monitor the energy experiments were performed in an indigenously designed and fabricated tank. The schematic diagram of the EDM set up is shown in Fig. 5.1(a). Experiments were performed on work piece of diameter 20mm with electrode of the same diameter on both electrodes a hole of diameter 2mm was created to avoid arcing and to facilitate controllable flushing conditions.

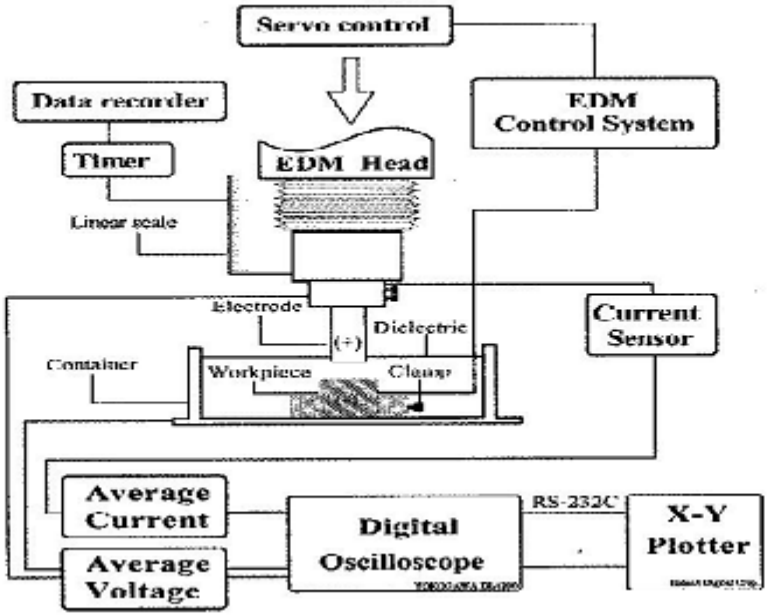

Fig. 5.1(a): Schematic diagram of the EDM set-up

The heat loss was minimized by putting insulating glass wool between two coaxial cylindrical walls of dielectric tank as shown in Fig. 5.1(b).

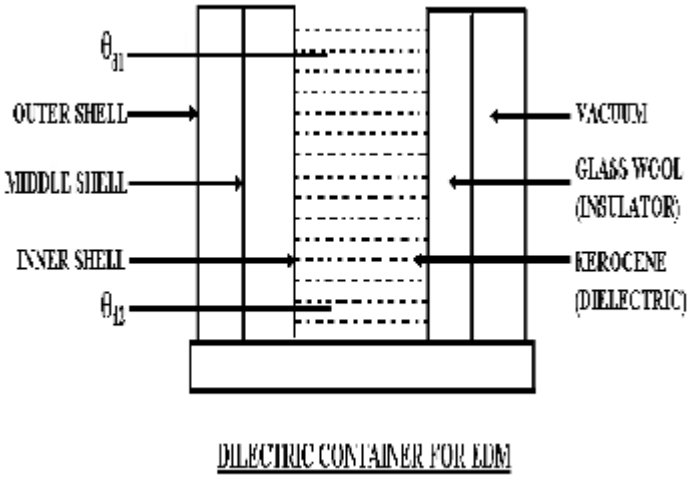

Fig. 5.1(b): Schematic view of insulation of dielectric

The temperature of the dielectric was measured at top and the bottom of dielectric fluid which is designated as θd_1 & θd_2 respectively. Tungsten Carbide (P20 grade) was used as work piece material. Copper tungsten (CuW) material having composition tungsten 78% and copper 22% by weight is used as an electrode. CuW has excellent wear characteristics and is suitable for machining of tungsten carbide by EDM. To minimize the energy loss teflon

cover was used in the work piece. The dielectric fluid tank was insulated from outside as shown in Fig. 1(b). The temperature at different locations of work piece, electrode and dielectric fluid was measured with J-type Iron/constantan thermocouples. These thermocouples were attached to temperature indicators which directly measure the temperature with resolution of ± 0.1° C. The volume of material eroded from the work piece was measured at the time when steady temperature was obtained. θ_1& θ_2 are the temperature of the electrode at lower and the upper end while θ_3 & θ_4 are the temperature of the work piece at upper and lower end as shown in Fig. 5.2.

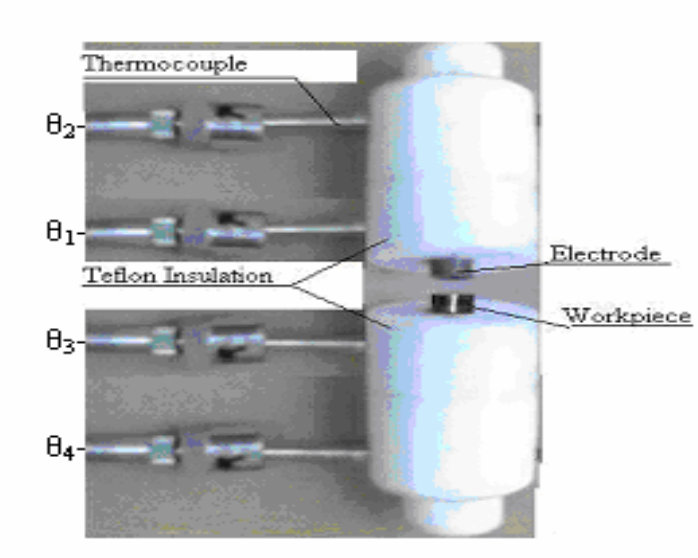

Fig. 5.2: Workpiece and electrode with insulation and thermocouples

5.3 Process Parameters

During EDM process electrode and workpiece materials are brought closer to each other to start the process of erosion on the surface of workpiece material. Electrode/workpiece with insulation is shown in Fig. 5.3. l_1, l_2 and l_3 are the distances from the point where temperature is taken with the help of thermocouples. The experiments were performed at different currents for different pulse durations which are shown in table 5.1 and 5.2. For each condition minimum of three experiments were performed. The values given in table 5.1 and 5.2 are the average values. From these data MRR values at different current and for different pulse durations were calculated which is shown in table 5.3.

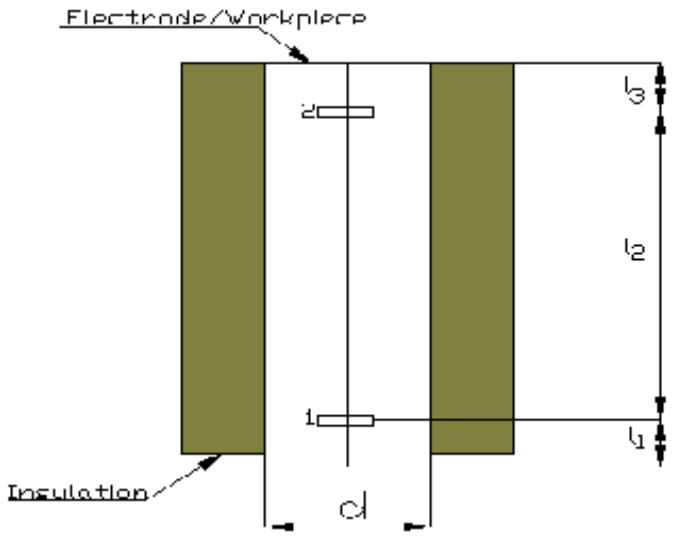

Fig. 5.3: Electrode/Work piece with Insulation (1&2 are positions of Thermocouples)

Table 5.1: Experimental Readings for work piece to calculate Energy Distribution V=60V, Initial temperature θ_o= 28 °C and off time t_o = 20µs, l_{2w} =36 and l_{3w}=2.24

Current (Amp)	Pulse Duration (µs)	θ_1 °C	θ_2 °C	θ_{d1} °C	θ_{d2} °C	l_{1w} (mm.)
4	25	52.4	35.5	35.6	32.9	11.52
4	50	63.7	37.4	36.8	34.1	11.18
4	100	76	40.1	38.3	36.2	10.75
4	200	81.4	43.3	41	38.9	10.42
10	25	56.6	40.3	35.3	32.5	10.06
10	50	63.4	40.9	37.1	34.3	9.56
10	100	77.3	50.8	39.4	37	8.7
10	200	82.2	54	39.4	36.9	7.76
16	25	58.2	40.5	39.4	38.7	7.26
16	50	66.3	41.8	39.5	38.7	6.56
16	100	78	48.8	40.4	39.6	5.66
16	200	86.7	54.2	40.4	39.6	4.86
24	25	76.3	63.2	45.3	44.6	9.83
24	50	75.4	60.1	45.1	44.3	7.48
24	100	88.2	70.1	45.2	44.2	4.91
24	200	112.3	93.4	46.2	45.7	2.66

Table 5.2: Experimental Readings for Electrode to calculate Energy Distribution V=60V, Initial temperature θ_o= 28 °C and off time t_o = 20µs l_{2w} =26.60 and l_{3w}=4.90

Current (Ampere)	Pulse Duration (µs)	θ_3 ^oC	θ_4 ^oC	θ_{d1} ^oC	θ_{d2} ^oC	l_{1E} (mm.)
4	25	44.3	36.4	35.6	32.9	7.89
4	50	50.1	39.3	36.8	34.1	7.64
4	100	53	40.2	38.3	36.2	7.28
4	200	61.9	43.6	41	38.9	6.90
10	25	45.3	37.3	35.3	32.5	6.79
10	50	52.3	39.1	37.1	34.3	6.53
10	100	63.3	42.4	39.4	37	6.16
10	200	68.9	44.2	39.4	36.9	5.77
16	25	47.4	35	39.4	38.7	5.40
16	50	60.5	39.3	39.5	38.7	4.65
16	100	70.4	42.4	40.4	39.6	3.76
16	200	75.9	44.6	40.4	39.6	2.86
24	25	72.3	61.1	45.3	44.6	5.27
24	50	84.4	62.3	45.1	44.3	4.27
24	100	90.3	62	45.2	44.2	3.05
24	200	109.6	72.3	46.2	45.7	1.45

Table 5.3: Effect of pulse duration on MRR

Discharge Current (A)	MRR (mm^3/min) 25µs	MRR (mm^3/min) 50µs	MRR (mm^3/min) 100µs	MRR (mm^3/min) 200µs
4	0.46	0.65	0.81	0.63
10	0.60	1.02	1.62	1.77
16	0.94	1.32	1.70	1.51
24	3.09	4.19	4.95	4.3

5.4 Thermal Modeling of the Discharge process in EDM

Since EDM is basically a thermal erosion process, where plasma (discharge channel) is a surface heat source in which large amount of heat is evolved. Heat which is propagated in the metal as a consequence of thermal conductivity is transmitted through the surface which forms the contact between the discharge channel and the electrode and thus passes into the workpiece [120]. Since the distance between the electrodes is very small in comparison to the electrode dimensions, the scattering of heat in the dielectric layer between the electrodes can be ignored and the heat source can be considered to be a surface one.

The mathematical models for the analysis of EDM process are based on the theory of heat conduction into the solids and use the following differential equation with suitable boundary conditions:

$$\frac{1}{a^2}\frac{\partial T}{\partial t} = \nabla^2 T \qquad (5.1)$$

where $a = \sqrt{\frac{k}{c\gamma}}$

The models, which have been employed for the study of the EDM process can be classified according to the idealized geometrical shapes of the heat source (discharge channel). These may be point, plane and circular heat source having a finite radius.

Zingerman [119] gave a mathematical relation to find the temperature distribution in a homogeneous body of infinite dimensions which is heated by a surface heat source for which the amount of heat evolved per unit time is known and specified by a time function.

Hocheng [117] has given the solution for induced temperature for instantaneous point heat source as:

$$T - To = \frac{P}{8(\pi\alpha t)^{3/2}} e^{(-r^2/4\alpha t)} \qquad (5.2)$$

where P is energy intensity.

In these equations coefficient of volume specific heat 'c' is used, which will not differ from normal temperature to temperature of diffusion (e.g. only 2% is for copper and by 1% for aluminium). Using these equations it is possible to find the effect of the magnitude of the area of the heat source upon depth of depression.

The knowledge of the heat source area is necessary in order to verify the theoretical derivations. The direct measurement of this area is not known as yet. It is only possible to measure the diameter of the depression reliably. Now diameter of depression can be determined by diameter of discharge channel. The diameter of the discharge channel can be determined according to the Drabkina formula [122]. Experimental verification of the Drabkina formula showed that this formula is in accordance with experimental data. This formula gives the correct relation between diameter of the column and the generated energy in the single spark. The results obtained indicate that the diameter of the column is a function of the energy generated in the column. The conclusions are based on two assumptions:

(1) The heat energy is liberated along the axis of the column.

(2) The process is adiabatic in character. The temperature gradient along the axis of the column, at the centre, is zero and in this part of the column the only energy losses may be due to radiation.

At the beginning of the process the energy is distributed primarily in the discharge channel and the electrodes surface layers (called primary distribution). The process is transient and

the energy distribution is changed towards the secondary distribution when steady state is reached (secondary distribution).

The heat distribution in the material after achieving the steady state can be calculated with the aid of the physical properties and on the assumption that all the electric energy will be transferred into heat on the material surface. Since the main mode of heat transfer in EDM process is by conduction only, a mathematical modeling can be done by heat transfer techniques. The power distribution between the tool (cathode) and the work (anode) depends on the effective voltage drop which in turn depends on the work function of material [77].

The theoretical and experimental work in EDM has demonstrated that crater size and dimensions are function of energy supplied at the discharge [3, 7 and 16].

Konig [7] has given relationship between volume of a crater and energy and is discussed below:

The input energy W_{in}= Sum of the pulse energies W_e of all the pulses

$$W_{in} = \sum_{x=1}^{n} W_e \tag{5.3}$$

The input energy per unit time is as follows:

$$\dot{W}_{in} = VIt_i f_p \eta \tag{5.4}$$

The input energy W_{in} can be split among all modes of energy in the primary energy distribution and appear in the three parts of the closed system: electrode, work piece and dielectric fluid with varying intensity and duration. The energy released in work piece and electrode can be divided into conducted energy, stored energy and energy used in the erosion (of the work piece) and the unwanted wear (of the electrode). Only stored and directly conducted energy are distinguished in the dielectric fluid. The remainder of the discharge which cannot be assigned to a particular element of the closed system appears as different form of energy like radiation, light, sound etc.

The components of the primary energy distribution [Fig. 5.4]

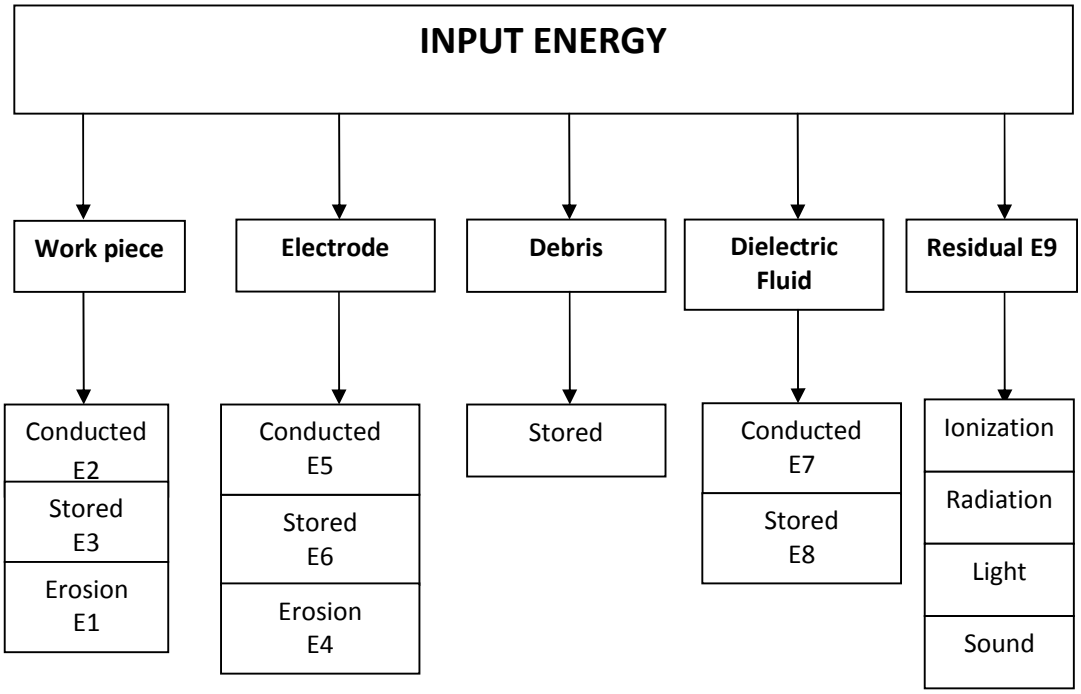

Fig. 5.4: Primary Energy Distribution in EDM Process

are defined by the following:

- E_1 - energy for erosion/removal of work piece material
- E_2 - energy conducted through the work piece
- E_3 - energy stored in the work piece
- E_4 - energy for erosion/removal of electrode
- E_5 - energy conducted through the electrode
- E_6 - energy stored in the electrode
- E_7 - energy conducted through the dielectric fluid
- E_8 - energy stored in dielectric fluid
- E_9 - residual energies like radiation , light , sound or ionization

Using above designations following energy balance can be obtained:

$$\sum_{x=1}^{n} \dot{W}_e = \dot{W}_{in} = \sum_{y=1}^{9} \dot{E}_y \qquad (5.5)$$

This primary energy distribution changes to the secondary distribution due to conversion and transfer processes between the different modes of energy and various components of the system. For example, the energies E_1 and E_4, causing erosion and wear respectively are

partly liberated by cooling subsequent to erosion. The major portion of this energy is dissipated in the electrodes by conduction of heat and in the dielectric fluid by convection and radiation. The secondary energy distribution can be divided into two groups, corresponding to the form of energy: All stored and conducted heats are collected in the first group. These are relatively easily measurable, by temperature sensors [123, 124]. The second group includes all other forms of energy that are not stored and given off, which are designated as residual energies and are difficult to measure.

The components of the secondary energy distribution [Fig. 5.5] are defined by the following:

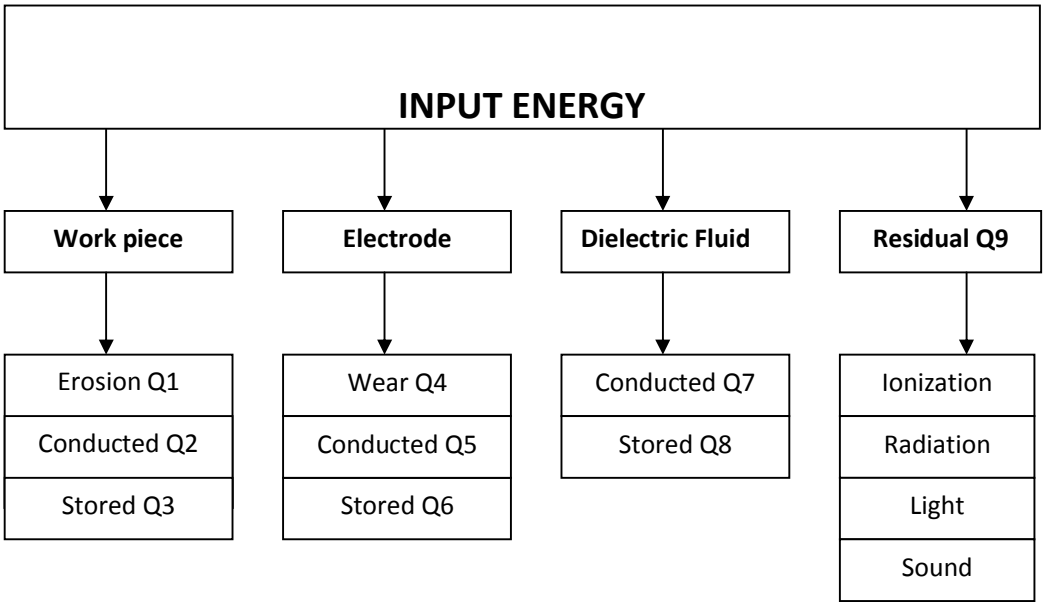

Fig. 5.5: Secondary Energy Distribution in EDM Process

Q_1 – Heat stored in eroded (from work piece) particles

Q_2 – Heat conducted through the work piece

Q_3 – Heat stored in the work piece

Q_4 – Heat stored in worn (from electrode) particles

Q_5 – Heat conducted through the electrode

Q_6 – Heat stored in the electrode

Q_7 – Heat conducted through the dielectric fluid

Q_8 – Heat stored in the dielectric fluid

Q_9 – Residual energies like radiation, light & sound energies

The sum for all components of both distributions per unit of time is equal to the input energy:

$$\dot{W}_{in} = \sum_{y=1}^{9} \dot{E}_y = \sum_{z=1}^{9} \dot{Q}_z \qquad (5.6)$$

Theoretically, the primary distribution is changed completely into the secondary distribution. The transformation can be described by the following linear relations:

$$\dot{E}_y = \sum_{z=1}^{9} K_{yz} \dot{E}_y, \quad y = 1, 2, 3, \ldots\ldots\ldots,9 \qquad (5.7)$$

For example, a portion $K_{11}\dot{E}_1$ of energy $\dot{E}_1$ goes to $\dot{Q}_1$, $K_{yz}\dot{E}_y$ goes to $\dot{Q}_z$, $K_{19}\dot{E}_1$ goes to $\dot{Q}_9$. The following relation must be valid for the coefficient to satisfy equation (5.7):

$$\sum_{z=1}^{9} K_{yz} = 1, \qquad y = 1, 2, 3, \ldots\ldots\ldots,9 \qquad (5.8)$$

Following linear relations can be written for the secondary distribution:

$$\dot{Q}_z = \sum_{y=1}^{9} K_{yz} \dot{E}_y, \quad z = 1, 2, 3, \ldots\ldots\ldots, 9 \qquad (5.9)$$

For example, the energy $\dot{Q}_1$ is obtained from the sum of portions $K_{11}\dot{E}_1$ of energy $\dot{E}_1$, $K_{21}\dot{E}_2$ of energy $\dot{E}_2$,….. , $K_{91}\dot{E}_9$ of energy $\dot{E}_9$

If primary and secondary distribution is expressed in matrix form, they may be related with the help of matrix (K):

$$(K)\,(\dot{E}) = (\dot{Q}) \qquad (5.10)$$

Thus from the secondary distribution primary distribution can be calculated by transposing Equation (5.10)

$$(\dot{E}) = (K^{-1})\,(\dot{Q}) \qquad (5.11)$$

for $(K^{-1}) = (R)$ the following relation is obtained:

$$(\dot{E}) = (R)\,(\dot{Q}) \qquad (5.12)$$

$$\text{or} \quad \dot{E}_y = \sum_{z=1}^{9} R_{yz} \dot{Q}_z, \quad y = 1, 2, 3, \ldots\ldots\ldots,9 \qquad (5.13)$$

When the process of EDM starts, at the beginning of the process both primary and secondary distribution is in transient state. A steady state energy distribution, appear after a certain period, depending on the operating conditions. Now on achieving steady state the heat stored in the electrodes approaches zero and can be neglected in drawing up the energy balance for

steady state. The part of the energy stored in the work piece, electrode and the dielectric fluid become significant if the energy distribution is evaluated from the start of the experiment the variation of energy as the process of EDM proceeds.

The results obtained at steady state have been used to evaluate secondary distribution of input energy by using equations. The primary energy distribution has been calculated from secondary distribution by using these equations. The fraction (in percentage) of primary energy distributed with respect to input energy has been calculated. The above procedure to calculate the energy distribution has been repeated by varying pulse duration (on time) and input current. Also discharge voltage and pulse interval off time has been kept constant for all experiments [67, 125]. The results obtained have been compared with the help of graphs using these equations.

5.5 Calculation of Energy Distribution

Some of the assumptions made for the calculation of energy distribution during electrical discharge machining are:

- The electrodes and the dielectric fluid are considered as continuum in calculating the stored and conducted heats.
- The radial conduction in the electrodes and the axial conduction in the dielectric fluid are neglected with respect to the axial and radial components respectively.

A numerical evaluation of the temperature as a function of time and of a single space coordinate enables calculation of the above mentioned components of the secondary energy distribution.

Heat stored in work piece and electrode can be written as:

$$Q_{3,6} = \pi \rho c r^2 l \{½ [(\theta_1 - \theta_2). (l_1 - l_3 / l_2) + \theta_1 + \theta_2] - \theta_0\} \quad (5.14)$$

Heat stored in the dielectric fluid Q_8 is calculated by similar linearization of the temperature profile in the dielectric fluid. Now after calculation of the stored energy from the start of machining to the momentary time of measurement t_x, the energy stored per unit of time is approximately obtained from:

$$Q_{3,6,8} = [Q_{3,6,8}(t_x) - Q_{3,6,8}(t_{x-1})] / (t_x - t_{x-1}) \quad (5.15)$$

$\dot{Q}_3$ and $\dot{Q}_6$ become negligible after a certain time t_x. Thus the transition region from transition to steady state can be determined from the heat stored in the electrodes.

Heat conducted by the work piece and electrode in the axial direction can be written as:

$$Q_{2,5} = \pi \quad d^2_{W,E} k_{W,E} (\theta_1 - \theta_2) / 4l_2 \quad (5.16)$$

Heat stored in eroded and worn particles will be:

$$Q_{1,4} = V_{W,E}\, \rho\, c\, (\theta_{d1} - \theta_0) \quad (5.17)$$

Heat conduction in the dielectric fluid can be written as:

$$Q_7 = 2\pi\, k_d\, h_d\, (\theta_{d1} - \theta_{d2}) / \ln (r_{d2} / r_{d1}) \quad (5.18)$$

The residual energy $\dot{Q}_9$ will be:

$$\dot{Q}_9 = \text{Input energy} - \text{sum of all other energy components} \quad (5.19)$$

Energy required to melt and evaporate the eroded particles is calculated as:

$$\dot{E}_{1,4} = V_{W,E}.\ \rho.\ \{c_{solid}\, (\theta_M - \theta_0) + S + K_v\, [c_{liquid}\, (\theta_V - \theta_M) + R]\} \quad (5.20)$$

The components of primary energy distribution are taken as percentage fraction of input energy:

$$M_y = E_y / W_{in} \qquad y = 1, 2, 3, \text{--------}, 9 \quad (5.21)$$

The components of the fraction of primary energy distribution are defined by the following:

- M_1 - fraction of energy for erosion/removal of work piece
- M_2 - fraction of energy conducted through the work piece
- M_3 - fraction of energy stored in the work piece
- M_4 - fraction of energy for erosion/removal of electrode
- M_5 - fraction of energy conducted through the electrode
- M_6 - fraction of energy stored in the electrode
- M_7 - fraction of energy conducted by the dielectric fluid
- M_8 - fraction of energy stored in dielectric fluid
- M_9 - fraction of residual energy losses

As described above a number of experiments were performed under the defined experimental conditions, the observations are already given in table 5.1 and 5.2. MRR was calculated from the results of table 5.1 and 5.2 and is given in table 5.3. From these experimental data the above mentioned energy components (M1 to M9) were calculated using above described equation with the help of Mathematica software. The calculated values are presented in table 5.4 and 5.5.

Table 5.4: Primary Energy Distribution

Voltage 60V		Work Piece			Electrode			Dielectric		
Off Time 20us	Pulse Duration (μs)	Energy stored in Eroded particles (Watts)	Energy conducted through work piece (Watts)	Energy stored (Watts)	Energy stored in worn particles (Watts)	Energy conducted (Watts)	Energy Stored (Watts)	Energy Stored (Watts)	Energy conducted (Watts)	Residual Energy (Watts)
Current (Amp.)		E1	E2	E3	E4	E5	E6	E7	E8	E9
4	25	0.137	1.080	11.067	0.056	3.245	12.160	0.483	17.640	87.460
4	50	0.197	1.665	21.120	0.127	4.393	22.630	0.485	44.150	76.660
4	100	0.243	2.260	23.600	0.183	5.180	24.600	0.393	52.980	90.570
4	200	0.190	2.430	23.782	0.195	5.690	25.970	0.385	57.870	101.670
10	25	0.181	1.031	20.399	0.057	3.258	40.100	0.510	30.100	237.690
10	50	0.306	1.390	41.499	0.132	5.356	81.214	0.487	74.200	223.980
10	100	0.486	1.655	68.850	0.186	8.387	147.600	0.430	91.300	181.090
10	200	0.532	1.779	87.436	0.199	9.941	189.217	0.457	114.220	141.690
16	25	0.283	1.074	65.493	0.188	4.930	59.990	0.119	35.300	365.950
16	50	0.398	1.460	90.033	0.381	8.450	175.540	0.138	105.870	299.870
16	100	0.512	1.872	112.880	0.454	11.280	214.880	0.147	129.840	328.220
16	200	0.454	2.078	133.530	0.462	12.550	237.120	0.145	149.760	336.610
24	25	0.927	0.681	134.100	0.300	3.664	39.640	0.102	52.880	591.760
24	50	1.257	0.878	153.200	0.513	7.410	112.840	0.111	147.170	605.230
24	100	1.485	1.011	193.320	0.621	10.322	147.480	0.163	176.600	668.930
24	200	1.290	1.116	222.680	0.810	16.084	185.950	0.086	206.040	676.810

Table 5.5: Percentage Fraction of Energy Distribution

Voltage 60V		Work Piece			Electrode			Dielectric		
Off Time 20μs	Pulse Duration	Energy stored in Eroded particles (%)	Energy conducted through work piece (%)	Energy stored (%)	Energy stored in worn particles (%)	Energy conducted (%)	Energy stored (%)	Energy stored (%)	Energy conducted (%)	Residual Energy (%)
Current (Amp.)	(μs)	M1	M2	M3	M4	M5	M6	M7	M8	M9
4	25	0.103	0.810	8.300	0.042	2.430	9.120	0.362	13.230	65.603
4	50	0.115	0.970	12.320	0.074	2.560	13.200	0.281	25.760	44.720
4	100	0.121	1.130	11.800	0.092	2.580	12.300	0.194	26.490	45.293
4	200	0.087	1.110	10.900	0.089	2.610	11.900	0.177	26.530	46.597
10	25	0.055	0.310	6.120	0.017	0.980	12.030	0.150	9.030	71.308
10	50	0.071	0.324	9.683	0.031	1.250	18.950	0.115	17.313	52.263
10	100	0.097	0.331	13.770	0.038	1.680	29.520	0.086	18.260	36.218
10	200	0.098	0.326	16.030	0.037	1.820	34.690	0.083	20.940	25.977
16	25	0.053	0.201	12.280	0.036	0.920	11.250	0.210	6.620	68.620
16	50	0.058	0.213	13.130	0.056	1.230	25.600	0.190	15.440	43.732
16	100	0.064	0.234	14.110	0.057	1.410	26.850	0.180	16.230	41.027
16	200	0.052	0.238	15.300	0.053	1.440	27.170	0.170	17.160	38.570
24	25	0.116	0.085	13.750	0.036	0.460	4.960	0.015	6.610	73.970
24	50	0.122	0.085	14.890	0.050	0.720	10.970	0.013	14.310	58.840
24	100	0.125	0.086	16.110	0.052	0.860	12.290	0.012	14.720	55.750
24	200	0.099	0.086	17.010	0.058	1.100	14.204	0.007	15.740	51.700

The Energy Distribution has been calculated by varying pulse duration and current by using equations given above. During calculations some of the assumptions taken are:

It is assumed that the relative frequency used in equation 5.13 to calculate input energy, $\eta = 1$

It is assumed that all the erosion during EDM process is due to melting. However, the energy due to evaporation is negligible i.e. K_V is negligible as shown in equation 5.20 for energy stored in work piece (M3), electrode (M6) and energy conducted by dielectric (M8). The

results are given below in table 5.6-5.8 indicate that F and P value are within acceptable limits.

5.6 Results and discussion

The machining parameters studied are the pulse duration and current, whilst the machining response factors evaluated are material removal rate (mm^3/min) and percentage fraction of distribution of primary energy. The experimentation has two stages i.e. unsteady state and steady state. During the steady state it was assured that the temperature at the bottom and the top of workpiece, electrode and dielectric is same. Variation of energy with respect to time showing transition from transient to steady state is shown in Fig. 5.6. The results have been presented in graphical forms for the purpose of comparison and discussion.

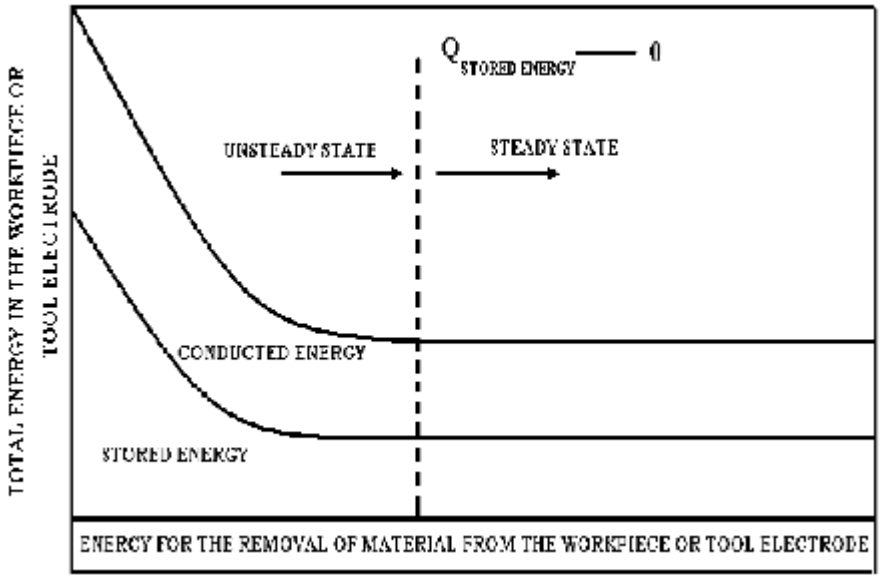

Fig. 5.6: Variation of energy with respect to time showing transition from transient to steady state

5.6.1 Material Removal Rate

The material removal rate (MRR) at different current density has been measured at different pulse duration after achieving the free steady state condition. MMR was calculated by measuring the diameter and depth of the cavity in work piece machined during EDM machining. The time of machining has been noted on the monitor of the machine and material removal rate has been calculated in mm^3/min. During machining the variation in peak current was controlled manually by percentage setting knob. The results obtained for

the MRR, using copper tungsten electrode for tungsten carbide workpiece have been shown in Fig. 5.7and Fig. 5.8

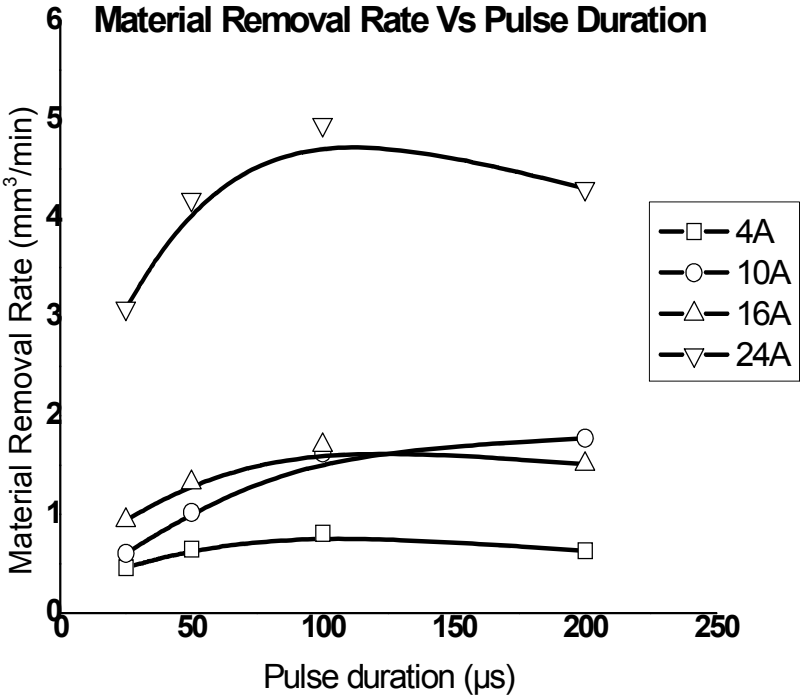

Fig. 5.7: Effect of Pulse Duration on Material Removal Rate

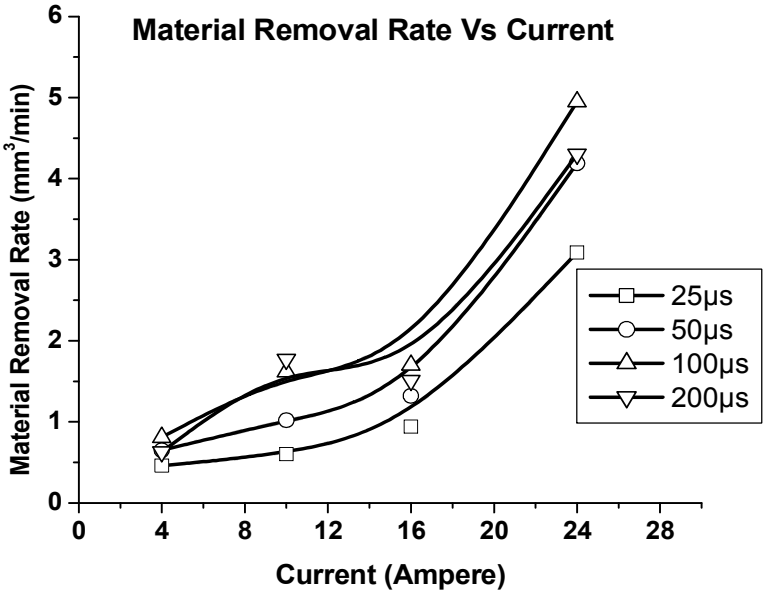

Fig. 5.8: Effect of Current on Material Removal Rate

as a function of pulse duration and current respectively. It has been seen that the highest value of MRR for tungsten carbide is obtained for pulse duration of 100 μs and after that a down ward trend is observed. It is expected that the MMR should increase with increasing pulse duration because higher pulse duration may give rise to higher electrode discharge energy which get accumulated at the surface and will rapidly melt and evaporate the substance. However, overlarge pulse duration will expand the plasma channel [123, 124]. This leads to expansion in EDM covered area. When the plasma channel becomes large, its energy density decreases and the heat energy absorbed by the work piece per unit area is reduced. This causes the reduction in MRR. Similar results were also obtained for other hard material [124]. Lee et al. [3] have studied the MRR over a wide range of current density for machining of WC. They have also reported the similar nature in their work. When the pulse duration was extremely short, the amount of electrical discharge conducted into the machining gap was very small. Therefore, the MRR was small as can be seen in Fig. 5.7. The cemented carbide has high melting point. For machining such a high melting point substance the energy level should be high. This can be obtained by increasing pulse duration till optimum condition is achieved [67].

Fig. 5.8 shows the variation in MRR at different current density when machined for different pulse on time. It is observed that there is no significance increase in MRR up to 16 ampere current. The MRR is considerably increased at 24 ampere current as compared to MRR at 4, 10 and 16 ampere for all pulse levels. Steep rise (2 to 3 times) in MRR is observed from 16 ampere to 24 ampere indicate that melting and evaporation of material is on higher side in this range of current. It is mainly due to the fact that in the beginning the energy is consumed in conduction of workpiece, electrode and dielectric. The saturation point is reached at the level of 16 ampere current and after this level when the current is increased to next level of 24 ampere the energy supplied to the system is consumed for removal of material from the work piece. This leads to steep rise in MRR. Singh et al. [77] have reported a steep rise in MRR beyond 9.0 ampere discharge current for EN-31 alloy. Lee et al. [20] have also reported a similar trend in machining of WC. They have also observed that MRR increases rapidly beyond 16 ampere current up to 32 ampere. After that increase is not so rapid. Results obtained in this work are also in similar lines as reported by Lee et al. [20].

5.6.2 Effect of Pulse Duration on Energy Distribution

In order to know the amount of energy utilized for the machining of WC, the study of distribution of energies in different segments using energy equations has been done. The formulation of heat equation and their respective amount distributed in different sectors has been described in previous sections. The effect of pulse duration on % fraction of primary energy (%FPE) on various parameters is shown in Fig. 9 to17.

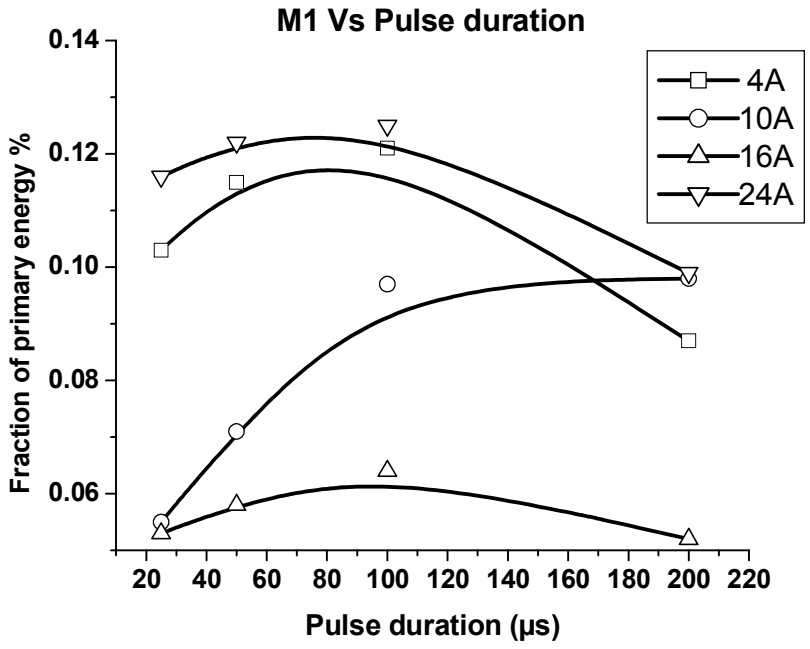

Fig. 5.9: Effect of pulse duration on % fraction of primary energy utilized for erosion of work piece at different currents

The effect of pulse duration on % FPE (M1) used for erosion of work piece at different currents using heat transfer equation is shown in Fig. 5.9. It is observed that the % FPE at 4 ampere current and 24 ampere current is maximum in this work. At 16 ampere current primary fraction of energy used is minimum during experimentation. However, for 24 ampere current it is maximum. Moreover, the important fact is that for all current densities 100 μs pulse duration gives optimum utilization of energy for all current values. For experimental results a variation in MRR with pulse duration for different current density (Fig. 5.7) shows that for low current densities (4A to 16A) the MRR varies in the range of 0.5 to 1.5 mm^3/mm whereas it is relatively high for 24A current (3 to 5mm^3/mm). The analysis done using energy equation indicate that fraction of energy utilized in case of 4A, 10A and 16A current is in decreasing order which jumps suddenly in case of 24 A current.

Since the total variation in energy is very less (0.052 to 0.125%) the above variation in nature does not make more impact though it is not in order. It has been found that the trend for utilization of the fraction of primary energy for all the levels of pulse duration is similar. For different current the impact of pulse duration on %FPE conducted through workpiece is shown in Fig. 5.10.

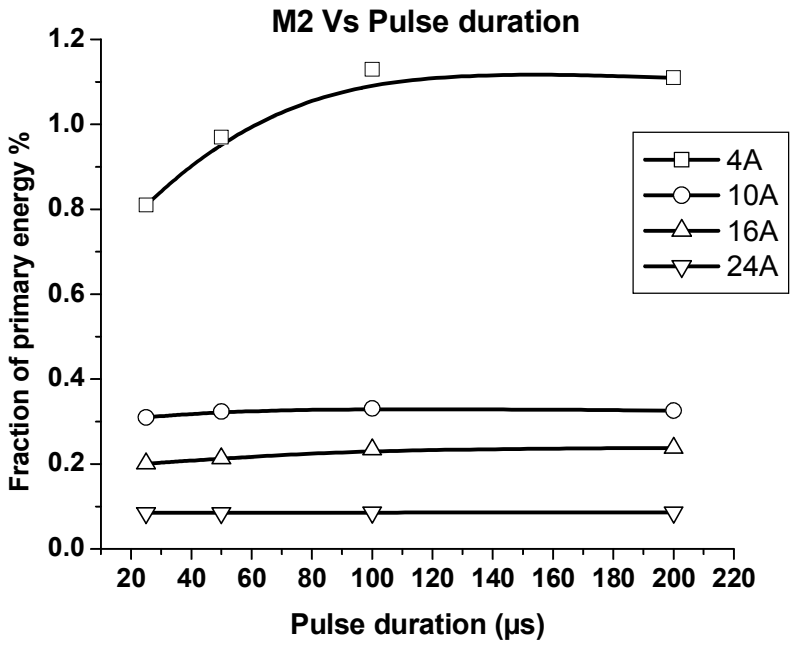

Fig. 5.10: Effect of pulse duration and fraction of primary energy conducted through work piece at different current

It is important to mention that the trend for all the pulse duration is similar. Some variation is seen at 4 ampere in utilization of fraction of primary energy whereas for 10, 16 and 24 ampere the variation is negligible. The effect of pulse duration on energy stored in work piece is shown in Fig. 5.11.

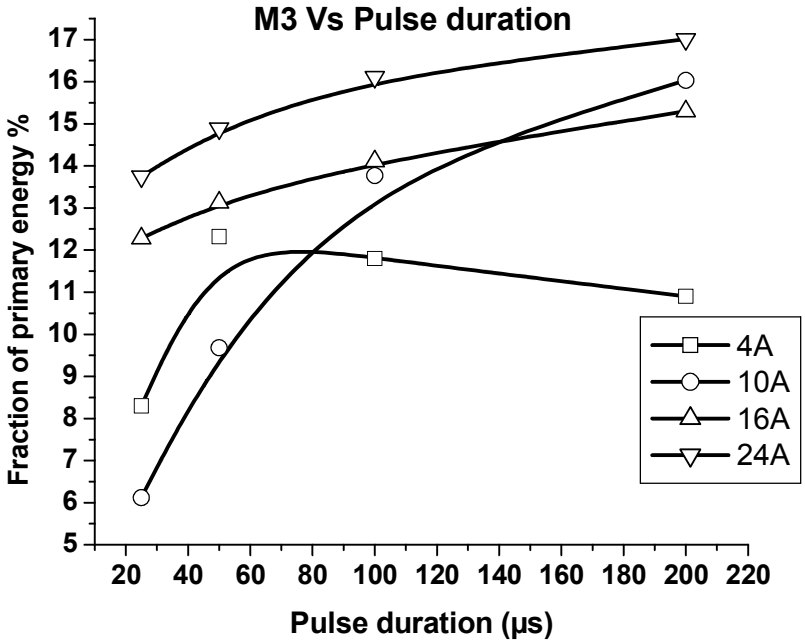

Fig. 5.11: Comparison between pulse duration and fraction of primary energy stored in work piece for different current

The trend for all the current levels is similar and is in line with the energy input i.e. more the energy supplied more energy is used for the machining of work piece. The exception is 10 ampere levels where steep increase is observed. Fig. 5.12 depicts the energy utilized for the erosion of electrode. It is observed that the energy conducted through both work piece and electrode is more for low current than for higher current. Due to fact that energy transferred to work piece and electrode is less so energy is used for erosion and unwanted wear of electrode and hence energy conducted is more at lower current. Looking at the nature of curves it appears that the 4 ampere and 24 ampere current values give different results whereas the nature for 16 ampere and 24 ampere is similar. Comparison between pulse durations and % FPE conducted through electrode for different current is shown in Fig. 5.13.

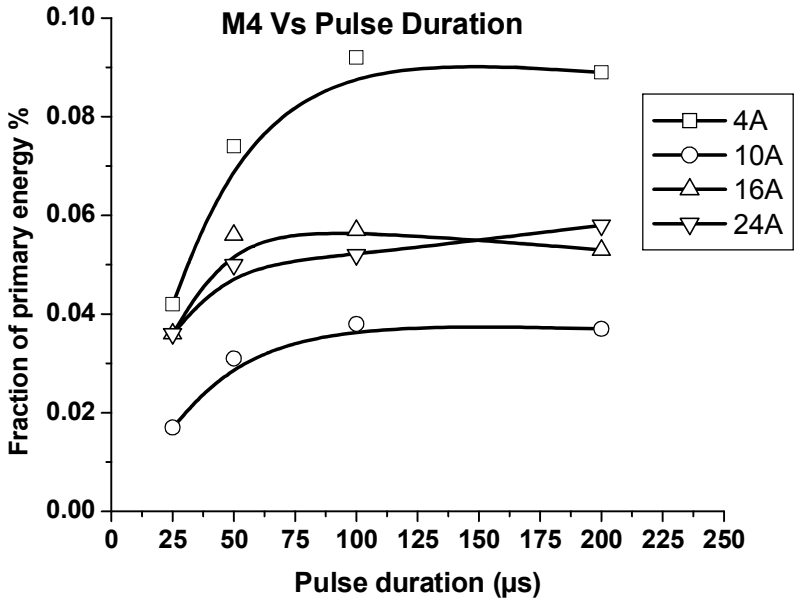

Fig. 5.12: Effect of pulse duration on % fraction of primary energy for erosion of electrode at different currents

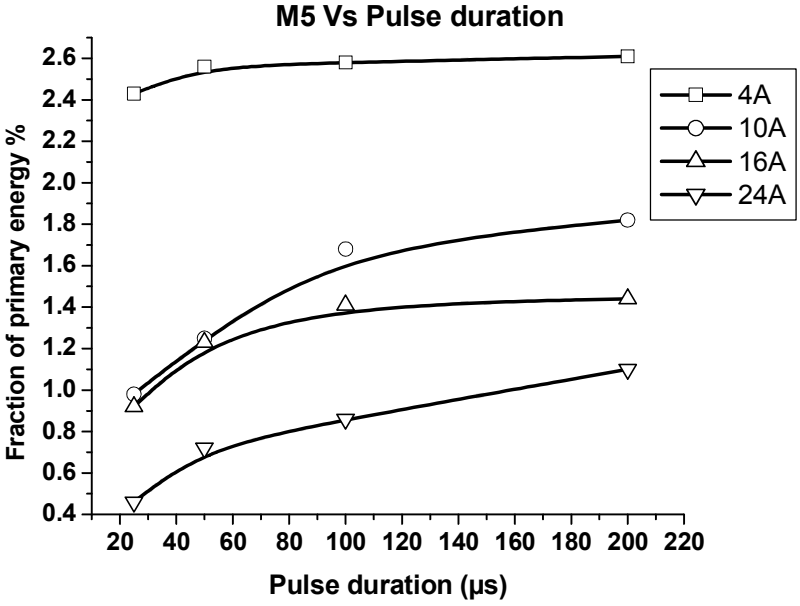

Fig. 5.13: Comparison between pulse duration and fraction of primary energy conducted through electrode for different current

It is important to mention that the trend for all the pulse duration is similar. Some variation is seen at 10, 16, 24 ampere in utilization of fraction of primary energy whereas for 4 ampere

current the variation is negligible. It confirms that raising the current means directly raising the input energy when the size of the electrode remains same with negligible change in size. Comparison between pulse duration and fraction of primary energy stored in electrode for different current is shown in Fig. 5.14.

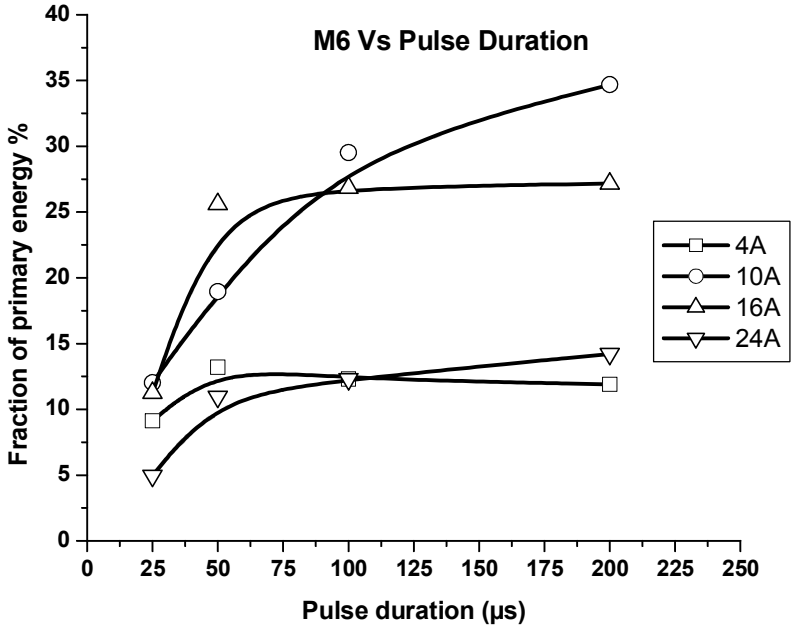

Fig. 5.14: Comparison between pulse duration and fraction of primary energy stored in electrode for different current

It is observed that 10 ampere and 24 ampere current showed similar increasing trend for all levels of pulse duration during experimentation. 16 ampere current and 4 ampere current followed the similar trend showing constant %FPE at pulse duration greater than 50 µs. These observations are favorable for higher current levels, since under such conditions the energy stored in the electrode will be less leading to more life of the electrode. The eroding energy increases steadily with increase of pulse duration. It is found that with pulse duration longer than 100µs, this energy either decreases or remains almost constant, due to arcing caused at longer pulse duration. Also MRR shows the same trend as of eroding energy as shown in Fig. 5.7, due to direct proportionality between MRR and eroding energy. It is observed that for all pulse durations useful energy that is energy used for erosion of work piece is highest for 24A current.

Relation between pulse duration and % FPE conducted through dielectric fluid for different current is shown in Fig. 5.15.

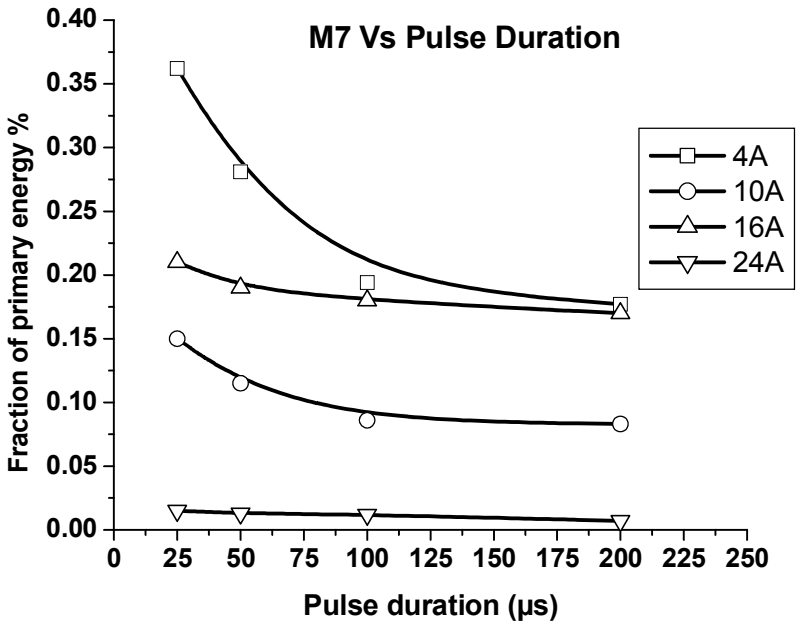

Fig. 5.15: Comparison between pulse duration and fraction of primary energy conducted through dielectric fluid for different current.

The energy conducted in dielectric is wastage of energy so it is proposed that higher current and higher pulse duration will be suitable for proper utilization of energy. Since for all practical purposes the dielectric will be circulated after filtration. This data is helpful for the purpose to have a proper utilization of energy observed in this study.

Variation of fraction of primary energy stored in dielectric fluid with different pulse duration for different current is shown in Fig. 5.16.

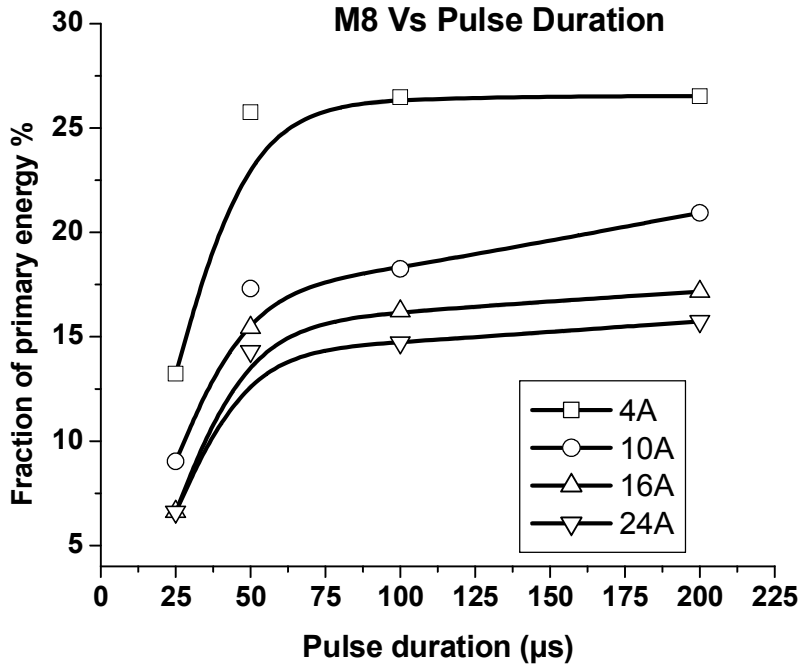

Fig. 5.16: Comparison between pulse duration and fraction of primary energy stored in dielectric fluid for different current

Similar trends are observed for all the currents with respect to pulse durations i.e. sudden rise in energy stored for 25 μs to 50 μs pulse duration levels and after that not much increase is observed up 200 μs pulse duration level. The variation of fraction of primary energy for different pulse duration as residual losses for different current is shown in Fig. 5.17.

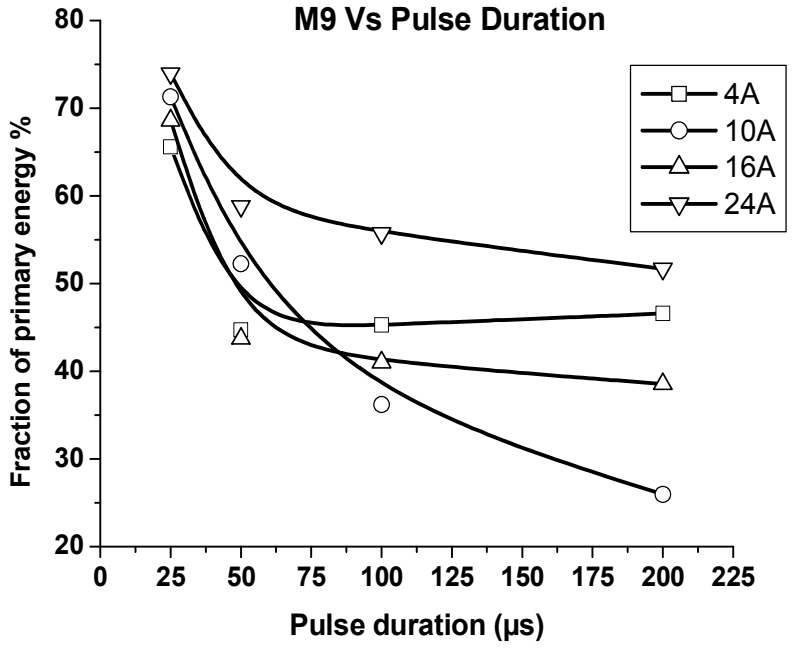

Fig. 5.17: Comparison between pulse duration and fraction of primary energy as residual losses for different current

The % FPE at 25 µs for all the current levels used for experimentation range varies from 65% to 75%. At higher pulse duration, the losses are reduced to 55%. These loses were observed lowest for 10 ampere current i.e. 25 %.

5.6.3 Effect of Current on Energy Distribution

The effect of current on % fraction of primary energy on variation parameters is shown in Fig 5.18 to 5.26. Comparison between current and fraction of primary energy for erosion of workpiece for different pulse duration is shown in Fig. 5.18.

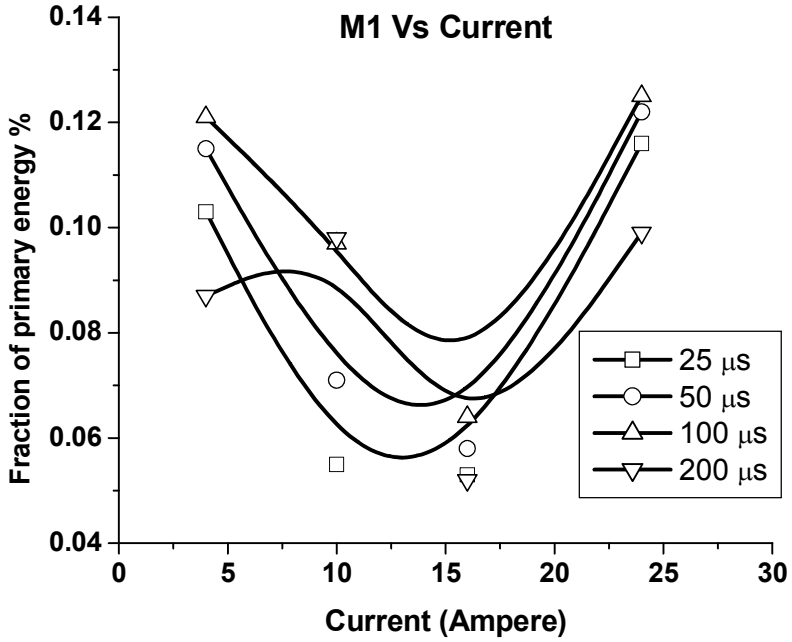

Fig. 5.18: Comparison between current and fraction of primary energy for erosion of work piece for different pulse duration

On increasing the current the % FPE firstly decreases up to lowest 0.05% and then increases in the %FPE is observed. As the pulse duration increases % FPE also increases, this variation is from 0.05-0.12% i.e. total variation is 0.07% at all pulse duration levels. Though this variation is very little but utilization factor for 200μs is less because of expansion of plasma channel. Comparison between current and fraction of primary energy conducted through workpiece for different pulse duration is shown in Fig. 5.19.

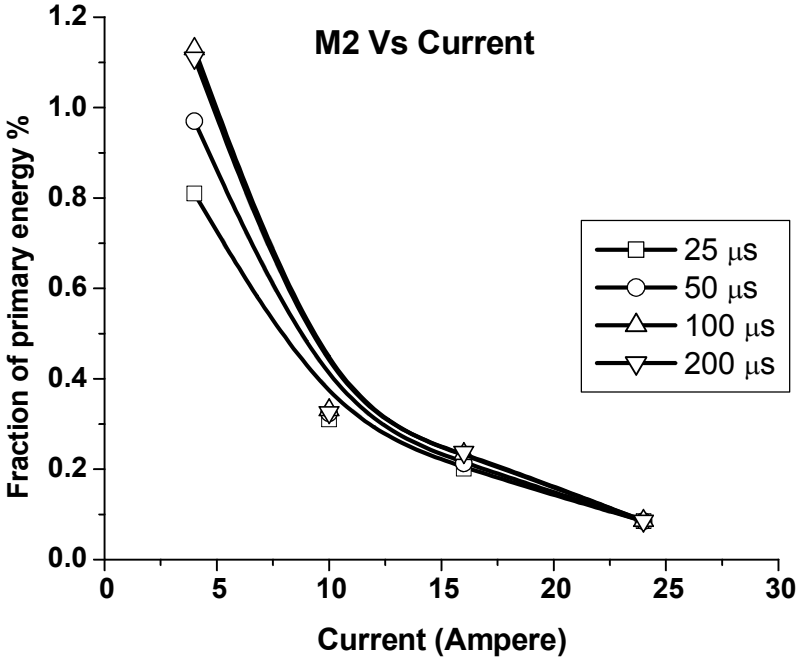

Fig. 5.19: Comparison between current and fraction of primary energy conducted through work piece for different pulse duration

The % FPE variation for all the pulse duration is small variation of 0.3% only. When the current is increased this variation comes closer to negligible for all the pulse durations.

The relation between current and fraction of primary energy stored in workpiece for different pulse duration is shown in Fig. 5.20.

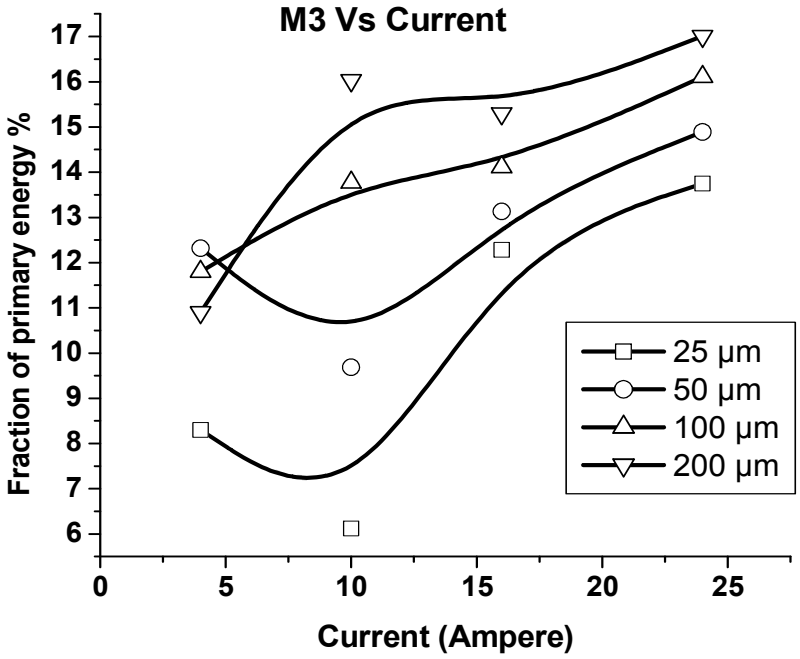

Fig. 5.20: Comparison between current and fraction of primary energy stored in work piece for different pulse duration

The % FPE drop down at 10 ampere level in case of 25 µs and 50 µs pulse duration. An increasing trend is observed for levels more than 10 ampere current.

Effect of current on fraction of primary energy for erosion of electrode for different pulse duration is shown in Fig. 5.21.

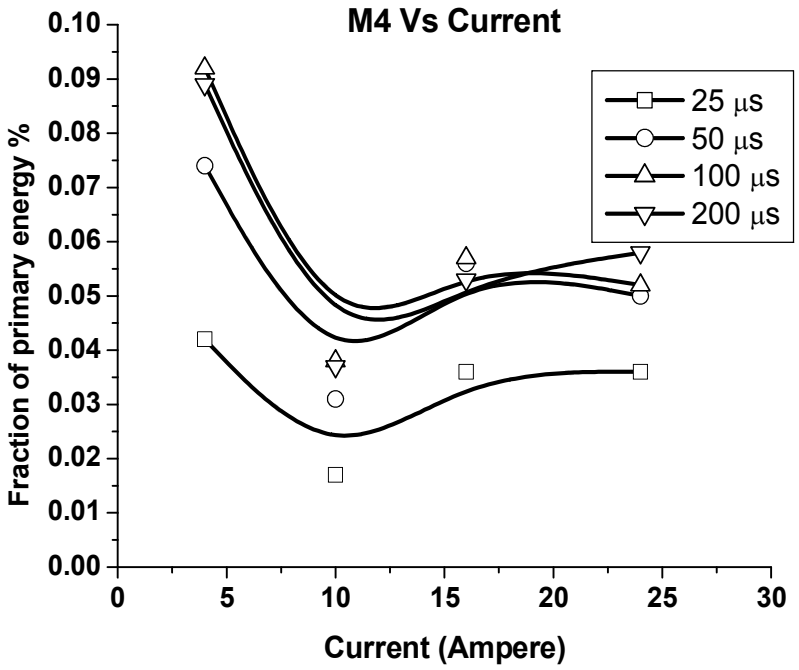

Fig. 5.21: Comparison between current and fraction of primary energy for erosion of electrode for different pulse duration

Utilization of % FPE for electrode varies from 0.04-0.09% at 4 ampere and 0.04-0.06% at 24 ampere with variation in pulse duration. This variation is negligible at all pulse currents.

Comparison between current and fraction of primary energy conducted through electrode for different pulse duration is shown in Fig. 5.22.

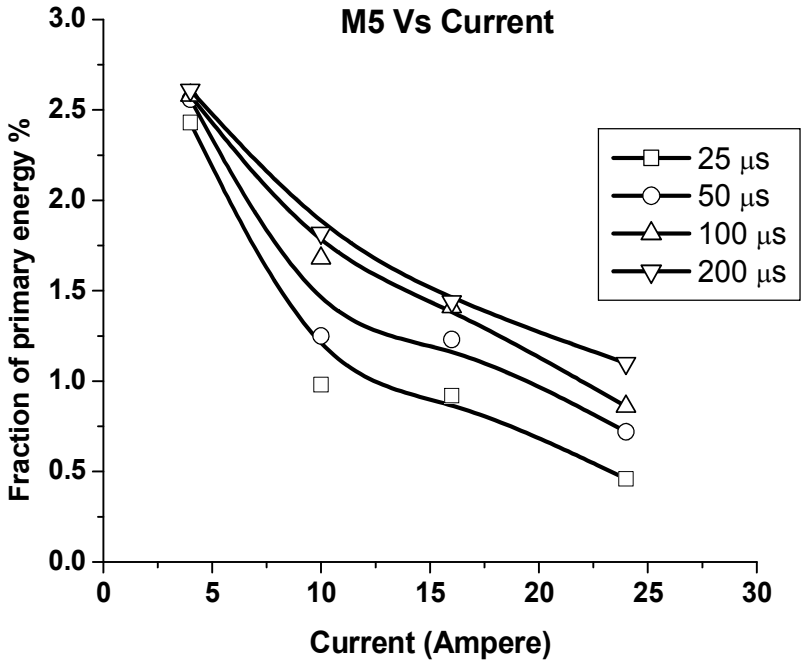

Fig. 5.22: Comparison between current and fraction of primary energy conducted through electrode for different pulse duration

There is no variation in %FPE a 4 ampere current which gradually increases at higher current. Lower %FPE is observed for 25 μs and higher %FPE at high pulse duration i.e. 200 μs. This variation is also with the range of 0.5-1.3% i.e. 0.7%. Fraction of primary energy stored in electrode for different pulse duration is shown in Fig. 5.23.

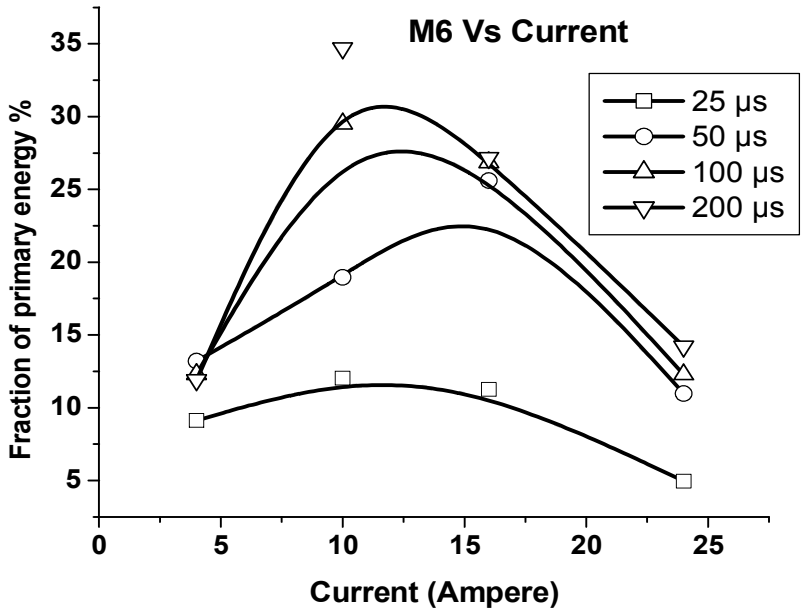

Fig. 5.23: Comparison between current and fraction of primary energy stored in electrode (M6) for different pulse duration

There is a variation of only 5% at 25µs pulse duration as the current is increased from 4 ampere to 24 ampere current. At 16 ampere current all the pulse duration showed maximum % FPE. At 200 µs pulse duration more than 30% FPE is observed. This variation in energy which is conducted through electrode for different pulse duration is shown in Fig. 5.24.

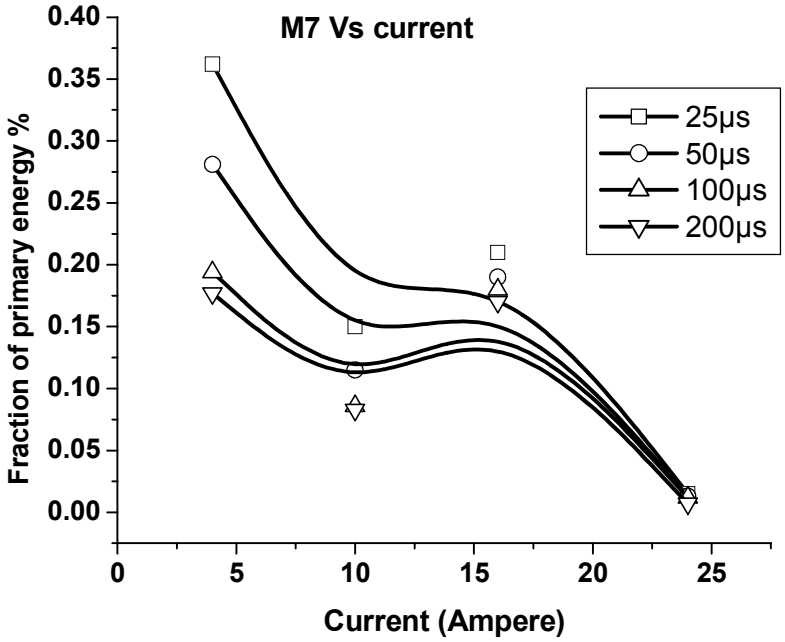

Fig. 5.24: Comparison between current and fraction of primary energy conducted through electrode for different pulse duration

At lower current of 4 ampere as the pulse duration increases the energy conducted though electrode decreases. At 24 ampere the % FPE is lowest and is equal for all levels of current. Comparison between current and fraction of primary energy stored in dielectric fluid for different pulse duration is shown in Fig. 5.25.

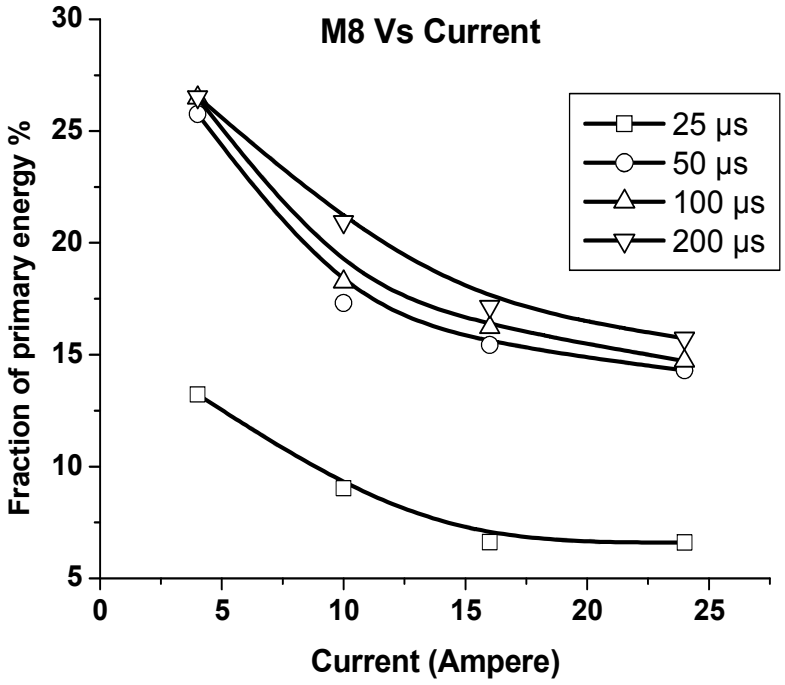

Fig. 5.25: Comparison between current and fraction of primary energy stored in dielectric fluid for different pulse duration

It is observed that for all pulse durations the % FPE is approximately 12 % as the discharge current is increased from 4 ampere to 24 ampere. The behavior observed for 25µs pulse duration is different as compared to 50, 100 and 200µs. For 50 to 200µs the %FPE observed is 27% which drops down to approximately 17% at 24 ampere current level. Comparison between current and fraction of primary energy stored as residual losses for different pulse duration is shown in Fig. 5.26.

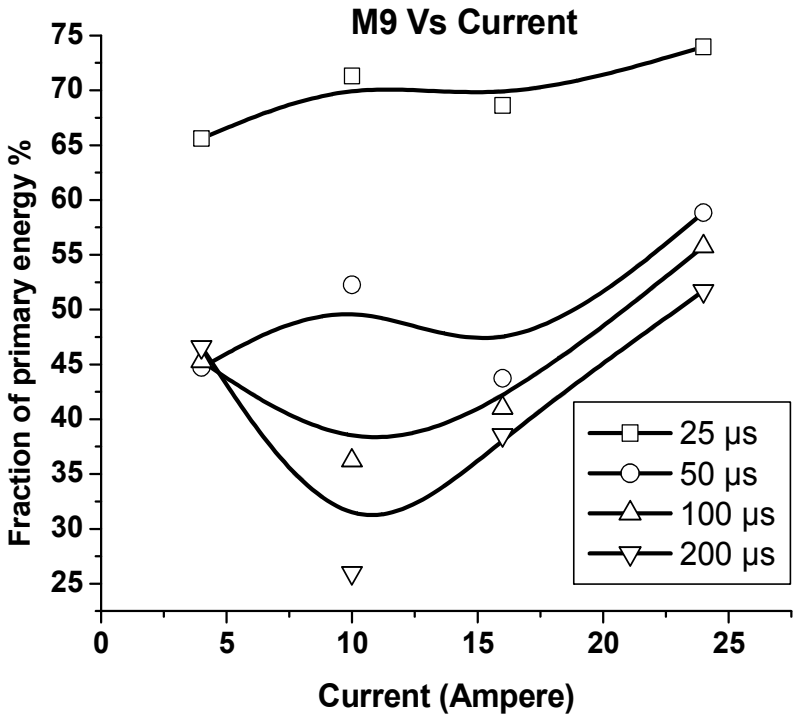

Fig. 5.26: Comparison between current and fraction of primary energy as residual losses for different pulse duration

The % FPE for the residual losses have been observed to be maximum at 25 µs pulse duration which varies from 65% to75% as the current is increased from 4 ampere to 24 ampere current levels. These losses drop down with increasing pulse duration. At higher current the variation in losses is very less.

5.6.4 Energy Distribution in Work piece, Electrode and Dielectric Materials

The percentage of energy distributed in workpiece, electrode, and dielectric has been calculated from the data given in table 6. It is observed that the total used energy by work piece, dielectric and electrode for all the currents at different pulse duration varies from 9.2 to 17.2 %.

The comparison between energy distributed between work piece, electrode and dielectric fluid for 4A, 10A, 16A and 24A current with variation pulse duration is given in Fig. 5.27-5.30 respectively.

This relation between pulse duration and % FPE distributed between work piece, electrode and dielectric fluid for current of 4 ampere is shown in Fig. 5.27.

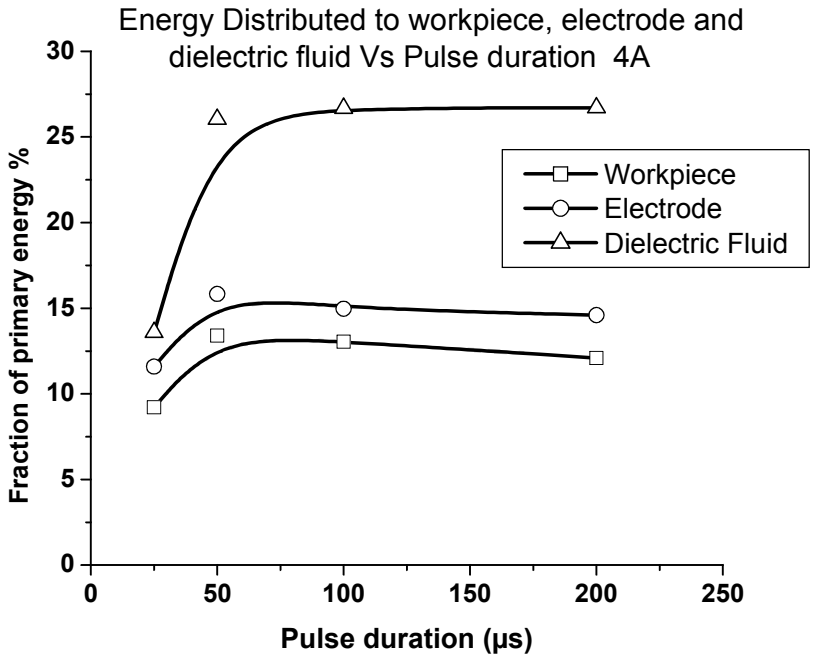

Fig. 5.27: Comparison between pulse duration and fraction of primary energy distributed between work piece, electrode and dielectric fluid for current of 4Amp

It is observed that maximum energy is consumed by the dielectric fluid. There is not much difference in trend except at for electrode and workpiece material where utilization of energy increases from 25 to 50 µs pulse duration after that it remains nearly constant. These results are the reverse of normal requirement for machining. The energy utilization for the work piece should be more. Comparison between pulse duration and %FPE distributed between work piece, electrode and dielectric fluid for 10 ampere current is shown in Fig. 5.28.

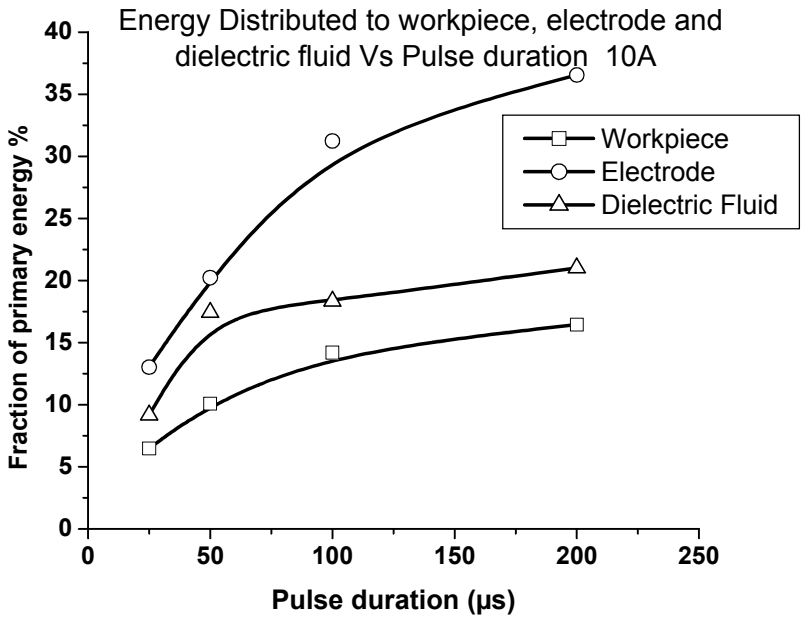

Fig. 5.28: Comparison between pulse duration and fraction of primary energy distributed between work piece, electrode and dielectric fluid for current of 10Amp

It is observed that maximum energy is consumed by the electrode. These results are also in the reverse order of normal requirement i.e. to optimize the process the energy utilization need to be optimized. Under such conditions reverse polarity can be considered to improve the results. Comparison between pulse duration and fraction of primary energy distributed between work piece, electrode and dielectric fluid for 16 ampere current is shown in Fig. 5.29.

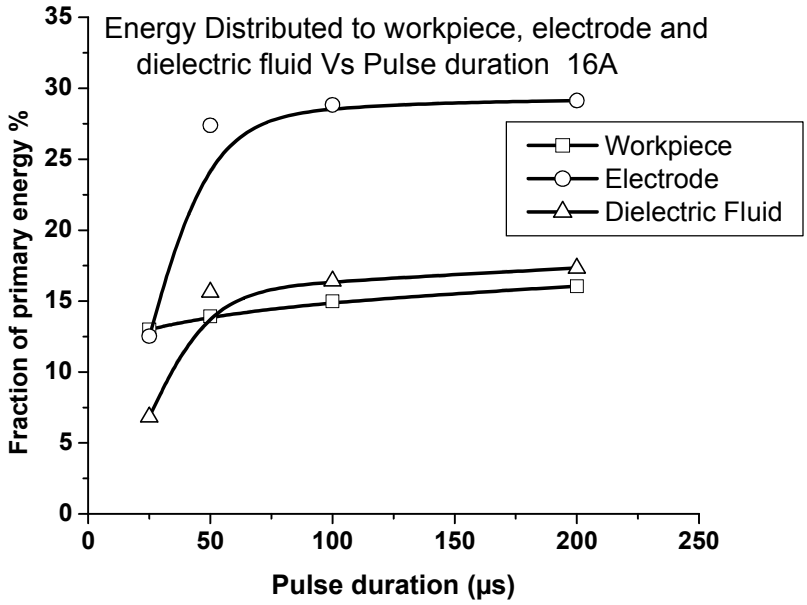

Fig. 5.29: Comparison between pulse duration and fraction of primary energy distributed between work piece, electrode and dielectric fluid for current of 16Amp

Here also the maximum energy is utilized by electrode.

Comparison between pulse duration and fraction of primary energy distributed between work piece, electrode and dielectric fluid of 24 ampere current is shown in Fig. 5.30.

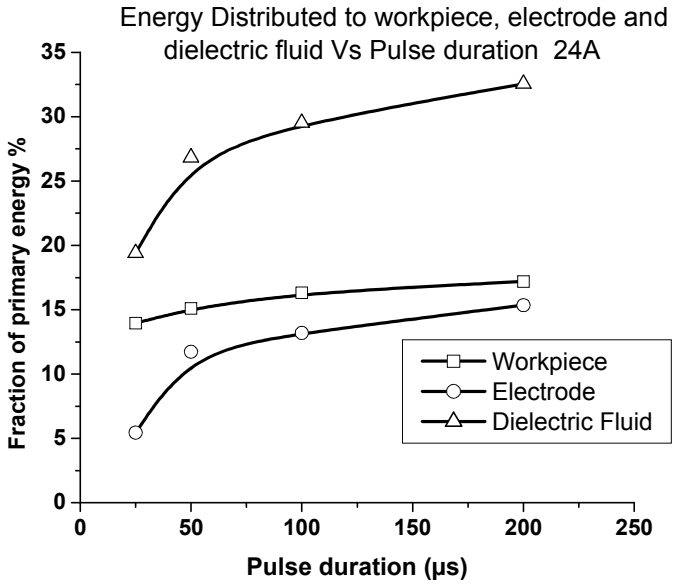

Fig. 30: Comparison between pulse duration and fraction of primary energy distributed between work piece, electrode and dielectric fluid for current of 24A

It is observed that maximum energy is consumed by the dielectric fluid. The utilization of energy for 50 μs, 100 μs and 200 μs pulse duration remains almost equal. In order to have maximum utility of energy, the work piece material should conduct more energy which is obtained in these conditions. Considering these factors it can be said that machining at 24 ampere current for all pulse duration will lead to maximum utilization of energy by the work piece material which is also observed in our experiments (Fig. 5.7).

5.6.5 ANOVA analysis of variance

Two way ANOVA analyses have been performed with the help of MINITAB software to find out the suitability of the experiments performed. These tests were performed on selected significance factors. These significant factors are selected on the basis of existing work of Scott [86]. Percentage fraction of energy distribution data shown in data shown in Table 5.5 have been used for these tests.

Table 5.6: Two way ANOVA: M6 versus current, pulse duration analysis of variance for M6

Source	DF	SS	MS	F	P
Current	3	593.9	198.0	10.40	0.003
Pulse Duration	3	375.9	125.3	6.58	0.012
Error	9	171.3	19.0	-	-
Total	15	1141.1	-	-	-

Table 5.7: Two way ANOVA: M8 versus current, pulse duration analysis of variance for M8

Source	DF	SS	MS	F	P
Current	3	250.43	83.48	63.78	0.000
Pulse Duration	3	319.49	106.50	81.36	0.000
Error	9	11.78	1.31	-	-
Total	15	581.71	-	-	-

Table 5.8: Two way ANOVA: M3 versus current, pulse duration analysis of variance for M3

Source	DF	SS	MS	F	P
Current	3	54.48	18.16	5.85	0.017
Pulse Duration	3	50.63	16.88	5.43	0.021
Error	9	27.96	3.11	-	-
Total	15	133.07	-	-	-

The results so obtained are shown in Tables 5.6-5.8. The P values vary from 0 to 0.017. These values are very near to zero and F value vary from 5.43 to 81.36 indicating that the experiments performed are well in standard acceptable value of ±5%. As expected the degree of freedom in all the cases is three.

Manufacturing of materials are usually done by improving the quality and productivity level by selecting shortest process time. Factors such as process energy, wastage of materials are ignored. There are other health and environmental problems which demand for proper utilisation of energy. The increase in uses of process energy directly impacts on the amount of waste created which leads to depletion of the resources. There is need to develop a methodology for optimising these parameters which include process time, process energy, quality and quantity of energy utilised. The present work is an effect to optimise the energy.

EDM employs thermal energy to cut or shape the work piece material. Energy generated by plasma is utilized for machining of the material. The thermal energy which in impart for material removal is very less. Rest of energy goes as waste. The wastage occurs due to cracking of hydrocarbon (kerosene) dielectric which is toxic in nature and cannot be recycled. The dielectric material (kerosene) also possesses high dielectric strength and is non-conductive until breakdown voltage reached. The process requires large amount of energy for machining where heat capacity of the dielectric fluid plays an important role.

In order to reduce the wastage one should use other dielectric fluid like water. The heat capacity of water is 1.5 times higher than kerosene and thus the amount lost through evaporation is lower. In order to increase the utility value of energy which goes as waste it is essential to address on type of dielectric material which will help from health point of view also for which in EDM is one of the substitute which has been discussed elaborately in Chapter 1.

Chapter 6

CONCLUSIONS AND SCOPE OF FUTURE WORK

Overview

The present chapter summarizes the results of the various experiments conducted during the course of investigations in reference to the objectives of study. The effect of different process parameters on MRR, surface integrity and energy distribution patterns for machining of tungsten carbide by electrical discharge machining (EDM) has been studied and reported. The study carried out on machining of WC-Co material has brought to surface a complex phenomenon where the formations of complex carbides like Co_3W_3C, Co_3W_6C was observed during machining. The causes of formation of cracks in the work piece material are related to machining conditions. For removing the surface cracks, finishing should be done at low current and low pulse duration. The phase transition should be avoided to retain the basic structure of WC-Co material which is possible only when the heat removal from the surface is fast. However, it is strongly felt that there is a need to study the phenomenon of formation of complex carbides and their role in influencing surface integrity in machining. This can be taken up as future research work.

Further, by varying the machining parameters it has been found that the MRR can be improved by synchronizing current, pulse on time and appropriate flushing conditions. A controlled current should be selected, which may have higher value in the beginning, to achieve a higher MRR.

Energy distribution between the process elements was also examined and has been reported accordingly. The effective energy distributed to the work piece material increases with increase of pulse duration at high current and that which goes into electrode and dielectric fluid decreases with decrease in pulse duration and increase in current. Optimum utilisation of energy occurs at 24Amp current and 100μs pulse duration. Also, the pulse duration at which utilisation of energy is optimum decreases with decrease in current.

6.1 Conclusions

The present work comprises of study conducted with a view to optimise the process parameters for machining of tungsten carbide (WC-Co) composite by EDM process. In order to improve MRR and also the surface roughness (R_a value), pulse-on time, the discharge current, electrode material and type of flushing were varied. The conclusions derived from the investigations are reported as below under separate heads.

1. Material removal rate and surface roughness:

Since one of the motivating factors in selecting the problem was to seek higher productivity of the process, conditions leading to higher MRR and better surface finish were investigated. It was found that both MRR and surface roughness (R_a) values increased with increase in the discharge current for all the three electrode materials viz graphite, copper tungsten and copper. The increase has been found to be linear for graphite electrode in the discharge current range of 10 Amp to 20 Amp. For copper tungsten electrode MRR varied almost linearly whereas surface roughness (R_a) was found to be nearly constant for the current range of 10 Amp to 15 Amp but this increase stopped at 15 Amp to 20 Amp which could be due to material being removed in the form of patches and non uniform distribution of heat. For copper electrode both MRR and Ra were observed to increase with increase in discharge current in the range of 10 Amp to 200 Amp. MRR varies non-linearly, whereas R_a value increases at a faster rate in the range of 10 Amp to 15 Amp but becomes slow between the current ranges of 15 Amp to 20 Amp. However, an important fact observed for copper and copper tungsten electrodes was that the variation of R_a is non-linear whereas that of MRR is linear for all the three electrodes under similar experimental conditions. The machining time has been observed to be lowest for graphite electrode as compared to that for copper tungsten whereas the highest time was taken by the electrolytic copper electrode. It was also confirmed that the material removal rate increased with increase in discharge current but over a specific range only.

2. Surface integrity and crack formation:

In electro discharge machining, material removal takes place due to surface melting followed by flushing action. The areas from where material is removed come up as craters. The depth of crater for small discharge current was less while for a large discharge current it was found to be more. Further, surface roughness for all the three types of electrodes increased with the increase in the discharge current. SEM of the tungsten carbide vividly reveals valuable information on surface modification, structural change and crack formation in the work piece

material. The structural features also confirmed the erosion of material by thermal melting during the spark erosion process.

The EDMed surface has a mattee appearance having craters, re-deposits and pits. It has been observed that the possible addition of eroded electrode material in the workpiece material during electric discharge machining process leads to the compositional change of different elements present in the work piece material.

There is a white layer deposition all over the workpiece material during electric discharge machining. This machined surface has many micro cracks. The width of the cracks formed varies from 448.9nm to 635.54nm for small cracks as compared to 20.96 μm to 28.08 μm for bigger size cracks. Crack width is more when machining is done at higher current and it is less when we use lower current because heat affected zone is larger when machining is done at higher value of discharge current.

EDX analysis of the machined samples indicates that there is a black phase which has the highest amount of cobalt and the grey phase which has the lowest amount of cobalt. The grey phase is also rich in tungsten while the black phase has lowest amount of tungsten. This situation might be responsible for non uniform heat distribution, difference in coefficient of expansion, both promoting crack formation and their aggravation.

3. *Energy Distribution*:

Thermal energy plays a vital role in formation of cracks during machining of WC-Co. The energy is a function of pulse current and pulse duration. Surface cracks are formed due to re-solidified layer which are confined to only few micron of the re-solidified layer. However, at higher discharge current, formation of detrimental phase Co_3W_6C occurs (due to loss of carbon) which causes formation of cracks inside the material which is also affected by difference in coefficient of thermal expansion . Grain size of tungsten carbide plays a vital role in the distribution of cracks and depth of cracks. Larger the grain size more is the possibilities of cracks formation which is extended deeper into the surface due to larger pool of cobalt component occupying the grain boundary. This situation can be redressed by using fine grained work piece material. Current and pulse duration have an optimum value for maximization of MRR for each set of machining .When any one of the two exceeds, the value the MRR decreases.

The effective energy distributed to work piece increases with the increase in pulse duration at high current and also the energy distributed to electrode and dielectric fluid decreases with decrease in pulse duration and increase in current. The effective energy is maximized and unwanted energy is minimized for 24A current for all pulse durations. The optimum utilization of energy occurs at 24A current and 100 μs pulse duration. Finally, the effective

utilization of energy is less for low current (4A) than for higher current, but if pulse duration is considered, it is observed that the optimum pulse duration at which utilization of energy is optimum also decreases with the decrease of current.

It is suggested that if fine machining is required, then for effective utilization of energy it should be done at low current and low pulse duration as compared to the machining at higher current. But, in order to obtain high value of MRR for tungsten carbide work piece material we should use high values of current for which utilization of energy is maximum.

Analysis of experimental results carried out in chapter 3 in case of all three electrodes has shown that observed experimental results if desired can be represented reasonably by an appropriate type of exponential curve. Our results again confirm that exponential model is more appropriate for the present set of experimental results.

6.2 Suggestion for Future Work

In this work, the process parameters have been optimised using Taguchi orthogonal array design, which reduces the number of experiments to a greater extent as compared to conventional parametric design. However, Taguchi design does not account for the interaction between process parameters, which is evident from the parametric design. Considering this fact, it is suggested that a comparison between the results obtained from Taguchi orthogonal array design with conventional parametric design be carried out to establish a correlation among them. The design of experiment can be further optimised with well described objectives, pin-pointing the predominant performance parameters with their significance statistically defined.

Energy distribution in EDM is at an infancy stage as yet. A little has been reported on this important aspect. However, it is well proven that energy is the function of pulse current and pulse duration in EDM process. A detailed investigation into this area can play a very important part if an in depth study is carried out, particularly on carbide die materials.

An in-depth study is also required to understand the phase transition during machining as it influences both the MRR and surface roughness. Role of complex carbides also need to be understood more deeply in order to achieve better surface integrity as well as longer life of EDMed die material.

It is proposed that further studies are required to find out the range of current and pulse duration. Before development of mathematical models for Material removal rate (MRR) or the Surface finish (R_a). For moulds and Forging dies, designing of EDM machines of different range will be required and accordingly different set of experiments need to be tried out and optimised.

References

1 Pandey, P.C., and Shan, H.S. (2008), "Modern Machining Process", Tata McGraw Hill, New Delhi.

2 Pandey P.C. (1980), "Some Developments in Unconventional Machining Methods", Keynote Paper, 9th AIMTDR Conf., IIT Kanpur.

3 Lee S. H., Li, S.P. (2001), "Study l of the effect of machining parameters on the machining characteristics in Electrical Discharge Machining of Tungsten Carbide", *J. of materials processing technology,* **115**, 344-358.

4 Snoeys, Dijck R., F. Van. (1971), "Investigations of EDM Operations by Means of Thermo – Mathematical Models", *Annals of the CIRP*, **20**, 35.

5 Gurumurthy T., Arvind B.M., Sudhendra G. (1986), "Development of a Data Bank for Electrical Discharge Machining", Proc. of 12th AIMTDR Conf. 11T Delhi.

6 Jeswani M.L., Ramasawmy N. (1970), "Technological Characteristics of Electrospark Machining Process", Proc. Of 4th AIMTDR Conf. IIT Madras, 499.

7 Konig W., Werheim R., Zivirin Y., Toren M. (1975), "Material Removal and Energy Distribution in Electrical Discharge Machining", *Annals of the CIRP*, **24** 95.

8 Paterson C. (1984), "EDM White Paper**",** Elox Division, Colt Industries, Davidson, NC.

9 Guitrau E.B., The EDM Handbook, Henser Gardner Publications, 1997.

10 Lee, Lim L.C., Narayanan V., Venkatesh V.C. (1988), "Quantification of Surface Damage of Tool Steel after EDM", *Int. J Mach Tools Manufacturing*, **28**, 359.

11 Panda D.K., Bhai R.K. (1996), "Thermal modeling to predict the crater shaper in EDM", Proc. of 17th AIMTDR Conf., NIT Warangal.

12 Abbas Norliana Mohd., Solomon Darius G., Bahari Md. Fuad (2007), "A review on current research trends in electrical discharge machining (EDM)", *International journal of Machine Tools & Manufacture*, **47**, 1214-1228.

13 Daryl D., Di Bitonto, Philip, Eubank T., Mukund Patel, Maria Barrufet (1989), "Theoretical Models of the Electrical Discharge Machining Process- The Anode Erosion Model", *Journal of Applied Physics*, **66/9**, 4095-4103.

14 Daryl D., Di Bitonto, Philip Eubank T., Patel Mukund, Maria Barrufet (1989), "Theoretical Models of the Electrical Discharge Machining Process- The Cathode Erosion Model", *Journal of Applied Physics*, **66/9**, 4104-4112.

15 Guu Y.H., Hocheng H., Chou C.Y., Deng C.S. (2003), "Effect of electrical discharge machining on surface characteristics and machining damage of AISI D2 tool steel", *Material Science and Engineering A*, **358**, 37-43.

16 Jeswani M.L. (1981), "Effect of addition of graphite powder to kerosene used as a dielectric fluid in electrical discharge machining", *Wear*, **70**, 133-139.

17 Ho K.H., Newman S.T. (2003), "State of the art electrical discharge machining (EDM)", *International journal of Machine Tools & Manufacture*, **43**, 1287-1300.

18 Marafona J., Wykes C. (2000), "A new method of optimizing material removal rate using EDM with copper tungsten electrode", *International Journal Machine Tools & Manufacture*, **40(2)**, 153-164.

19 Juhr, Schulze H. (2004), "Improved Cemented Carbide Properties after Wire EDM by Pulse Shaping", *Journal of Materials Processing Technology*, **149**, 178-183.

20 Lee S.H., Li Xiaoping (2003), "Study of the Surface Integrity of the Machined Workpiece in the EDM of Tungsten Carbide", *Journal of Materials Processing Technology*, **139**, 315-321.

21 Kansal H.K., Singh S., Kumar P. (2005), "Parametric optimization of powder mixed electrical discharge machining by response surface methodology", *International Journal of materials Processing Technology*, **149**, 427-436.

22 Liao Y.S., Yu Y. P. (2004), "The energy aspect of material property in WEDM and its applications", *International journal of Machine Tools & Manufacture*, **149**, 77-82.

23 Montgomery D.C. (2005), "Design and analysis of experiments", 5th Edition, John Wiley & Sons, ISBN 9971-51-329-3.

24 Navas V. Garcia, Ferreres I., Maranon J.A., Gracia-Rosales, Sevillano J. Gil (2008), "Electro-discharge machining versus hard turning and grinding- Comparison of residual stresses and surface integrity generated in AISI O1 tool steel", *Journal of Materials Processing Technology*, **195**, 186-194.

25 Pandit S.M., Rajurkar K.P. (1983), "A stochastic approach to thermal modeling applied to electro-discharge machining", *J. of Heat Transfer*, **105**, 555-562.

26 Puertas I., Luis C.J., Alvarez L. (2004), "Analysis of the Influence of EDM Parameters on Surface Quality, MRR and Electrode Wear of WC-CO", *Journal of Materials Processing Technology*, **153**, 1026-1032.

27 Ramasawmy H., Blunt L. (2002), "3D topography assessment of the effect of different electrolytes during electrochemical polishing of EDM surfaces", *International journal of Machine Tools & Manufacture,* **42**, 567-574.

28 Rebelo, J.C., Morao, D.A., Kremer D., Lebrun J.L. , 1998, Influence of EDM Pulse Energy on the Surface Integrity of Martensitic Steels, *Journal of Materials Processing technology*, **84**, 90-96.

29 Singh, S., Maheshwari, S., Pandey, P.C., 2004, Some Investigations into the Electric Discharge Machining of Hardened Tool Steel Using Different Electrode Materials, *Journal of Materials Processing Technology*, **149**, 272-277.

30 Shu Kuen-Ming, Tu G.C. (2001), "Fabrication and characterization of Cu-SiC composites for Electrical Discharge Machining applications", *International journal of Machine Tools & Manufacture*, **16(4)**, 483-502.

31 Simao, J., Lee H.G., Aspinwall, D.K., Dewes, R.C., Aspinwall, E.M., 2003, Work Piece Surface Modification Using Electrical Discharge Machining, *International Journal Machine Tools and Manufacture*, **43**, 121-128.

32 Yadav Vinod, Jain Vijay K., Dixit Prakash M. (2002), "Thermal stresses due to electrical discharge machining", *International Journal Machine Tools & Manufacture*, **42**, 877-888.

33 Kangarajan D., Kerthkeyan R., Palani Kumar K., Davim J. Paulo (2008), "Optimization of electrical discharge machining characterization of WC-Co composites using non dominated sorting genetic algorithm", *International Journal of Advanced Manufacturing Technology*, Springer, **36**, 1124-1132.

34 Singh Sehijpal, Shan H.S., Kumar Pradeep (2002), "Parametric optimization of magnetic field assisted abrasive flow machining by Taguchi method", *Journal of Quality and reliability engineering International*, **18**, 273-283.

35 Hwa-Teng Lee,Fu-Chuan Hsu, Tzu-Yao Tai (2004), "Study of surface integrity using the small area EDM process with a copper-tungsten electrode", *Material Science and Engineering*, **A364**, 346-356.

36 Kunieda M, Nakashima T. (1998), "Factor determining discharge location in EDM", *International Journal Electrical Machining,* **3**, 53.

37 Heuvelman C.J., Horn B.L. (1974), "Review of Co-operative work on EDM in STCE of CIRP", *Annals of the CIRP*, **23/2**, 213.

38 Takashi Endo, Tsujimoto Takayuki, Mitsui Kimiyuki, (2008), "Study of vibration assisted micro- EDM – The effect of vibration on machining time and stability of discharge", *Precision Engineering*, **32**, 269-277.

39 Cole M.., Bucklow I.A., Grigson, C.W.B. (1961), "Technique for Rapid, Accurate and Strain Free Machining of Metallic Single Crystals", *Brit. J. Appl. Physics,* **12/6**, 296.

40 Thoe T.B., Aspinwall D.K., Killey N. (1999), "Combined ultrasonic and electrical discharge machining of ceramic coated nickel alloy", *Journal of Materials Processing Technology*, **92/93**, 323-328.

41 Lazarenko B.I., Lazarenko N.I. (1964), "Technological Characteristics of Electrospark

Machining of Current Conducting Materials", *Electrospark Machining of Metals*, Consultants Bureau, N.Y., **2,** 1.

42 Williams E.M. (1952), "Theory of Electric Spark Machining", *AIEE Trans. (Application & Industry)*, **71**, 105

43 Rudorff, D.W. (1957), "Principles and Applications of Spark Machining", *Proc. Instrumentation Mechanical Engineering, London,* **171/14**, 495.

44 Lin H.C., Lin K.M., Cheng I.S. (2001), "The electro discharge machining characteristics of Ti Ni shape memory alloys", *Journal of Materials Science,* **36,** 399-404.

45 Manna A., Bhattacharaya B. (2001), "Investigation for effective tooling system to machine A1/SiC-MMC", Proc. of National Conf. on Recent Advances in Materials Processing, *Annamalai University,* September 7-8.

46 Fuzhu Han, Kunieda Masanori (2004), "Development of parallel spark electrical discharge machining", *Precision Engineering,* **28**, 65-72.

47 Chen S.L., Hsu Q.C. (2003)," Studies on electric-discharge machining of non-contact seal face grooves", *Journal of Materials Processing Technology,* **140**, 363–367.

48 Greene J.E., Guerrero-Alverez (1974), "Electro Erosion of Metal Surfaces", *Metall. Trans.,* **5**, 695.

49 Heuvelman C.J. (1969), "Some Aspects of the Research on Electro-Erosion Machining", *Annals of the CIRP,* **17/1**, 195.

50 Bucklow I.A., Cole M., (1969), "Spark Machining". *Metall. Rev.*, **3/6**, 103.

51 Kojima H., Kunieda M., Nishiwaki N. (1992), "Understanding discharge location movement during EDM", *Proceedings International Symposium Electro machining,* **10**, 144.

52 Mironoff N. (1970), "Introduction into the Study of Spark-Erosion", 2nd Ed., *Microtecnic-Scriptar Ltd.,* Switzerland.

53 Deng Jianxin, Lee Taichiu (2002), "Effect of ultrasonic surface finishing on the strength and thermal shock behavior of the EDMed ceramic composite", *International Journal of Machine Tools & Manufacture,* **42,** 245-250.

54 Namitokov K.K. (1965), "Physics of the Electrical Erosion of Metals by Low Voltage Pulse Discharges", *Electro spark Machining of Metals,* Consultants Bureau, N.Y., **3**, 45.

55 Ghanem F., Braham C., Sidhom H. (2003), "Influence of steel type on electrical discharge machined surface integrity", *Journal of Materials Processing (Placeholder1) Technology,* **142,** 163-173.

56 Nekrashevich I.G., Bakuto I.A. (1965), "Present State of the Theoretical Concepts of the

Electric Erosion of Metals", *Electrospark Machining of Metals, Consultants Bureau,* N.Y., **3**, 17.

57 Guu Y.H., (2005), "AFM surface imaging of AISI D2 tool steel machined by the EDM process", *Applied Surface Science,* **242**, 245–250.

58 Willey P.C.T. (1976), "Analysis of Debris from the Electro-Discharge Machining Processing and the Conclusions to be Drawn about the Physical Process of Metal Removal", *Proc. Of 17th Int. M.T.D.R. Conf.,* UMIST, **2,** 291.

59 Crookall J.R., Heuvelman C.J. (1971), "Electro-Discharge Machining – The State of the Art", *Annals of the CIRP,* **20/2**, 113.

60 Haoyu Huang, Noritaka Yusa, Kenzo Miya, (2006), "Eddy current testing and sizing of fatigue cracks", 12th A-PCNDT, *International institute of universality,* Tokyo, Japan.

61 Snoeys R., Van Dijck F. (1973), "Physico-Mathematical Analysis of the EDM Process", *Proc. N. Am. Metal Work, Res. Conf.,* Hamilton, **2**, 181.

62 Zolotych B.N. (1960), "The Mechanism of Electrical Erosion of Metals in Liquid Dielectric Media", *Sov. Phy.-Tech. Phy.,* **4**, 1370.

63 Van Dijck F., Snoeys R. (1975), "A Theoretical and Experimental Study of the Main Parameters Governing the Electro-Discharge Machining Process", *Mecabnique,* **9**, 301-302.

64 Crookall J.R., Khor B.C (1974), "Electro- Discharge Machined Surfaces", *Proc. of 13th Int. M.T.D.R. Conf., Birmingham,* 373.

65 Jeswani M.L., Basu S. (1979), "Electron Microprobe Study of Deposition and Diffusion of Tool Material in Electrical Discharge Machining", *Int. J. Prod. Res.*, **17/1,** 100-110.

66 Venkatesh V.C., Parasnis S. (1972), "Surface Transformation in High Speed Steel after EDM", *Proc. of 5th AIMTDR Conf., I.I.T. Roorkee,* 639.

67 Kun Ling Wu, Biing Hwa Yan, Fuang Yuan Huang, Shin Chang Chen (2005), "Improvement of surface finish and surfactant added dielectric", *International Journal of Machine Tools & Manufacture,* **45,** 1195-1201.

68 Carslaw H.S., Jaeger J.C. (1959), "Conduction of Heat in Solids", *Oxford University Press*, Oxford.

69 Mohri N., Saito N., Takawashi T., Kobayashi K. (1985), "Mirror Like finish by EDM", *Proceedings of the 25th Machine Tool Design and research Conference,* 329.

70 Lim H.S., Wong Y.S., Rahman M., Edwin Lee M.K. (2003), "A study on the machining of high-aspect ratio micro-structures using micro-EDM", *Journal of Materials Science Processing Technology,* **140,** 318–325.

71 Aleksandrov V.P. (1965), "Residual Stresses and the Long-Term and Fatigue Strengths of Heat-Resistant Materials after Electrospark Machining", *Electrospark Machining of Metals, consultants Bureau,* N.Y., **3**, 98.

72 Crookall J.R., Khor B.C. (1972), "Residual Stresses and Surface Effects in EDM", *Proc. Of 13th Int. M.T.D.R. Conf., Birmingham,* 331.

73 Mahdavinejad R. A., Mahdavinejad A. (2005), "ED machining of WC-CO", *Journal of Material Processing Technology,* **163,** 637-643.

74 Chetverikov S.S., Foteev N.K. (1964), "Electrospark Machining of the Cutting Elements of Sintered Carbide Blanking and Piercing Dies", *Electrospark Machining of Metals, Consultants Bureau,* N.Y., **2**, 85.

75 Barash M. (1962), "Electric Spark Machining", *Int. J. Mach. Tool Des. Res.,* **2/3**, 281.

76 Lee H.T., Tai T.Y. (2003), "Relationship between EDM parameters and surface crack formation", *Journal of Material Processing Technology,* **142**, 676–683.

77 Shankar Singh , Maheshwari S., Pandey P.C. (2004), "Some investigations into the electric discharge machining of hardened tool steel using different electrode materials", *Journal of Material Processing Technology*, **149,** 272–277.

78 Simao J., Lee H.G., Aspinwall D.K., Dewes R.C., Aspinwall E.M. (2003), "Work piece surface modification using electrical discharge machining", *International Journal Machine Tools and Manufacture*, **43**, 121-128.

79 Opitz H. (1960), "Metallurgical Aspects and Surface Characteristics, Spark Machining", *Symposium of Metal Treatment and Drop Forging,* **27/177**, 237.

80 Lee L. C., Lim L. C., Wong Y. S. (1992), "Towards crack minimization of EDMed surfaces", *Material Processing Technology,* **32***,* 45-54.

81 Wang Z.L., Fang Y., Wu P.N., Zhao W. S., Cheng K. (2002), "Surface modification process by electrical discharge machining with a Ti powder green compact electrode", *Journal of Materials Science Processing Technology*, **129,** 139-142.

82 Mathar J. (1934), "Determination of initial stresses by measuring the deformation around drilled holes", *Transaction of the ASME*, **56,** 249-254.

83 Barash M. (1965), "Effect of EDM on Surface Properties of Tool & Die Steels", *Metals Engineering Quarterly,* **5/4**, 48.

84 Longfellow J.D, Wood J.D, Palme R.D. (1968), "Effect of Electrode Material Properties on Wear Ratio in Spark Machining", *Inst. Metals J.,* **96/2**, 43.

85 Bhattacharya S., Kanshawy M.E., Carber S., Wallbank J. (1981), "A Correlation between Machining Parameters and Machinability in EDM", *Int. J. Prod. Res.,* **19/2**, 111.

86 Dan Scott, Sreedhar Boyina, Rajurkar K.P. (1991), "Analysis and Optimization of Parameter Combinations in Wire Electrical Discharge Machining", *Int. J. Prod. Res*, **29/11**, 2189-2207**.**

87 Rajurkar K.P., Pandit S.M. (1994), "Formation and Ejection of EDM Debris", *ASME Transaction*, **108,** 22.

88 Luis Llanes, Begona Casas, Eva Idanez, Montserrat Marsal, Marc Anglada (2004),"Surface integrity effects on the fracture resistance of electrical discharge machined WC-Co cemented carbides", *Journal of American ceramic society*, **87**, 1687-1693.

89 Casas B., Wiklund U., Hogmark S., Llanes L. (2008), "Adhesion and abrasive wear resistance of TiN deposited on electrical discharge machined WC-Co cemented carbides", *Wear*, **265**, 490-496.

90 Jeswani M.L. (1978), "Roughness and Wear Characteristics of Spark Eroded Surfaces", *Wear*, **51**, 227–236.

91 Lee H.T., Hsu F.C., Tai T.Y. (2004), "Study of Surface Integrity Using the Small Area EDM Process with a Copper-Tungsten Electrode", *Mater. Sci. Eng.*, **A364**, 346–356.

92 Kai Egashira, Akihiro Matsugasako, Hachiro Tsuchiya, Makoto Miyazaki (2006), "Electrical discharge machining with ultra low discharge energy", *Precision Engineering*, **30**, 414–420.

93 Ramaswamy H., Blunt L. (2004), "Effect of EDM Process Parameters on 3D Surface Topography", *Journal of Materials Science Processing Technology*, **148**, 155-164.

94 Sahin Y., Kok M., Celik H. (2002), "Tool wear and surface roughness of Al_2O_3 Particle-reinforced alluminium alloy composites", *Journal of Materials Science Processing Technology*, **128**, 280–291.

95 Zhao Wangsheng, Zhenlong , Di Shichun, Chi Guanxin, Wei Hongyu (2002), "Ultrasonic and electric discharge machining to deep and small hole on titanium alloy", *Journal of Materials Processing Technology,* **120**, 101–108.

96 Tzu-Yao Tai (2006), "Application of EDM Hole-drilling Method to the Measurement of Residual Stress in Tool and Carbon Steel", *Journal of Engineering Materials and Technology*, **128**, 468-475.

97 Ramasawmy R., Raj S.L. (1973), "A Study of Wear and Surface Finish During Spark Erosion Machining of High Speed Tool Steel", *Wear*, **24**, 156-157.

98 Stanislao J., Richman M. H. (1971), "EDM die making", *Precis. Met.*, **29**, 50.

99 Yih-fong T., Fu-Chen C. (2005), "Investigation into some surface characteristics of

electrical discharged machined SKD-11 using powder-suspension dielectric oil", *J. Mater. Process. Technol*., **170**, 385–391.

100 Walker W. F. (1970), "Fundamentals of economic manufacture-65", *Tooling*, **24**, 22.

101 Blake A. (1985), "Handbook of mechanics, materials and structures", **357**, Wiley IEEE.

102 Barash M. M. (1958), "Investigation into some aspects of the spark erosion process and its effects on some mechanical properties of the workpiece", PhD thesis, Victoria University, Manchester, UK.

103 Hasan F., Iqbal J. (2006), "Consequential rupture of gas pipe line", *Engineering Failure Analysis*, **13**, 127–135.

104 Singh Shankar, Maheshwari S., Pandey P. C. (2004), "Some investigations into the electric discharge machining of hardened tool steel using different electrode materials", *Journal of Material Processing Technology*, **149**, 272–277.

105 Khatter C. P., Pandey O. P. (2008), "Effect of processing parameters on structural features of tungsten carbide after electrical discharge machining (EDM)", *International journal of tribology* , **2**, 65-71.

106 Wansheng Zhao, Wang Zhenlong, Di Shichum, Chi Guanxin, Wei Hongyu (2002), "Ultrasonic and electric discharge machining to deep and small hole on titanium alloy", *Journal of Materials Processing Technology*, **120**, 101-106.

107 Soo Hiong Lee, Xiaoping Li (2003), "Study of the surface integrity of the machined workpiece in the EDM of tungsten carbide", *Journal of Material Processing Technology*, **139**, 315–321.

108 Khanra A. K., Patra S., Godkhindi M. M. (2006), "Electrical discharge machining studies on reactive sintered FeAl", *Bull. Mater. Sci*., **29**, 277-280.

109 Jacobs L., Hyland M. M. (1999), "Study of the influence of microstructural properties on the sliding –wear behavior of HVOF and HVAF sprayed WC-cermet coatings", Journal of Thermal Spray Technology, **8**, 125-132.

110 Li C.J., Ohmori A., Harada Y. (1996), "Effect of Powder Structure on the Structure of Thermally Sprayed WC-Co coatings",*J. Mater . Sci.*, **31**,785-794.

111 Subrahmanyam J., Srivastava M.P., Sivakumar R.(1986), "Characterization of plasma sprayed WC-Co coatings", *Mater. Sci. Eng.,* **84**,209-214.

112 Hwang S.Y., Seong B.G., Kim M.C. (1996) Charactrization of WC-Co Coatings Usings HP/HVOP Process", *Thermal Spray: Practical Solutions of Engineering Problems,* C.C. Berndt, Ed., ASM International 107-112.

113 Chang Jiu Li, Ohmori A., Harada Y. (1996), "Effect of powder structure on the structure of themally sprayed WC-Co coating", *Journal of Material Science*, **31**,785-794.

114 Yeo S. H., New A. K. (1999), "A method for green process planning in electric discharge machining", *The International Journal of Advanced Manufacturing Technology*, **15**, 287-291.

115 Raman K.S., Gupta H.R., Singhal A.R., Das P.K., Saha P., Mishra P.K. (1996), "Edming of GT-20 Grade of Carbide", *Proc of 17th AIMTDR Conf.*, NIT Warangal.

116 Jain V.K. (2002), "Manufacturing Technology", Indira Gandhi National Open University, Delhi.

117 Rappaz Michel (2005), Metallurgical processes occurring at surfaces submitted to high melting and cooling rates during electrical–discharge machining, Project No. 5777.2.

118 Hocheng H., Lei W.T. Hsu H. S. (1997), "Preliminary study of material removal in EDM of SiC/Al", *Journal of Materials Processing Technology*, **63**, 813-818.

119 Daryl D., Eubank T. (1989), "Theoretical Models of the Electric Discharge Machining Process – A Simple Cathode Erosion Model", *Journal of Applied Physics*, **66/9**, 4095-4103.

120 Zingerman A.S. (1956), "Propagation of a Discharge Column", *Journal of Soviet Physics*, **4**, 992.

121 Van Osenbruggen, High Precision Spark Maching, Philips Tech Rev., **30** (6/7).

122 Panda D. K., Bhoi R. K., Mishra B. (1996), "Study of Crater Profile and its Temperature Distribution in EDM", Proc. Of 17th AIMTDR conf., NIT, Warangal.

123 Drabinka S. I. (1954), "The theory of the development of the channel in the spark discharge", *Journal of Experimental Physics*, **21**, 473.

124 Bozkurt B., Gadalla A. M., Eubank P.T. (1996), "Simulation of Erosion in a single discharge EDM process", M*aterials and Manufacturing Processes*, **11**, 555-563.

125 Lin H.C., Lin K.M., Cheng I.S. (2001), "Modeling of Material Removal in Mechanical Type Advanced Machining Processes: A State-of-Art Review", *Int. J. of Machine Tools & Manufacture*, **36**, 1573.